Title
X-ray Absorption Spectroscopy and EPR Studies of Oriented Spinach Thylakoid Preparations

Author
Andrews, Joy C.

Publication Date
1995-08-01

LBL-37695
UC-408

Lawrence Berkeley Laboratory
UNIVERSITY OF CALIFORNIA

STRUCTURAL BIOLOGY DIVISION

X-ray Absorption Spectroscopy and EPR Studies of Oriented Spinach Thylakoid Preparations

J.C. Andrews
(Ph.D. Thesis)

August 1995

Prepared for the U.S. Department of Energy under Contract Number DE-AC03-76SF00098

DISCLAIMER

LBL-37695
UC-408

X-ray Absorption Spectroscopy and EPR Studies of Oriented Spinach Thylakoid Preparations

Joy Cooke Andrews
Ph.D. Thesis

Department of Chemistry
University of California

and

Structural Biology Division
Lawrence Berkeley Laboratory
University of California
Berkeley, CA 94720

August 1995

This work was supported by the Director, Office of Energy Research, Office of Energy Biosciences Division, of the U. S. Department of Energy under Contract No. DE-AC03-76SF00098

X-ray Absorption Spectroscopy and EPR Studies of Oriented Spinach Thylakoid Preparations

by

Joy Cooke Andrews

B. A. (Barnard College) 1978
M. S. (California State University, Hayward) 1989

A dissertation submitted in partial satisfaction of the

requirements for the degree of

Doctor of Philosophy

in

Chemistry

in the

GRADUATE DIVISION

of the

UNIVERSITY of CALIFORNIA at BERKELEY

Committee in charge:

Professor Kenneth Sauer, Chair
Professor Robert Harris
Professor Bob Buchanan

1995

Abstract

X-ray Absorption Spectroscopy and EPR Studies
of Oriented Spinach Thylakoid Preparations

by

Joy Cooke Andrews

Doctor of Philosophy in Chemistry

University of California at Berkeley

Professor Kenneth Sauer, Chair

In this study, oriented Photosystem II (PS II) particles from spinach chloroplasts are studied with electron paramagnetic resonance (EPR) and x-ray absorption spectroscopy (XAS) to determine more details of the structure of the oxygen evolving complex (OEC). The nature of halide binding to Mn is also studied with Cl K-edge and Mn EXAFS (extended x-ray absorption fine structure) of Mn-Cl model compounds, and with Mn EXAFS of oriented PS II in which Br has replaced Cl.

In chapter 2, oriented PS II particles from spinach were studied with EPR spectroscopy. The mosaic spread for these samples was determined by comparison of the oxidized cytochrome b_{559} (cyt b_{559}^+) signal measured at angles of 0° to 360° between the EPR magnetic field and sample membrane normal with simulations of oriented cyt b_{559}^+. The tyrosine Y_D^+ signal was measured for these oriented samples at 0° and 90°, and a linear relationship was found between the dichroism found in the tyrosine Y_D^+ signal and the mosaic spread.

In chapters 3 and 4, Mn XAS was performed on oriented PS II membrane particles isolated from spinach. These studies were on control samples (chapter 3) and on samples treated with ammonia (chapter 4), a water analog which can yield insight into the binding of water by the OEC. Structural features of the tetranuclear Mn cluster and the orientation of the cluster with respect to the lipid bilayer were determined in the S_2 state of the Kok cycle

for control samples, and on the annealed S_2 state for the ammonia-treated samples. Variation of the sample orientation with respect to the x-ray **e**-vector yields highly dichroic EXAFS, indicative of an asymmetric tetranuclear cluster. Mn-Mn vectors at 2.72 Å and 3.38 Å are resolved from the control samples. Vectors at 2.73 Å, 2.86 Å and 3.3 Å are resolved from the ammonia-treated samples. The 2.72 Å vector for the control samples is oriented at an angle of 59° to the membrane normal (an average for at least two component vectors) with an average of 0.98 interaction per Mn atom. In the ammonia-treated samples it is further resolved into a 2.73 Å vector at 54° and a 2.85 Å vector at 61°. Thus, asymmetry of the two di-μ-oxo bridged Mn-Mn binuclear units of the OEC is directly observed. The 3.38 Å vector, also likely to be an average of two vectors, makes an angle of 40° with respect to the membrane normal, with an average of 0.41 backscatterers per Mn atom in the control samples. An angle of 41° with an average of 0.76 backscatterers per Mn were found for the 3.3 Å vector in the ammonia-treated samples.

In chapter 5, the binding of halide to Mn was studied using Cl K-edge XAS and Mn EXAFS on Mn-Cl model compounds, and Mn EXAFS on oriented Br-treated PS II. From the Cl K-edges of model compounds, direct ligation of Cl to Mn could be confirmed with the presence of a pre-edge feature: a forbidden 1s to 3d transition which is seen due to mixing of Mn 3d orbitals with Cl 3p orbitals. Bridging and terminal Cl bonds to Mn could be distinguished. EXAFS of Mn-Cl model compounds revealed that Mn-Cl interactions, especially bridging interactions, make an important contribution to the EXAFS.

EXAFS of oriented Br-treated PS II showed differences from EXAFS of control Cl-treated PS II that were on the same order as the variation from sample to sample. Fits to Br-treated and Cl control samples were also inconclusive. Thus, it is not possible to establish or rule out direct ligation of Cl to Mn in the OEC with these studies.

Table of Contents

Chapter 1

Introduction to Photosynthesis and the Oxygen Evolving Complex

Chapter 2

Determination of Mosaic Spread in Oriented Photosystem II Particles from Signal II EPR Measurements

Chapter 3

Oriented EXAFS: Studies of PS II in the S_2 State

Chapter 4
Structural Changes in PS II as a Result of Treatment with Ammonia: EPR and XAS Studies

Chapter 5

Studies of Halide Binding to Mn: Cl K-edge and Mn EXAFS of Mn-Cl Model Compounds and Mn EXAFS of Oriented Br-Treated Photosystem II

List of Abbreviations

ATP	adenosine triphosphate
Chl	chlorophyll
Cyt	cytochrome
dbm	dibenzoylmethane
EDTA	ethylenediamine tetraacetic acid
EPR	electron paramagnetic resonance
ESEEM	electron spin echo envelope modulation
EXAFS	extended x-ray absorption fine structure
Hepes	4-(2- hydroxyethyl)-1-piperazineethanesulfonic acid
HOMO	highest occupied molecular orbital
HP	high potential
IP	intermediate potential
kDa	kilo Daltons
LCAO	linear combination of atmic orbitals
LHC I	light harvesting complex I
LHC II	light harvesting complex II
LP	low potential
MES	4-morpholineethanesulfonic acid
NADP	nicotinamide adenine dinucleotide phosphate
NSLS	National Synchrotron Light Source
OEC	oxygen evolving complex
Phe	pheophytin
PPBQ	phenyl-*p*-benzoquinone
PS I	photosystem I
PS II	photosystem II
py	pyridine
SALPN	1,3-bis(salicylideneiminato)propane
SSRL	Stanford Synchrotron Radiation Laboratory
XAS	x-ray absorption spectroscopy

Acknowledgments

Here, in the place which is reserved for expressing our thanks, I would first like to express gratitude for being alive, in such a beautiful place.

At Calvin Lab, I have appreciated the guidance and friendship of Ken Sauer. He has always encouraged me to be what I am and to pursue my own goals, including bringing my love of teaching into these graduate years. He has not tried to force me into a role which does not fit, someone's idealized version of a scientist, and I appreciate that. Mel Klein has been an inspiring scientific leader, very interested in science, and open to new exploration. Both he and Ken are good role models in that they are very involved in life; they do not live with tunnel vision, and they do careful, thoroughly contemplated research. They have encouraged their graduate students to grow as scientists by treating them as colleagues rather than as students. I would like to express warm gratitude to Vittal Yachandra, who has been patient enough to show me details of how to perform the work, and also how to write about it. He has been demanding and exacting - he does not spoon-feed, as he would say, but encourages us to find it in ourselves to do the best science that we can. I have also really enjoyed getting down to the basics and discussing science with colleagues, and working as part of a team. I am also proud to be part of a legacy which has involved excellent science and exciting new discoveries.

I would like to thank my lab-mates. They are a nice bunch of people, compassionate and also smart. Special thanks among my colleagues goes to Annette, whose presence and support has gotten me through long nights of EPR and beamline. It's also imperative to thank the rest of the people who have helped to collect the data in this dissertation. I literally could not have done it without you, as sometimes family commitments kept me away from the beamline entirely. So, thank you Roehl, Matthew, Wen, Theo, Gary and Henk. This work is definitely a group effort. I have also enjoyed the friendship and company of Mary, Jana, Shelley and Aimee, who have helped to make the lab a fun, human place. I would also like to thank Maria for her friendship, encouragement and humorous perspective on the business of being a graduate student. Humor has amazing healing power.

I would like to thank Ishita Mukerji and Holger Dau for their help and earlier work on oriented PS II. Michael Wemple of Georges Christou's group at the Indiana University, and Neil Law of Vincent Pecoraro's group at the University of Michigan, have shown wonderful initiative in supplying us with model compounds. I would also like to thank the faculty at California State University, Hayward, for their support, inspiration and friendship.

I would like to thank some special friends, who have encouraged me to nurture what is at the very core: Steven, Cathy, Rob, Cecilia, Carol, Andrea, and many others. Special thanks goes to Steven, who has pointed the way to what is most essential and simple, and who has encouraged me to find what I needed to complete this work. They have all inspired me by being brave enough to live life from what they truly are, whenever they can. Thanks, guys.

I would like to express thanks to my family - to grandparents, who have helped me to make time for retreat, so essential in keeping a busy life in perspective. To Lennie, who encouraged me to be a scientist in a very real, practical way, and who also was a kind and generous benefactor to my family. To my siblings, especially Janet and Jill - all a part of life; so different, yet sharing a common thread. We are mirrors for eachother, helping to show eachother different aspects of life. To my children Maxwell and Janine, delights of my life, who are wonderful people to grow with. And to my Mom who, by her own example, showed that a woman can raise a family and live an inspired, satisfying life. And most of all, to my husband Floyd, who has been my anchor and support, and best friend. I don't know how this could have been possible without you.

Dedicated to Nature:

for whom all of this is quite simple.

Chapter 1:

Introduction to Photosynthesis and the Oxygen Evolving Complex

If you want to know what water is you need science, and the scientist needs a laboratory. In the laboratory there are various ways in which to study what water is. Thus it is possible to know what kind of elements water has, the various forms it takes, and its nature. But it is impossible thereby to know water itself. Shunryu Suzuki, **Zen Mind, Beginner's Mind**
(Walker/Weatherhill, New York, 1970)

Life is wondrous. Plants, which are relatively low on the evolutionary scale, are able to harness photons of light and, through a series of charge transfer reactions, convert water and carbon dioxide to stored food. As a byproduct of the process they perform the feat of splitting water into hydrogen ions, electrons and the oxygen that we breathe. Scientists in the laboratory can accomplish this only with tremendous amounts of energy and have come nowhere close to the efficiency and competence that nature achieves. In this study we will address the manner in which plants oxidize water during photosynthesis, with the primary goal of understanding a process which is essential for most of life on earth, and secondarily for its possible applications to generation of energy from the sun.

Photosynthetic Membrane Structure and Function

About 2% of all the sunlight on the earth is captured and stored by photosynthetic organisms (Sauer, 1986). A photon is absorbed by an initial chromophore, usually a chlorophyll (chl) molecule. The electronic excitation is then funneled through antenna molecules into the reaction center, with a very high quantum yield. In oxygenic photosynthesis, which is the focus of this work, the entire process facilitates electron transfer from water in photosystem II (PS II), to reduced ferredoxin and NADPH in photosystem I (PS I) (see Figure 1.1). The electron transfer process has been reviewed for bacterial reaction centers (Friesner & Won, 1989; Giacometti & Carbonera, 1990; Bixon 1992; see articles in Deisenhofer and Norris 1993), and higher plants (Melis 1991;

Nechushtai 1992; Witt 1991) but will be summarized here. In thylakoid membranes PS II, cytochrome b_6f, PS I and ATP synthase act in a concerted manner to produce a strong oxidant (PS II) to oxidize water on the lumenal side, and a strong reductant to reduce $NADP^+$ on the stromal side. The membrane potential and proton gradient produced in this process, which is driven by light absorption by PS I and PS II, facilitates the production of ATP by ATP synthase.

Photosystem I

The structure and symmetry of PS I have been reviewed by Lagoutte & Mathis (1989). PS I has at its core a 84 kDa heterodimer that contains non-covalently bound P_{700} (a chl dimer), two electron acceptors A_0 (chl a monomer) and A_1 (phylloquinone, or Vitamin K1), and the primary 4Fe-4S iron-sulfur cluster F_X. ·Approximately 100 Chl are associated with the core. A cysteine-rich 9 kDa protein contains the 4Fe-4S clusters F_A and F_B. There are also extrinsic proteins associated with PS I ranging in size from 9 to 22 kDa, which are probably involved in interactions with ferredoxin and plastocyanin (Lagoutte & Mathis, 1989). There are also proteins which range from 22-29 kDa that are involved with the antenna complexes.

Upon photoexcitation P_{700}, which has an oxidation potential of ~0.5 V (reviewed in Golbeck 1987) donates electrons to A_0, which then transfers the electron to A_1 and on to the iron-sulfur proteins F_X, F_B and F_A. Electrons are transferred to ferredoxin on the stromal surface of PS I, which eventually reduces $NADP^+$ (Pschorn et al., 1988). The accessory light-harvesting antennae for PS I, Light Harvesting Complex I (LHC I), contain 80 - 120 chl a and chl b in a chl a / chl b ratio of about 3.5:1.

Photosystem II

PS II is found mainly in the grana of the thylakoid membranes, with less than 30% residing in the stroma-exposed thylakoids. The composition and function of PS II have been reviewed by Melis (1991), Debus (1992), and Vermaas (1993). All of the electron transfer components of PS II reside on the D1 and D2 proteins, which are heterodimers of

32 and 34 kDa, respectively (Nanba & Satoh, 1987). The D1/D2 heterodimer helps to stabilize the 4 Mn on the lumenal side of the thylakoid. Each contains one tyrosine: Y_Z on D1, which acts as an intermediate in electron transport, and Y_D on D2, which has a much lower redox potential than Y_Z (Vass & Styring 1991) and forms a stable radical. Tyrosine Y_D can donate electrons to PS II, but it does not play an active role in electron transfer. The Y_D^+ radical is discussed further in Chapter 2. The role of the Y_D^+ and Y_Z^+ radicals in PS II is reviewed by Barry (1993). Although there is structural symmetry, the function is asymmetric. The electron transfer path is from Mn (on D1 and D2) to Y_Z to P_{680}, a monomeric chl with high oxidation potential of ~1.1 V (Jursinic & Govindjee 1977), and Pheophytin (Phe) (all on D1), then to Q_A (a plastoquinone on D2) and on to Q_B (secondary quinone acceptor on D1). Closely associated with the reaction center is cytochrome b_{559} (cyt b_{559}), which consists of 2 polypeptides of 9 kDa and 4 kDa, with a b-type heme bound by histidine ligands (Cramer et al., 1986). There may also be a secondary electron transfer cycle involving cyt b_{559}, rather than reduction of plastoquinone (Arnon & Tang, 1988). There are three extrinsic proteins, of 33, 23 and 17 kDa associated with PS II (reviewed by Coleman, 1990) which play a role in the stability of the Mn and regulation of Ca^{2+} and Cl^- binding. Ca^{2+} and Cl^- are cofactors which are required for oxygen evolution (reviewed by Ghanotakis & Yocum, 1990; Debus 1992; & Rutherford 1992; for Cl^-: Coleman 1990; and Homann, 1987). They are thought to stabilize the structure of the oxygen evolving complex and, in the case of Cl^-, to neutralize charge accumulation by the OEC. Cl^- can be replaced by Br^- with retention of nearly full activity (Coleman 1990; Homann 1987; Sandusky & Yocum 1983 and 1986; DeRose 1990), but oxygen evolution is inhibited by replacement with F^- (Coleman 1990; Homann 1987). The role of chloride in PS II is discussed in Chapter 5.

Other polypeptides associated with PS II are a 10 kDa protein which undergoes phosphorylation and dephosphorylation which is regulated by the plastoquinone pool, and others whose function are not known at present. The light harvesting complex associated with PS II (LHC II) contains approximately 200 chl (a+b) of the 250 chl associated with PS II. The PS II reaction center, consisting of D1, D2, Cyt b_{559} and the 33 kDa extrinsic polypeptide, plus two antenna proteins CP47 and CP43 constitute the PS II core. Approximately 37 chl are associated with the core complex. A typical PS II preparation contains the core complex plus the extrinsic 17, 24 and 33 kDa polypeptides (Berthold et al., 1981). In spinach and other higher plants, the ratio of PS II to PS I is about 1.8, although this ratio varies with the quality of light. The organism adjusts synthesis of either photosystem to balance the absorption of light to maintain a high quantum efficiency (Chow et al., 1990).

The Oxygen Evolving Complex: Spectroscopic Methods and Current Model

The oxygen evolving complex (OEC) has been recently reviewed by Debus (1992), Ghanotakis & Yocum (1990), Klein et al. (1993); Pistorius (1993), Renger (1993); Rutherford (1992) and Sauer et al. (1992). Oxidation of water by the OEC does not occur in a single step. The stepwise accumulation of four positive charges on the oxidizing side of PS II is necessary for the oxidation of $2H_2O$ (reviewed by Joliot & Kok, 1975), and the release of 4 electrons, 4 protons and one molecule of O_2: $2H_2O \longrightarrow 4e^- + 4H^+ + O_2$. Kok et al. (1970) found that, upon a series of flashes, oxygen is released upon every fourth flash. The cycle that was proposed, called the Kok cycle, is depicted in Figure 1.2. The subscripts on the S-states S_0 to S_4 refer to the number of oxidizing equivalents accumulated by the OEC. It has been established that 4 protons are released during the O_2 evolution cycle (reviewed in Debus 1992). However, it is unclear what the pattern of release is for the four S-state transitions. Lübbers et al. (1993) found that the pattern of proton release is 1:1:1:1 from reaction center core preparations, and approximately 0.5:1:1.5:1 in thylakoid preparations. The proton release pattern also varied with pH. Their conclusion was that the pattern of measured proton release from the membrane is highly dependent on the chemical environment of the proton; release can be delayed by proton interaction with amino acids and other species in the membrane.

When PS II is dark-adapted, S_1 is the predominant state: reduced tyrosine YD causes a rapid decay of S_2 and S_3 to S_1, and oxidized YD slowly converts S_0 to S_1 (Messinger et al. 1993). S_2 and S_3 also exhibit slower decay paths to S_1 via interaction with the acceptor side of PS II. After a photon is absorbed by dark-adapted PS II, the S_2 state is formed. This state has a characteristic 16-20 line multiline electron paramagnetic resonance (EPR) spectrum, discovered by Dismukes and Siderer (1981), which is due to magnetic interaction between the Mn atoms. Upon acceptance of two successive additional photons, the S_3 state is formed, and then the S_4 state, which spontaneously releases O_2 with a return to S_0. Water is thought to bind either during the S_3 or S_4 states, with possible peroxo bond formation in the S_3 state (Renger 1993). The two peroxo oxygens are then released as molecular O_2 during the S_4 to S_0 transition.

Electron Paramagnetic Resonance

One way in which the components of PS II can be studied is with EPR spectroscopy (reviewed by Miller & Brudvig, 1991). EPR signals arise from unpaired electrons, and hyperfine interactions arise from coupling between nuclear spins with electron spins. The signal for the dark-adapted S_1 state can be detected only with parallel-polarization EPR (Dexheimer & Klein 1992), but upon absorption of one flash of light or upon continuous illumination at 195 K, the S_2 state is formed. The EPR multiline spectrum from this state is thought to arise from a $S = 1/2$ ground state configuration (Britt et al. 1992). Upon illumination of S_1 at 140 K, a $g = 4.1$ signal is seen, which is thought to arise from an $S = 5/2$ configuration of the S_2 state (Haddy et al. 1992). It is possible that some rearrangement which alters the exchange coupling must occur in the structure to convert from the configuration which produces the $g = 4.1$ signal to the state which produces the multiline signal. This would be thermodynamically unfavorable at 140 K, but occurs readily during 195 K illumination. Differences in the structure of the S_2 states produced upon 140 K illumination vs. 195 K illumination have been studied by Liang et al. (1994). The EPR of PS II is further discussed in Chapter 2.

X-ray Absorption Spectroscopy

X-ray absorption spectroscopy (XAS) has also been a fruitful method for studying the structure of the OEC. This method is described in detail in Koningsberger & Prins (1988). X-ray absorption spectra are named after the Bohr atomic level of the electron which is excited. Thus, K-shell XAS arises from excitation and photoionization of a 1s electron from the absorbing atom. A sample Mn K-edge is shown in Figure 1.3. The pre-edge and edge regions of the spectrum arise from transitions of the excited electron to atomic and molecular orbitals on the absorbing atom, and are subject to electric dipole selection rules. The pre-edge is due to a dipole-forbidden 1s-3d transition, which becomes allowed due to mixing of orbitals of p-character with the d-orbitals. Ligand XAS can give information on the degree of covalence between ligand and metal based on the intensity of these pre-edge transitions. XAS of Cl ligands bound to Mn will be discussed briefly in Chapter 5. The edge region is due to the dipole-allowed s-p transitions, and the edge position is dependent on the charge density of these bound states. Thus, XAS edge spectra can give information on the oxidation state and ligand environment of the absorbing atom.

Extended X-ray absorption fine structure (EXAFS) arises from interaction of the photoionized electron with electrons or nearby atoms. The photoelectron wave interacts with neighboring atoms, and the backscattered waves interfere with the outgoing wave creating an interference pattern. This information can be deconvoluted into information on the number, type and distance of backscattering atoms about the absorbing atom. In the case of the Mn tetramer in the OEC, the information obtained from EXAFS is an average for the four Mn absorbing atoms.

An advantage to the use of XAS for the study of PS II is that it is element-specific. We take advantage of the fact that Mn is rare in plants, and is present in PS II preparations only in the OEC . Care is taken to wash free Mn from the preparation before measurement. Thus, information on the oxidation state and environment of the Mn atoms can be obtained despite the fact that they are surrounded by lipids, proteins, and chromophores. Electrons emitted from the Mn K-shell, at about 6550 eV, are fairly well separated from absorption by other atoms found in PS II preparations. Iron does not begin to absorb until about 7100 eV, which gives a workable range wide enough for both Mn K-edge and EXAFS studies.

Oxidation States of Mn in the OEC

The oxidation states of the four Mn in the S_1 state of the OEC have been found to be Mn(III,III, IV,IV) by comparison of Mn K-edges of dark-adapted PS II with spectra of model compounds with known Mn oxidation states (Yachandra 1993). One of the Mn atoms becomes oxidized during the S_1 to S_2 transition, resulting in a Mn(III,IV,IV,IV) configuration for the S_2 state. This is in agreement with the configuration of Mn(III,IV,IV,IV) for the S_2 state based on analyses of the S_2 multiline EPR signal by Kusunoki (1992) and Bittl (1993).

There are several studies which indicate that Mn is not oxidized during the S_2 to S_3 transition, but rather a nearby aromatic residue, possibly histidine, is oxidized. S_3 does not give an EPR signal, but calcium-depleted PS II has an S_3 signal (Boussac et al. 1990). Pulsed EPR has revealed that the S_2 signal is still present in this calcium-depleted S_3 state, but is masked by the interaction of an organic radical (which could be histidine) with manganese (Zimmerman et al. 1993). The application of this information to the normal O_2 cycle is limited, however, because the Ca-depleted sample is not a native PS II preparation. UV spectroscopy of native PS II has shown significant variations in the UV difference spectra for the (S_2 - S_1) vs. (S_3 - S_2) states (Lavergne 1991). This indicates that the changes from S_1 to S_2 are significantly different from those occurring during the S_2 to S_3 transition, and is further evidence that Mn is not oxidized during the S_2 to S_3 transition. However, X-ray absorption spectroscopy results by Ono et al. (1992) have shown nearly equivalent edge jumps from S_1 to S_2 and S_2 to S_3, and they claim that Mn is oxidized during both transitions. Others have found that there is a significant increase in the edge position and changes in the edge shape from S_1 to S_2, but very small changes from S_2 to S_3 (Andrews et al. 1995; Liang 1994). The latter results agree with an earlier XAS study which found very small differences in edge position between the S_2 state and a chemically-induced S_3 state (Guiles et al. 1990a). Thus, S_3 is thought to be in the configuration Mn(III,IV,IV,IV). The S_0 state has been found to have the configuration Mn(II,III,IV,IV) in native PS II (Andrews et al. 1995; Liang 1994) and in S_0* produced by reduction of S_1 with hydroxylamine (Guiles et al. 1990b).

Model for the OEC

EXAFS has also yielded important information on the structure of the OEC (reviewed in Debus 1992; and Sauer et al. 1992; see also DeRose et al. 1994; Mukerji et al. 1994; and Dau et al. 1995). The Fourier transform of the Mn EXAFS of PS II has three main peaks. The first peak corresponds to approximately two O or N ligands per Mn at about 1.8 Å. The second peak has been assigned to at least one Mn-Mn interaction at 2.7 Å per Mn absorber. This distance has been found to occur in model compounds in di-μ-oxo bridged Mn-Mn complexes (Wieghardt, 1989). Based on this information from the first and second peaks and from model compounds, two Mn-Mn di-μ-oxo bridged binuclear units have been included in the Klein/Sauer model for the OEC in Figure 1.4 (Yachandra et al. 1993, Sauer et al. 1992). The third EXAFS peak corresponds to a Mn-Mn interaction, probably mono-μ-oxo bridged, and a Mn-Ca interaction, both at about 3.4 Å (Latimer et al. 1995). EXAFS studies of oriented native PS II (George at al. 1989) and of PS II in which Br^- has replaced Cl^- (DeRose 1990) indicate that the existence of one Cl per 4 Mn cannot be ruled out, but a Cl bridging between two Mn atoms is unlikely (DeRose 1990). Thus Cl is added as a ligand to Mn in the model. Histidine is also added to the model based on ESEEM studies of PS II from *Synechococcus* grown in ^{14}N vs. ^{15}N, which indicate ligation of N to Mn (DeRose 1991). This is a working model -- the arrangement of the components may change as more becomes known about the structure of the OEC.

One way in which we can discover more about the relative orientation of these components is with spectroscopy of oriented PS II. Because the OEC is embedded in the thylakoid membranes, we can orient the membranes in at least one plane. An extensive

EPR study of the components in PS II oriented by drying onto a flat substrate has been done by Rutherford (1985). EPR of oriented PS II is further discussed in Chapter 2. Oriented XAS has also been done on PS II (George et al. 1989, Mukerji et al. 1994, Dau et al. 1995), on cytochrome-c-oxidase (George et al. 1993), and on crystals of plastocyanin (Scott et al. 1982). With oriented XAS, the degeneracy of information from multi-nuclear absorbers can be reduced by selecting for various absorber-backscatterer interactions which lie at specific angles with respect to the membrane normal. XAS of oriented PS II is the subject of Chapters 3, 4 and 5 of this dissertation.

References

Andrews, J. C.; Cinco, R. ; Dau, H.; Latimer, M. J.; Liang, W.; Roelofs, T. A.; Rompel, A.; Sauer, K.; Yachandra, V. K. & Klein, M. P. (1995) *Physica B 208 & 209*, 657-659.

Arnon, D. I. & Tang, G. M.-S. (1988) *Proc. Natl. Acad. Sci. USA 85*, 9524-9528.

Barry, B. A. (1993) *Photochem. Photobiol. 57*, 179-188.

Berthold, D. A.; Babcock, G. T. & Yocum, C. F. (1981) *FEBS Lett. 134*, 231-234.

Bixon, M. (1992) *Israel J. Chem. 32*, 422-427.

Boussac, A.; Zimmerman, J.-L.; Rutherford, A. W. & Lavergne, J. (1990) *Nature (London) 347*, 303-306.

Britt, R. D.; Lorigan, G. A.; Sauer, K.; Klein, M. P. & Zimmerman, J.-L. (1992) *Biochim. Biophys. Acta 1040*, 95-101.

Chow, W.-S.; Melis, A. & Anderson, J. M. (1990) *Proc. Natl. Acad. Sci. USA 87*, 7502-7506.

Coleman, W. J. (1990) *Photosynth. Res. 23*, 1-27.

Dau, H.; Andrews, J. C.; Roelofs, T. A.; Latimer, M. J.; Liang, W.; Yachandra, V. K.; Sauer, K. & Klein, M. P. (1995) *Biochemistry 34,* 5274-5287.

Debus, R. J. (1992) *Biochim. Biophys. Acta 1102*, 269-352.

DeRose, V. J. (1990) Thesis, University of California, Berkeley: *Lawrence Berkeley Laboratory Report LBL-29795* (Univ. of California, Berkeley, 1990)

DeRose, V. J.; Yachandra, V. K.; McDermott, A. E.; Britt, R. D.; Sauer, K. & Klein, M. P. (1991) *Biochemistry 30*, 1335-1341.

DeRose, V. J.; Mukerji, I.; Latimer, M. J.; Yachandra, V. K.; Sauer, K. & Klein, M. P. (1994) *J. Amer. Chem. Soc. 116,* 1335-1341.

Deisenhofer, J. & Norris, J. R. (Eds.) (1993)*The Photosynthetic Reaction Center, Vols. I & II*, Academic Press Inc., San Diego.

Dismukes, G. C. & Siderer, Y. (1981) *Proc. Natl. Acad. Sci. U.S.A. 78*, 274-278.

Friesner, R. A. & Won, Y. (1989) *Photochem. Photobiol. 50*, 831-839.

George, G. N.; Prince, R. C. & Cramer, S. P. (1989) *Science 243*, 789-791.

George, G. N.; Cramer, S. P.; Frey, T. G. & Prince, R. C. (1993) *Biochim. Biophys. Acta 1142*, 240-252.

Ghanotakis, D. F. & Yocum, C. F. (1990) *Annu. Rev. Plant Physiol. Mol. Biol. 41*, 255-276.

Giacometti, G. & Carbonera, D. (1991) in *Ecological Physical Chemistry*, C. Rossia & E. Tiezzi, Eds., Elsevier, Amsterdam, p. 57-65.

Golbeck, J. H. (1987) *Biochim. Biophys. Acta 895*, 167-204.

Guiles, R. D.; Zimmerman, J.-L.; McDermott, A. E.; Yachandra, V. K.; Cole, J. L.; Dexheimer, S. L.; Britt, R. D.; Wieghardt, K.; Bossek, U.; Sauer, K. & Klein, M. P. (1990a) *Biochemistry 29*, 471-485.

Guiles, R. D.; Yachandra, V. K.; McDermott, A. E.; Cole, J. L.; Dexheimer, S. L.; Britt, R. D.; Sauer, K. & Klein, M. P. (1990b) *Biochemistry 29*, 486-496.

Haddy, A.; Dunham, W. R.; Sands, R. H. & Aasa, R. (1992) *Biochim. Biophys. Acta 1099*, 25-30.

Homann, P. H. (1987) *J. Bioenerg. Biomembr. 19*, 105-123.

Joliot, P. & Kok, B. (1975) in *Bioenergetics of Photosynthesis* (Govindjee, Ed.), Academic Press, New York, pp. 387-412.

Jursinic, P. & Govindjee (1985) *Photochem. Photobiol. 26*, 617-628.

Klein, M. P.; Sauer, K. & Yachandra, V. K. (1993) *Photosynth. Res. 38*, 265-277.

Kok, B.; Forbush, B. & McGloin, M. (1970) *Photochem. Photobiol. 11*, 457-475.

Koningsberger, D. C. & Prins, R., Ed. (1988) *X-ray Absorption: Principles, Application, Techniques of EXAFS, SEXAFS and XANES,* John Wiley & Sons, New York.

Lagoutte, B. & Mathis, P. (1989) *Photochem. Photobiol. 49*, 833-844.

Latimer, M. J.; DeRose, V. J.; Mukerji, I.; Yachandra, V. K.; Sauer, K. & Klein, M. P. (1995) *Biochemistry*, in press.

Lavergne, J. (1991) *Biochim. Biophys. Acta 1060*, 175-188.

Liang, W.; Latimer, M. J.; Dau, H.; Roelofs, T. A.; Yachandra, V. K.; Sauer, K. & Klein, M. P. (1994) *Biochemistry 33*, 4923-4932.

Liang, W. (1994b) Ph.D. Dissertation, University of California, Berkeley, *Lawrence Berkeley Laboratory Report LBL-36632*.

Lübbers, K.; Haumann, M. & Junge, W. (1993) *Biochim. Biophys. Acta 1183*, 210-214.

Melis, A. (1991) *Biochim. Biophys. Acta 1058*, 87-106.

Messinger, J.; Schröder, W. P. & Renger, G. (1993) *Biochemistry 32,* 7658-7668.

Miller, A. -F. & Brudvig, G. W. (1991) *Biochim. Biophys. Acta 1056*, 1-18.

Mukerji, I.; Andrews, J. C.; DeRose, V. J.; Latimer, M. J.; Yachandra, V. K.; Sauer, K. & Klein, M. P. (1994) *Biochemistry 33*, 9712-9721.

Nanba, O. & Satoh, K. (1987) *Proc. Natl. Acad. Sci. USA 84*, 109-112.

Nechushtai, R. (1992) *Israel J. Chem. 32*, 441-448.

Ono, T.; Noguchi, T.; Inoue, Y.; Kusunoki, M.; Matsushita, T. & Oyanagi, H. (1992) *Science 258*, 1335-1337.

Pistorius, E. K. (1993) *Physiologia Plantarum 87*, 624-631.

Pschorn, R.; Rühle, W. & Wild, A. (1988) *Photosynth. Res. 17*, 217-229.

Renger, G. (1993) *Photosynth. Res. 38*, 229-247.

Rutherford, A. W.; Zimmerman, J.-L., & Boussac, A. (1992) in *The Photosystems: Structure, Function and Molecular Biology* (Barber, J., Ed.) Elsevier, Amsterdam, pp. 179-229.

Rutherford, A. W. (1985) *Biochim. Biophys. Acta 807*, 189-201.

Sandusky, P. O. & Yocum, C. F. (1983) *FEBS Lett. 162*, 339-343

Sandusky, P. O. & Yocum, C. F. (1986) *Biochim. Biophys. Acta 849*, 85-93.

Sauer, K. (1986) in *Encyclopedia of Plant Physiology, Vol. 19*, Springer-Verlag, pp. 85-97.

Sauer, K.; Yachandra, V. K.; Britt, R. D. & Klein, M. P. (1992) in *Manganese Redox Enzymes,* (V. L. Pecoraro, Ed.), VCH Publishers, New York, 141-175.

Scott, R. A.; Hahn, J. E.; Doniach, S.; Freeman, H. C. & Hodgson, K. O. (1982) *J. Am. Chem. Soc. 104*, 5364-5369.

Vass, I. & Styring, S. (1991) *Biochemistry 30*, 830-839.

Vermaas, W. F. J.; Styring, S.,;Schröder, W. P. & Andersson, B. (1993) *Photosynth. Res. 38*, 249-263.

Wieghardt, K. (1989) *Angew. Chemie, Int. Ed. Eng. 28*, 1153-1172.

Witt, H. T. (1991) *Photosynth. Res. 29*, 55-77.

Yachandra, V. K.; DeRose, V. J.,;Latimer, M. J.; Mukerji, I.; Sauer, K. & Klein, M. P. (1993) *Science 260*, 675-679.

Zimmerman, J.-L.; Boussac, A. & Rutherford, A. W. (1993) *Biochemistry 32*, 4831-4841.

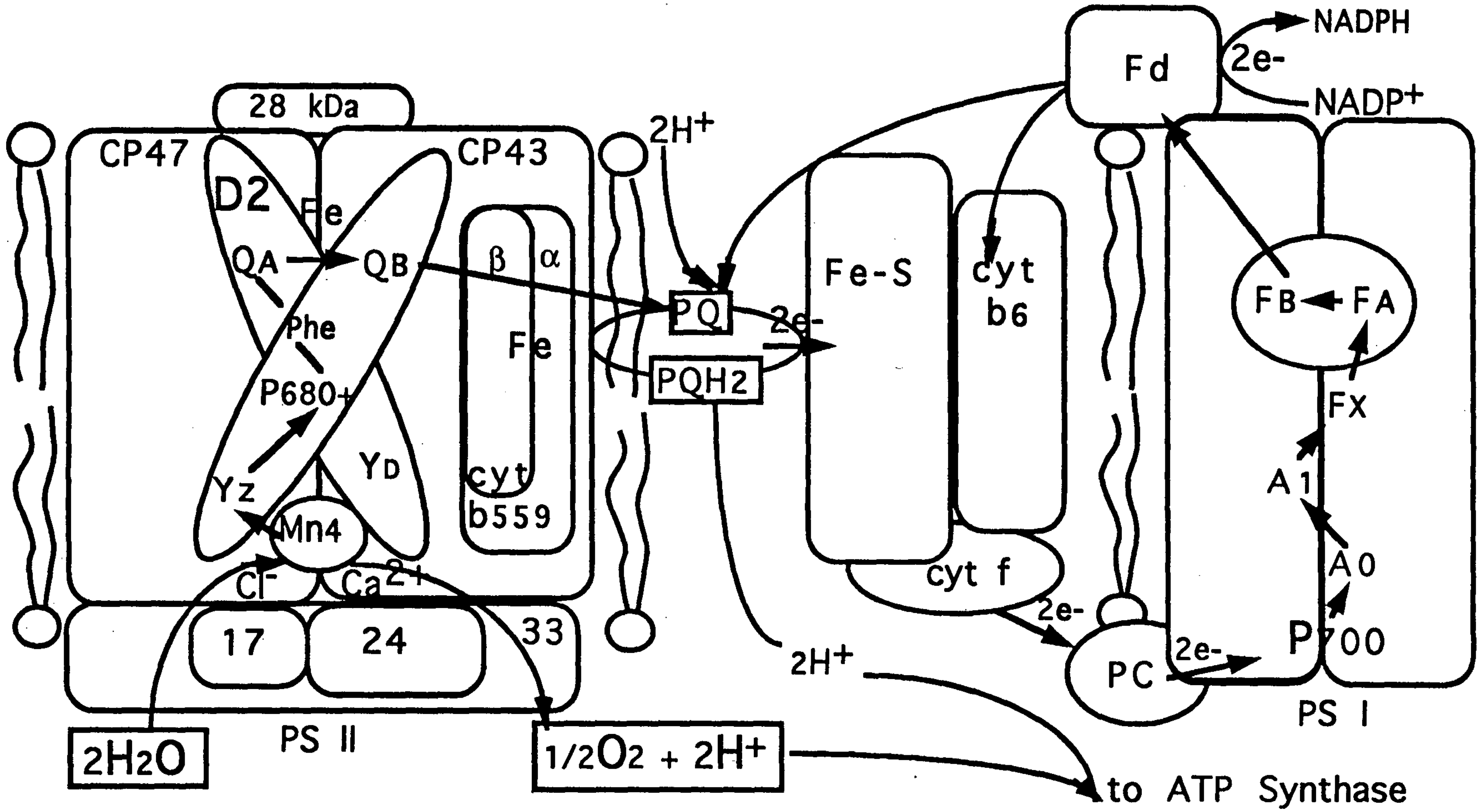

Figure 1.1: Electron transfer pathway in higher plants. In PS I light is absorbed by P700, initiating electron transfer to A_0, A_1, F_X, F_A, F_B and ferredoxin (Fd), which facilitates reduction of $NADP^+$ to NADPH. In PS II, light is absorbed by P680. $P680^+$ donates electrons to pheophytin (Phe), Q_A, and Q_B, which is replenished by the plastoquinone (PQ) pool. Electrons are transferred from the PQ pool through the cytochrome b_6f complex to plastocyanin, which donates electrons to P700. Electron donation to $P680^+$ is from Yz, which receives electrons from the Mn-containing oxygen-evolving complex (OEC). Protons shuttled across the membrane via the PQ pool, and produced by the OEC, are used by ATP synthase in the production of ATP.

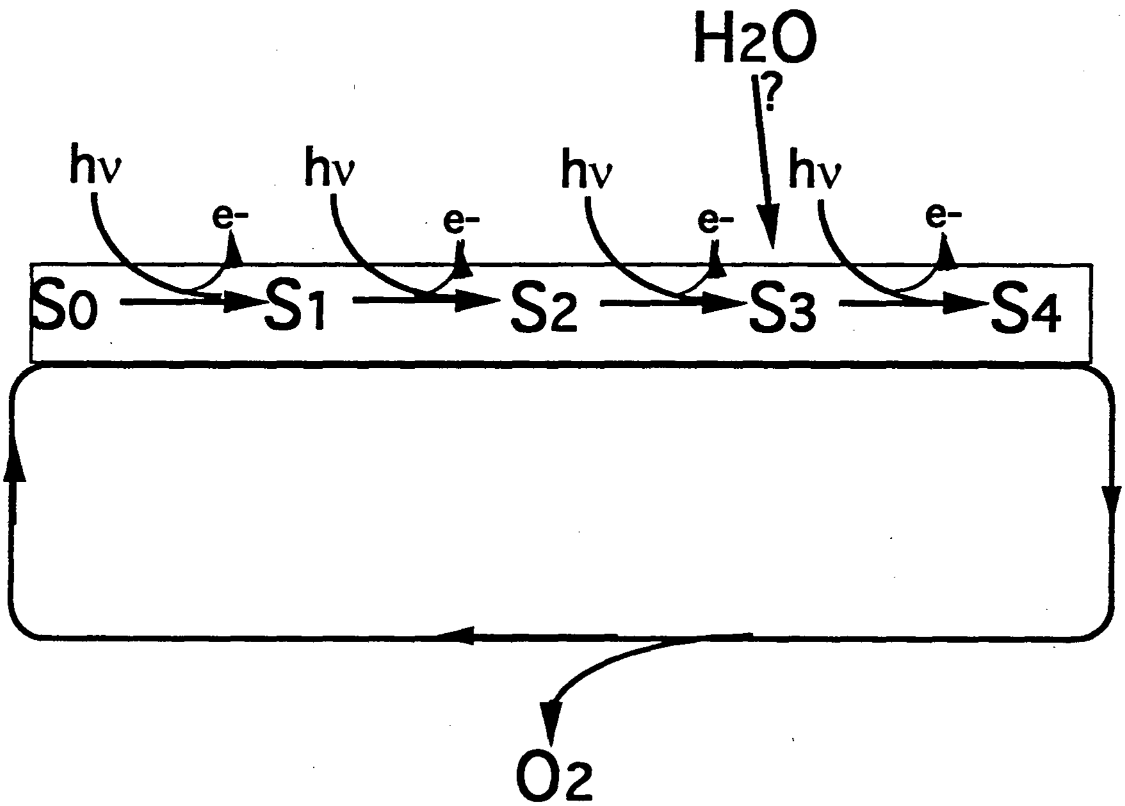

Figure 1.2: The Kok Cycle. The Mn Oxygen-evolving complex accumulates four oxidizing equivalents upon the stepwise absorbance of photons, from the S-states S0 through S4. Water binds to the OEC at either the S2 or the S3 state. Upon absorbance of a photon by S3, oxygen is released and the OEC spontaneously returns to S0, its most reduced state.

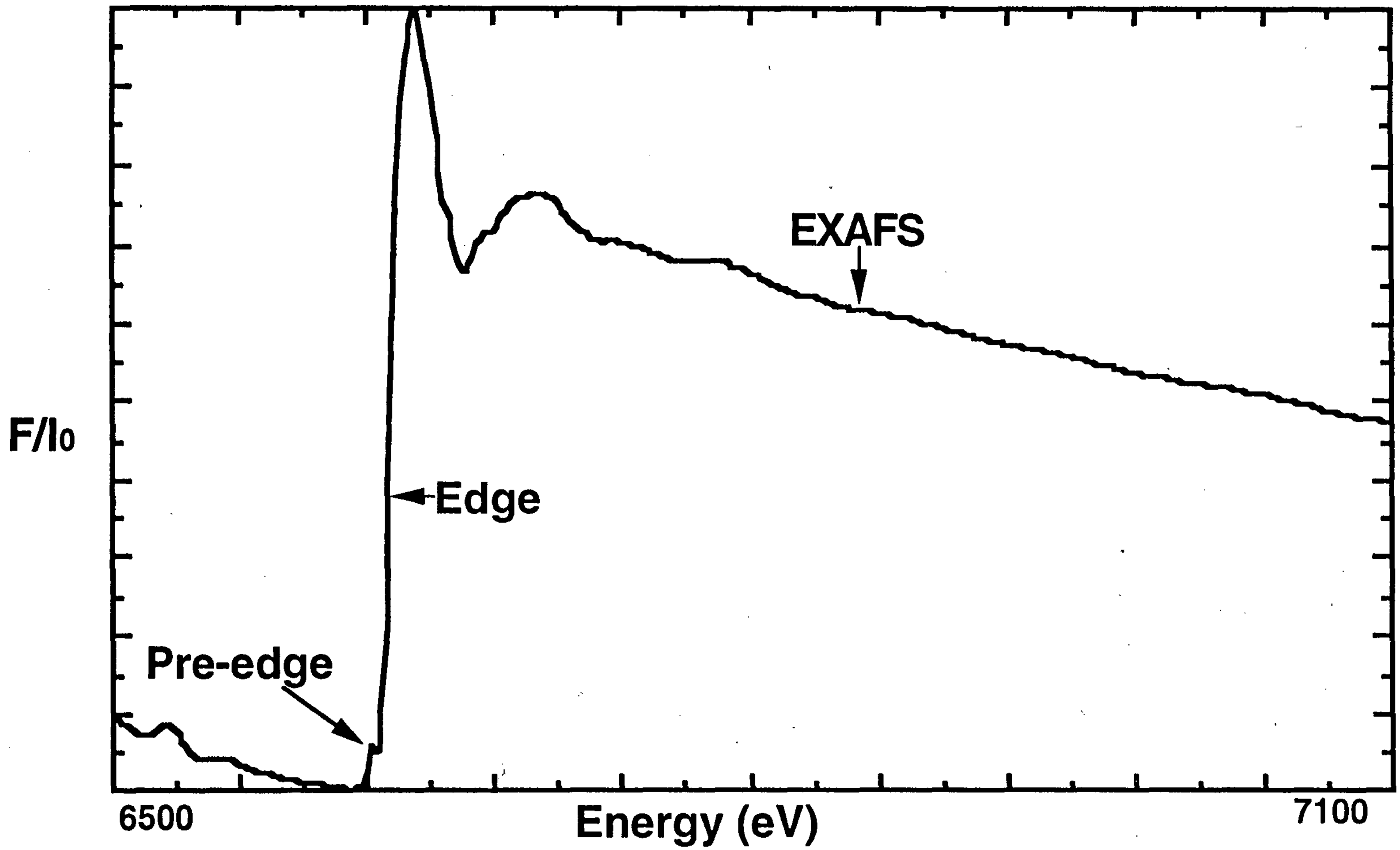

Figure 1.3: Mn K-edge of PS II, measured as fluorescence divided by the incoming beam intensity, F/I0. The pre-edge and edge regions are bound-state transitions, subject to dipole selection rules. The pre-edge is due to dipole-forbidden 1s-3d transitions, which become allowed due to mixing of d-orbitals with orbitals of p-character. The edge region is governed by s-p transitions. The EXAFS region is due to interference of the photoionized electron wave vector with backscattered waves from the surrounding atoms.

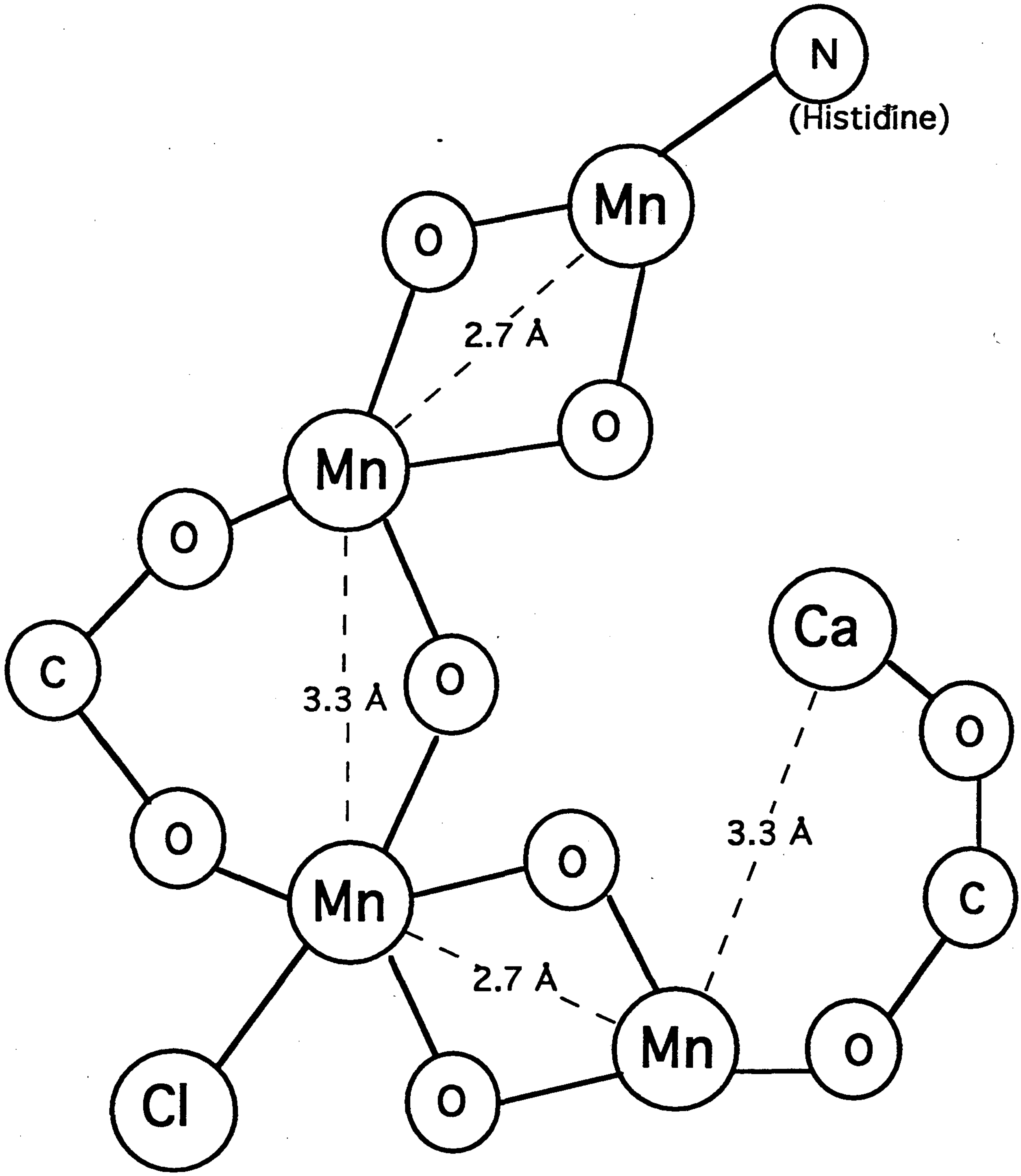

Figure 1.4: Klein/Sauer working model for the OEC. The four Mn atoms are arranged as two di-μ-oxo bridged binuclear units joined by a mono-μ-oxo bridge. Histidine, Cl and carboxylato-bridged Ca are added as ligands to Mn. Carboxylato bridges are proposed to be due to binding with amino acids. The arrangement of these components may be different from that drawn.

Chapter 2:

Determination of Mosaic Spread in Oriented Photosystem II Particles from Signal II EPR Measurements

Introduction

Electron paramagnetic resonance spectroscopy (EPR) is suitable for the study of various components in the electron transport network in photosynthesis, because EPR signals arise due to unpaired electrons. For texts on EPR, see Knowles et al. (1976); Poole (1983); and Wertz & Bolton (1986). EPR of the components of photosynthesis has been reviewed by Miller & Brudvig (1991) and Hoff (1987). EPR has also been done on oriented species of PS II (reviewed by Rutherford 1985). The spectroscopic study of oriented components can yield insight into the electron transfer between them, which is affected by their relative orientation and distance.

There are various methods for the orientation of biological membranes. The use of magnetic fields (Dismukes et al., 1984; Geacintov et al., 1972) and viscous flow methods such as stretching or compression of a gel (Dismukes & Sauer 1978) allow control of the ambient potential and pH of a sample. Orientation can also be achieved by painting and slow drying of a substance. This method has been used by many researchers (Blum et al. 1978a,b; Kim et al. 1992; Salerno et al. 1979), and it is the method used for orientation of Photosystem II (PS II) particles from spinach in this report. When orientation is achieved by drying, the membranes lie flat in the plane of the mylar. They are randomly oriented in the plane of the tape, but the membrane normal lies perpendicular to the tape plane. Thus, orientation of vectors relative to the membrane normal can be obtained from these oriented samples.

The orientation of a sample can be detected by various methods, including linear dichroism (Breton 1974; Vermeglio et al. 1980), absorbance-detected magnetic resonance (van der Vos et al. 1992) and EPR (e.g. Dismukes et al. 1978; Kim et al. 1992; Prince et al. 1980; Rutherford 1985; Salerno et al. 1979). The magnitude of the first derivative of the EPR spectrum is at a maximum when the magnetic field is parallel to the axis of the paramagnetic center. The orientation dependence of various components of PS II has been studied using EPR (reviewed in Miller & Brudvig 1991; Rutherford 1985). Information obtained from studies of the orientation of PS II components has helped in understanding the path of energy transfer. These paths have been described extensively (reviewed in Debus 1992).

There is disorder in an oriented sample, also called mosaic spread, due to variation either in the angle between the membrane and the mylar (due to inhomogeneous painting or drying of the sample), between the proteins and the membranes ("stacking disorder"), or between chromophore and protein ("chromophore disorder") (Salerno et al. 1979). In the absence of disorder, or mosaic spread, the g values of the spectrum change as the angle between the magnetic field **H** and the sample is changed. Disorder in a sample causes the g-values to remain constant at the principal g-values. As mosaic spread increases further, the powder spectrum is obtained.

The Tyrosine Y_D^+ EPR Signal

The role of tyrosine and other redox-active amino acids in PS II has been recently reviewed by Barry (1993). The Signal II "slow" EPR spectrum is produced by a photooxidized tyrosine radical, Y_D^+ (Barry & Babcock, 1987), which has been identified as tyrosine 160 on the D2 protein of PS II in *Synechocystis* (Debus et al. 1988; Vermaas et al. 1988). Upon dark adaptation of PS II, those centers which had been in the S_0 state (about 25%) reduce Y_D^+ upon advancement to S_1: $S_0Y_D^+ \rightarrow S_1Y_D$. Y_D can donate electrons to the Mn cluster in the oxygen evolving complex (OEC), but the pathway is much slower than for donation by the tyrosine Y_Z (Miller & Brudvig, 1991), and does not play a major role in the evolution of oxygen (Debus et al. 1988; Vermaas et al. 1988). Y_D^+ can be produced in about 100% of the centers by illumination at 273 K and trapping at 77 K. This signal has constant lineshape from 10 K to room temperature (Nishi et al.

1980), but it saturates easily at low temperature (Styring & Rutherford 1988).

The EPR spectrum of Y_D^+ as measured at X-band (9 GHz) is centered at about g = 2.0046 (Barry & Babcock 1987) in unoriented samples, and in oriented samples (see Fig 2.4) it varies from g=2.0032 with the membrane normal at 0° with respect to the magnetic field to g= 2.0061 at 90° (Rutherford 1985). The Y_D^+ spectrum at X-band is dominated by hyperfine interaction between electron spin and neighboring protons. In EPR studies of oriented preparations, the intensities of the hyperfine couplings were found to be 1:3:3:1 (O'Malley et al. 1984), suggestive of 3 protons with similar hyperfine coupling constants (O'Malley et al. 1984). The protons involved were found to be two ring protons and one methylene proton. The g-anisotropy of the Y_D^+ signal can be better resolved at high magnetic field strengths (the corresponding microwave frequencies are 100-250 GHz) (Gerfen et al. 1993; Gulin et al. 1992; Un et al. 1994). The g-anisotropy is dependent on the orientation of the tyrosine molecule with respect to the magnetic field, and so it can yield information on the effect of the orientation of Y_D^+ on the electron transfer process. The g-values for the tyrosine radical are quite dependent on the surrounding protein matrix, as different values have been found in vitro (Barry et al. 1990; Gulin et al. 1992) vs. in vivo (Gerfen et al. 1993; Un et al. 1994). Un et al. (1994) have found using high-field studies of oriented PS II that the phenyl ring plane of Y_D^+ lies an angle of 65 - 75° with respect to the membrane.

We have found that for oriented PS II, measurement of Signal II can provide a quantitative determination of the uniformity of orientation of a sample. If a sample is well oriented, the ratio of the height of the first low field peak measured at 90° (membrane normal with respect to the magnetic field) to the amplitude of this same peak measured at 0° will be between 3:1 and 5:1. We call this ratio the "Signal II ratio".

Cytochrome b559⁺ EPR Signal

Another EPR signal which reflects the degree of orientation of a sample is that of cytochrome-b559 (cyt b559). The structure and function of cyt b559 has been recently reviewed by Cramer et al. (1993). Cyt b559 consists of either one (Buser et al. 1992) or two (Cramer et al. 1986; Erixon & Butler 1971; Takehashi & Asada, 1989) heterodimers of alpha and beta proteins, with a hexacoordinate heme iron coordinated to a histidine residue on each protein. It exists in at least three forms: high (375 - 430 mV) potential (HP), intermediate (170-230 mV) potential (IP), and low (5 -80 mV) potential (LP) (Ahmad et al. 1993; Cramer & Whitmarsh 1977; Galvan et al. 1983; Thompson et al. 1989). The HP and LP forms have different g-values: $g_z = 3.08$ vs. 2.94 and $g_y = 2.16$ vs. 2.26, respectively, with g_x fairly constant at 1.56 (Bergström & Vänngård 1982; Crowder et al. 1982; Hootkins & Bearden 1983; Rutherford 1985). This shift in g-values has been interpreted as arising due to changes in the geometry of the two axial histidine imidazole rings from a parallel configuration in HP cyt b559 to a perpendicular arrangement in LP cyt b559 (Babcock et al. 1985). Both the HP and LP forms of cyt b559 have been found to have the same orientation with respect to the membrane normal (Bergström & Vänngård 1982). In whole chloroplasts, approximately 2/3 of the cyt b559 is in the HP form, and 1/3 is in the LP form. It converts completely and irreversibly to LP when the membrane system is severely distressed and distorted in conditions such as heat, sonication, high pH, or detergent/chemical treatments (Bendall et al. 1971; Cramer et al. 1971; Ortega et al. 1992), and in PS II which is under repair (Tae et al. 1993). Conversion between the HP and LP forms has slow kinetics, and therefore probably does not contribute to the main electron transport chain (Cramer et al. 1979). The exact role of cyt b559 in PS II is unknown. It may play a role in electron transfer on the oxidizing side of PS II (Knaff & Arnon 1969) or in the assembly of the oxygen evolving complex (Cramer et al. 1986). It is also thought that since cyt b559 can be reduced as well as oxidized by PS II, it may possibly play a protective role against photoinhibition (Buser et al. 1992; Canaani et al. 1990; Galvan et al. 1982; Heber at al. 1979; Thompson et al. 1988).

Rutherford found that for cyt $b559^+$ in an oriented PS II sample, the g_z peak was at a maximum with the magnetic field **H** parallel to the membrane plane ($\omega = 0°$) and the g_y

peak was at a maximum with **H** perpendicular to the membrane plane ($\omega = 90°$) (Rutherford 1985). Based on this information and on previous work (Bergström & Vänngård 1982; Crowder et al. 1982; Hootkins & Bearden 1983) it was proposed that the cytochrome heme plane is perpendicular to the membrane surface.

Cyt $b559^+$ can be used to determine the mosaic spread, or gaussian distribution of orientation about a single vector, of PS II samples. It does not have hyperfine features, and simulation is straightforward. Using an algorithm written by Blum et al. (1978b), it is possible to generate EPR spectra and examine differences in the spectra due to variation in the angle of the sample with respect to the magnetic field (ω) and in the degree of disorder (Ω). By comparison of these curves with EPR spectra generated at various ω values, the mosaic spread Ω can be determined. The above method has been used to determine mosaic spread for iron-sulfur complexes (Blum et al. 1980; Hootkins & Bearden 1983; Prince et al. 1980; Salerno et al. 1979), and for cytochrome c-oxidase (Blum et al. 1978a,b).

The algorithm of Blum et al. has been used in this lab to write a FORTRAN program to generate curves of g_y and g_z amplitudes vs. ω for various mosaic spread values for cyt $b559^+$. These simulations were compared with EPR measurements of oriented spinach PS II particles to determine the best match to mosaic spread. These values were then compared to a ratio of the height of the first peak of Signal II taken at 90° vs. 0°. The Signal II ratio versus mosaic spread relationship obtained from this comparison can be used to determine the mosaic spread in PS II using the spectra of Signal II alone. The two measurements of Signal II (at 90° and 0°) required for this determination are simple compared with the 24 measurements required to obtain a pattern of cyt $b559^+$ versus magnetic field angle, which must subsequently be compared with simulations to determine mosaic spread. Another advantage of using the Signal II measurements is that it can be done at room temperature, vs. 20 K for cyt $b559^+$.

Materials and Methods

PS II particles were prepared as previously described (Berthold et al. 1981). The membranes were resuspended in 50 mM MES, pH = 6.0 buffer containing 0.4 M sucrose and 5 mM $CaCl_2$ and pelleted by centrifugation at 4°C (39,000 g; 1h). One or two drops of 50 mM MES buffer were added to the pellet and the resulting paste was painted onto mylar tape. The PS II membranes were slowly dried under a stream of cold N_2 gas at 4°C in the dark, as previously described (Rutherford 1985). This process was repeated 5-7 times, with the drying time starting at 10 mins for the first layer and increasing by 10 mins with each successive layer. X-band EPR spectroscopy was performed with a Varian E-109 spectrometer, a standard TE_{102} cavity and an Air Products liquid helium cryostat. Both Signal II and cyt $b559^+$ were measured at 20 K. For Signal II measurements samples were dark-adapted for 30 min. at 4° C. Dark-adapted samples were used because the intensity of the signal increases by a factor of 40 after illumination, and shows less resolution of individual peaks. The approximate 0° sample position was found with the oscilloscope, such that the cavity dip moves to the lowest frequency. Fine adjustments to the angle were made to obtain a minimum amplitude of the first low-field peak. This is necessary because Chl also generates a large signal at g=2. This first low-field peak was chosen as convenient for measurement of the dichroism of Signal II measured at 0° and 90° because a baseline can be drawn next to it, providing a more accurate measurement of peak amplitude. The ratio of the amplitudes of this peak measured at 90° and 0° was called the "Signal II ratio".

After illumination at 77 K for 6 min, the cyt $b559^+$ signal was measured every 15° from 0° to 360°. A goniometer was used to set the angle between the membrane normal and the magnetic field. The mosaic spread was determined by comparison of the height of the g_y peak of cyt $b559^+$ (normalized relative to the height at 90°) with simulations of oriented cyt $b559^+$ with various mosaic spread values, which were generated as described under Results. A fit parameter was determined by a sum of the data minus simulation values squared, divided by the number of data points. The simulation which yielded the lowest fit parameter was determined to be the mosaic spread for the sample.

Results

Simulation of cyt b559^{+} EPR Spectra

Using an algorithm by Blum et al. (1978b), a FORTRAN program was written to produce a series of simulations by systematically varying both the angle ω with respect to the magnetic field **H** and the mosaic spread Ω. The simulation program was first checked by reproducing the results of Blum et al. for cytochrome c-oxidase (Blum et al. 1978a). Simulation of the cyt b559^{+} powder spectrum was done using g-values $g_x = 1.54$, $g_y = 2.22$ and $g_z = 2.97$ from Rutherford (1985). These g-values are between those of HP and LP cyt b559, but because the HP and LP forms are oriented the same with respect to the membrane normal (Bergström & Vänngård 1982), they do not require separate simulations. A diagram of the angles used to describe sample orientation and mosaic spread is given in Fig. 2.1.

According to Blum et al., the orientation of a g tensor is given by

$$g^2 = g_x^2 l_x^2 + g_y^2 l_y^2 + g_z^2 l_z^2 \qquad (2.1)$$

where l_x, l_y and l_z are the direction cosines of the principal axes g_x, g_y and g_z, respectively:

$$\begin{aligned} l_x &= \cos\omega' \sin\theta\cos\phi + \sin\omega' (\sin\alpha\sin\phi - \cos\alpha\cos\theta\cos\phi), \\ l_y &= \cos\omega' \sin\theta\sin\phi - \sin\omega' (\sin\alpha\cos\phi + \cos\alpha\cos\theta\sin\phi), \qquad (2.2) \\ l_z &= \cos\omega' \cos\theta + \sin\omega' \cos\alpha\sin\theta \end{aligned}$$

Integration is done over a sphere with $\alpha = 0$ to 360°, and magnetic field angle $\omega' = 0°$ to 180° (see Fig. 2.1B), and θ and ϕ are the angles between g_x and the x axis, and g_y and the projection of the membrane normal on the xy plane, respectively, as shown in Fig. 2.1A. Angles $\theta = 90°$ and $\phi = 90°$ were used for the orientation of the g_x, g_y and g_z axes based on the findings of Rutherford (1985) that the cyt b559 heme is perpendicular to the membrane. The transition probability g_p is given by

$$2g^3 g_p = g_x^2 g_y^2 (1 - l_z^2) + g_y^2 g_z^2 (1 - l_x^2) + g_z^2 g_x^2 (1 - l_y^2) \qquad (2.3)$$

and the orientation-dependent lineshape is given as

$$\Delta H^2 = \Delta H_x^2 l_x^2 + \Delta H_y^2 l_y^2 + \Delta H_z^2 l_z^2 \qquad (2.4)$$

where ΔH_x, ΔH_y and ΔH_z are the linewidths. Linewidths were obtained by comparison of the simulations with a powder spectrum of cyt b559$^+$. Mosaic spread is accounted for by weighting the spectrum at a given angle ω' from the membrane normal by a factor W, where

$$W = \Omega^{-1} \exp[-\ln 2 \cdot (\omega')^2 / \Omega^2]. \qquad (2.5)$$

Using the parameters θ, ϕ, ω, Ω, g_x, g_y, g_z, ΔH_x = 185 G, ΔH_y = 60 G, ΔH_z = 80 G and microwave frequency ν = 9.215 GHz, spectra were simulated for Ω = 15° to 45° in 2.5° intervals. As seen in Fig. 2.2, as mosaic spread increases, there is less variation in the spectra as the magnetic field angle ω varies from 0° to 90°. The powder pattern is obtained for all ω when the mosaic spread is infinite. The amplitudes of the g_y peaks of these simulations were normalized with respect to the g_y amplitude at 90° for each set of simulations (ω = 0° to 90°) with a given mosaic spread. These values are presented in Table 2.1. As can be seen in Fig. 2.3, a plot for g_y vs. ω has a very steep increase with ω for low mosaic spread (A: 20°) and decreases as mosaic spread increases (B: 30° and C: 40°).

EPR Spectra of Signal II and Cyt b559

Oriented PS II samples were dark adapted, and EPR spectra of Signal II were taken at 0° and 90° for the membrane normal with respect to the magnetic field. Typical spectra for Signal II are given in Fig. 2.4. A straight line was drawn through the baseline of the spectrum, as shown in the figure, and the height of the first peak was measured at 90° (A) and 0° (B). The ratio of these heights (the "Signal II ratio") was then noted.

After illumination of the sample at 77 K, the cyt b559$^+$ spectrum was taken. The g_z peak was maximum at 0° and the g_y peak was maximum at 90°, as reported by

Rutherford (1985). The changes in the g_y amplitude were much more pronounced and consistent than those in the g_z amplitude, so the g_y amplitudes were used for the determination of mosaic spread. The g_y peaks were measured and normalized with respect to the g_y amplitude at 90°. These normalized curves were compared with those from simulations at various Ω values until the best fit using least squares analysis was found. A comparison of g_y amplitudes for an oriented PS II sample vs. simulated curves for $\Omega = 15°$ (A), 20° (B) and 25° (C) is shown in Fig. 2.5. The best match (a lowest fit value as described in Materials and Methods) for this sample was a mosaic spread of 20°.

The measurement of Signal II ratio and mosaic spread was repeated for samples with various degrees of disorder, and we have generated a plot of Signal II ratio vs. mosaic spread as derived from measurements of cyt b_{559}^{+} (Fig. 2.6). The plot is essentially linear over the region shown, although it may take an asymptotic shape when extended out to higher Signal II ratios. More data are required to determine whether this is the case.

Discussion and Conclusions

In summary, the correlation of mosaic spread with Signal II ratio for oriented PS II particles will serve as a useful timesaving method. Measurement of Signal II at two angles is much quicker than the many measurements required for the determination of mosaic spread from cyt b_{559} measurements. It is also possible to measure Signal II at room temperature, and it may be worthwhile to set up a plot of Signal II vs. mosaic spread for this temperature as well. This would eliminate the need for low-temperature EPR measurement to determine mosaic spread.

Determination of the mosaic spread is an important indication of the quality of orientation of a given sample, and it is necessary for the calculation of absorber-backscatterer vectors from extended X-ray absorption fine structure (EXAFS) data (Dau et al. 1995; George et al. 1989; Mukerji et al. 1994).

Most of the samples in this study had 5 to 7 painted PS II layers and had mosaic

spreads from 25 to 35°. Lower mosaic spreads (17.5° - 20°) were found for thin samples of only three painted layers, in which disorder due to painting is at a minimum. George et al. (1989) found a mosaic spread of 17° for oriented PS II chloroplasts. This low degree of disorder may be possible due to the fact that in whole chloroplasts the thylakoid membranes are still stacked in their natural form. In PS II preparations the thylakoid membrane has been opened with detergent treatment, and the membrane stacking is disturbed.
However, with PS II preparations with mosaic spread of 20° to 30° there is significant dichroism in X-ray absorption edge spectra and EXAFS (Dau et al. 1995; Mukerji et al. 1994).

References

Ahmad, I.; Giorgi, L. B.; Barber, J.; Porter, G. & Klug, D. R. (1993) *Biochim. Biophys. Acta 1143*, 239-242.

Babcock, G. T.; Widger, W. R.; Cramer, W. A.; Oertling, W. A. & Metz, J. G. (1985) *Biochemistry 24*, 3638-3645.

Barry, B. (1993) *Photochem. Photobiol. 57*, 179-188.

Barry, B. A. & Babcock, G. T. (1987) *Proc. Natl. Acad. Sci. USA 84*, 7099-7103.

Barry, B. A.; El-Deeb, M. K.; Sandusky, P. O. & Babcock, G. T. (1990) *J. Biol. Chem. 265*, 20139 - 20143.

Bendall, D. S.; Davenport, H. E.; and Hill, R. (1971) *Methods in Enzymology, Vol. 23* (San Pietro, A., Ed.) Academic Press, New York, p. 327.

Bergström, J. & Vänngård, T. (1982) *Biochim. Biophys. Acta 682*, 452-456.

Berthold, D. A.; Babcock, G. T. & Yocum, C. F. (1981) *FEBS Lett. 134*, 231-234.

Blum, H. I.; Harmon, H. J.; Leigh, J. S.; Salerno, J. C. & Chance, B. (1978a) *Biochim. Biophys. Acta 502*, 1-10.

Blum, H.; Salerno, J. C. & Leigh, J. S., Jr. (1978b) *J. Magnetic Resonance 30*, 385-391.

Blum, H.; Poole, R. K.; & Ohnishi, T. (1980) *Biochem. J. 190*, 385 - 393.

Breton, J. (1974) *Biochem. Biophys. Res. Commun. 59*, 1011.

Buser, C. A.; Diner, B. A. & Brudvig, G. W. (1992) *Biochemistry 31*, 11441-11448.

Canaani, O. & Havaux, M. (1990) *Proc. Natl. Acad. Sci. USA 87*, 9295-9299.

Cramer, W. A.; Fan, H. N. & Böhme, H. (1971) *J. Bioenergetics 2*, 289.

Cramer, W. A.; Tae, G.-S.; Furbacher, P. N. & Böttger, M. (1993) *Physiologia Plantarum 88*, 705-711.

Cramer, W. A.; Theg, S. & Widger, W. R. (1986) *Photosynth. Res. 10*, 393-403.

Cramer, W. A. & Whitmarsh, J. (1977) *Annu. Rev. Plant Physiol . 28*, 133-172.

Cramer, W. A.; Whitmarsh, J. & Horton, P. (1979) in *The Porphyrins, Vol. 7* (Dolphin, D., Ed.) Academic Press, New York, p. 71.

Crowder, M. S.; Prince, R. C. & Bearden, A. J. (1982) *FEBS Lett. 144*, 204-208.

Dau, H.; Andrews, J. C.; Roelofs, T. A.; Latimer, M. J.; Liang, W.; Yachandra, V. K.; Sauer, K. & Klein, M. P. (1995) *Biochemistry 34*, 5274-5287.

Debus, R. J. (1992) *Biochim. Biophys. Acta 1102*, 269-352.

Debus, R. J.; Barry, B. A.; Babcock, G. T. & McIntosh, L. (1988) *Proc. Natl. Acad. Sci. USA 85*, 427-430.

Dismukes, G. C.; Frank, H. A.; Friesner, R. & Sauer, K. (1984) *Biochim. Biophys. Acta 764* , 253-271.

Dismukes, G. C. & Sauer, K. (1978) *Biochim. Biophys. Acta 504*, 431-445.

Erixon, K. & Butler, W. L. (1971) *Biochim. Biophys. Acta 234*, 381.

Galvan, F.; DeLa Rosa, F. F.; Hervas, M. & Losada, M. (1983) *Bioelectrochemistry and Bioenergetics 10*, 413-426.

GGeacintov, N. E.; van Nostrand, F.; Becker, J. F. & Tinkel, J. B. (1972) *Biochim. Biophys. Acta 267*, 65.

George, G. N.; Prince, R. C. & Cramer, S. P.. (1989) *Science 243*, 789-791.

Gerfen, G. J.; Bellew, B. F.; Un, S.; Bollinger, J. M. Jr.; Stubbe, J.; Griffin, R. G. & Singel, D. J. (1993) *J. Am. Chem. Soc. 115*, 6420-6421

ulin, V. I.; Dikanov, S. A.; Tsvetkov, Y. D.; Evelo, R. G. & Hoff, A. J. (1992) *Pure and Appl. Chem. 64*, 903-906.

Heber, U., Kirk, M. R. & Boardman, N. K. (1979) *Biochim. Biophys. Acta 546*, 292-306.

Hoff, A. J. (1987) *New Comprehensive Biochemistry: Photosynthesis* (Amesz, J., ed.), Elsevier, Amsterdam, pp. 97-123.

Hootkins, R. & Bearden, A. (1983) *Biochim. Biophys. Acta 723*, 16-29.

Kim, D. H.; Britt, R. D.; Klein, M. P. & Sauer, K. (1992) *Biochemistry 31*, 541-547.

Knaff, D. B. & Arnon, D. I. (1969) *Proc. Natl. Acad. Sci. USA 63*, 956-962.

Knowles, P. F.; Marsh, D.; & Rattle, H. W. E. (1976) *Magnetic Resonance of Biomolecules*, John Wiley & Sons, New York.

Miller, A.-F. & Brudvig, G. W. (1991) *Biochim. Biophys. Acta 1056,* 1-18.

Mukerji, I.; Andrews, J. C.; DeRose, V. J.; Latimer, M. J.; Yachandra, V. K.; Sauer, K. & Klein, M. P. (1994) *Biochemistry 33*, 9712-9721.

Nishi, N.; Hoff, A. J. & Van der Waals, J. H. (1980) *Biochim. Biophys. Acta 590*, 74-88.

O'Malley, P. J.; Babcock, G. T. & Prince, R. C. (1984) *Biochim. Biophys. Acta 766*, 283-288.

Ortega, J. M.; Hervás, M. & Losada, M. (1992) in *Research in Photosynthesis, Vol. II* (Murata, N., Ed.), Kluwer, Netherlands, pp. 697 -700.

Poole, C. P., Jr. (1983) *Electron Spin Resonance*, John Wiley & Sons, New York.

Prince, R. C.; Crowder, M. S. & Bearden, A. J. (1980) *Biochim. Biophys. Acta 592*, 323-337.

Rutherford, A. W. (1985) *Biochim. Biophys. Acta 807*, 189-201.

Salerno, J. C.; Blum, H. & Ohnishi, T. (1979) *Biochim. Biophys. Acta 547*, 270-281.

Styring, S. & Rutherford, A. W. (1988) *Biochemistry 27*, 4915-4923.

Tae, G.-S.; Everly, P. M.; Cramer, W. A.; Madgwick, S. A. & Rich, P. R. (1993) *Photosynth. Res. 36*, 141-146.

Takehashi, M. & Asada, K. (1989) *Plant Cell Physiol. 30*, 915-921.

Thompson, L. K. & Brudvig, G. W. (1988) *Biochemistry 27*, 6653-6658.

Thompson, L. K.; Miller, A.; Buser, C. A.; de Paula, J. C. & Brudvig, G. W. (1989) *Biochemistry 28*, 8048-8056.

Un, S.; Brunel, L.-C.; Brill, T. M.; Zimmerman, J.-L. & Rutherford, A. W. (1994) *Proc. Natl. Acad. Sci. USA 91*, 5262-5266.

van der Vos, R; van Leeuwen, P. J.; Braun, P. & Hoff, A. J. (1992) *Biochim. Biophys.*

Acta 1140, 184-198.

Vermaas, W. F. J.; Rutherford, A. W. & Hansson, Ö. (1988) *Proc. Natl. Acad. Sci. USA 85*, 8477-8481.

Vermeglio, A.; Breton, J.; Barouch, Y & Clayton, R. K. (1980) *Biochim. Biophys. Acta 593,* 299-311.

Wertz, J. E. & Bolton, J. R. (1986) *Electron Spin Resonance,* Chapman and Hall, New York.

Table 2.1: Normalized g_y amplitudes for simulations at Ω = 15° to 47.5°

angle	Ω = 15°	20°	25°	30°	35°	40°	45°
ω =							
0°	.00	.00	.00	.00	.00	.00	.19
15°	.00	.00	.00	.01	.00	.11	.18
30°	.00	.00	.00	.06	.18	.27	.36
45°	.00	.00	.19	.32	.42	.50	.59
60°	.44	.46	.57	.67	.73	.78	.82
75°	1.0	.97	.97	.97	.98	.98	.98
90°	.80	1.0	1.0	1.0	1.0	1.0	1.0

	Ω = 17.5°	22.5°	27.5°	32.5°	37.5°	42.5°	47.5°
ω =							
0°	.00	.00	.00	.00	.00	.05	.10
15°	.00	.00	.00	.03	.08	.14	.22
30°	.00	.00	.05	.13	.22	.31	.40
45°	.00	.00	.24	.37	.47	.55	.62
60°	.43	.52	.62	.70	.76	.80	.84
75°	.47	.96	.97	.97	.98	.98	.98
90°	1.0	1.0	1.0	1.0	1.0	1.0	1.0

Table 2.2: Signal II Ratio and Mosaic Spread Values for Oriented PS II Samples

Signal II Ratio	Mosaic Spread
2.3	37.5°
2.3	42.5°
3.1	27.5°
3.1	32.5°
3.2	30.0°
3.3	27.5°
3.3	27.5°
3.4	27.5°
3.4	27.5°
4.5	20.0°

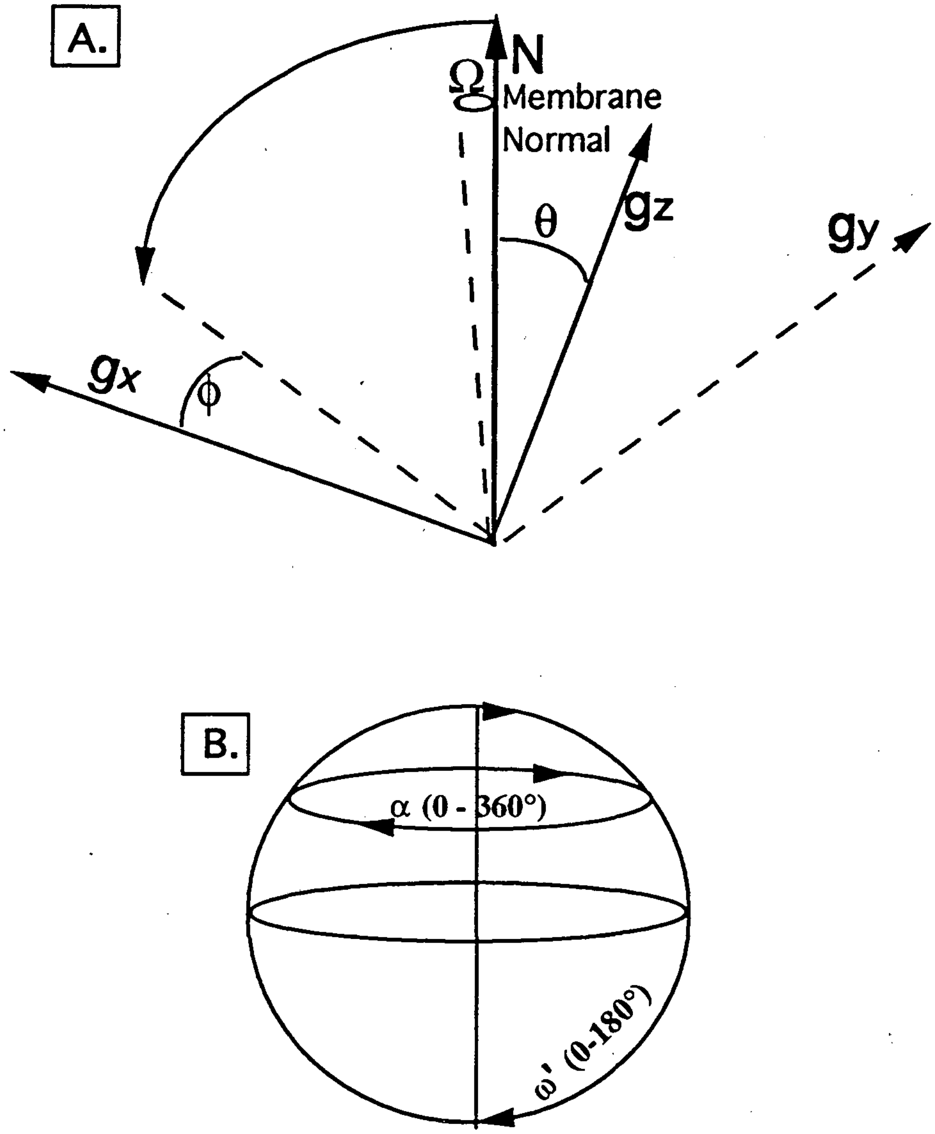

Figure 2.1 Angles used for oriented samples. A: The cone around the membrane normal represents the mosaic spread Ω, or half-width of the gaussian distribution in the orientation of any vector in the sample. θ is the angle between the gz and the membrane normal, and φ is the angle between gx and the projection of **N** on the gxy plane. B: The transition probability is evaluated over a sphere, with $\alpha = 0°$ to 360°and $\omega' = 0°$ to 180°.

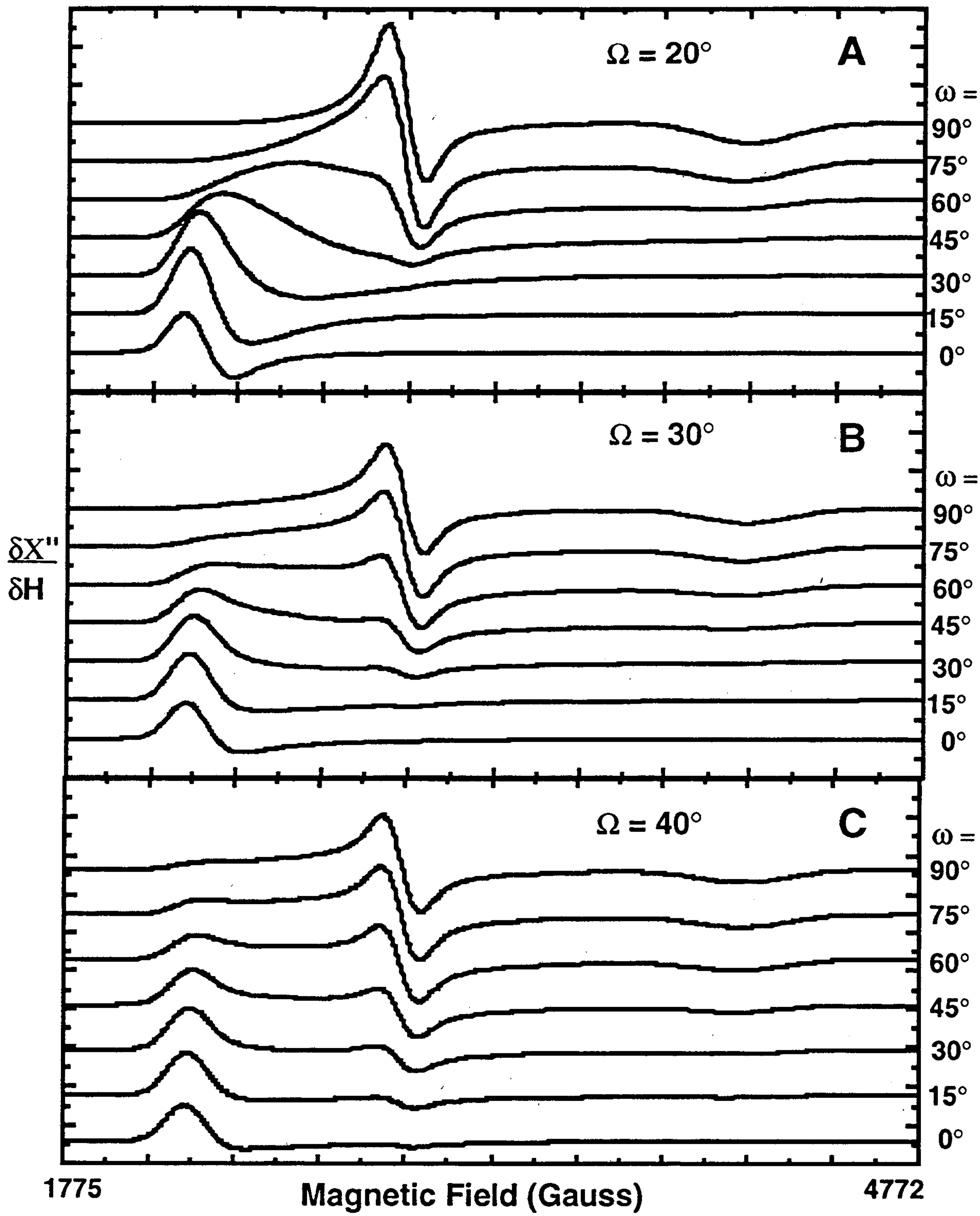

Fig. 2.2 Simulation of cyt b559+ with (A) Ω = 20°; (B) Ω = 30°; (C) Ω = 40°. Simulation parameters were θ = 90°, ϕ = 90°, ω = 0° (bottom) to 90° (top), gx = 1.54, gy = 2.22, gz = 2.97, ΔHx = 185 G, ΔHy = 60 G, ΔHz = 80 G and microwave frequency ν = 9.215 GHz.

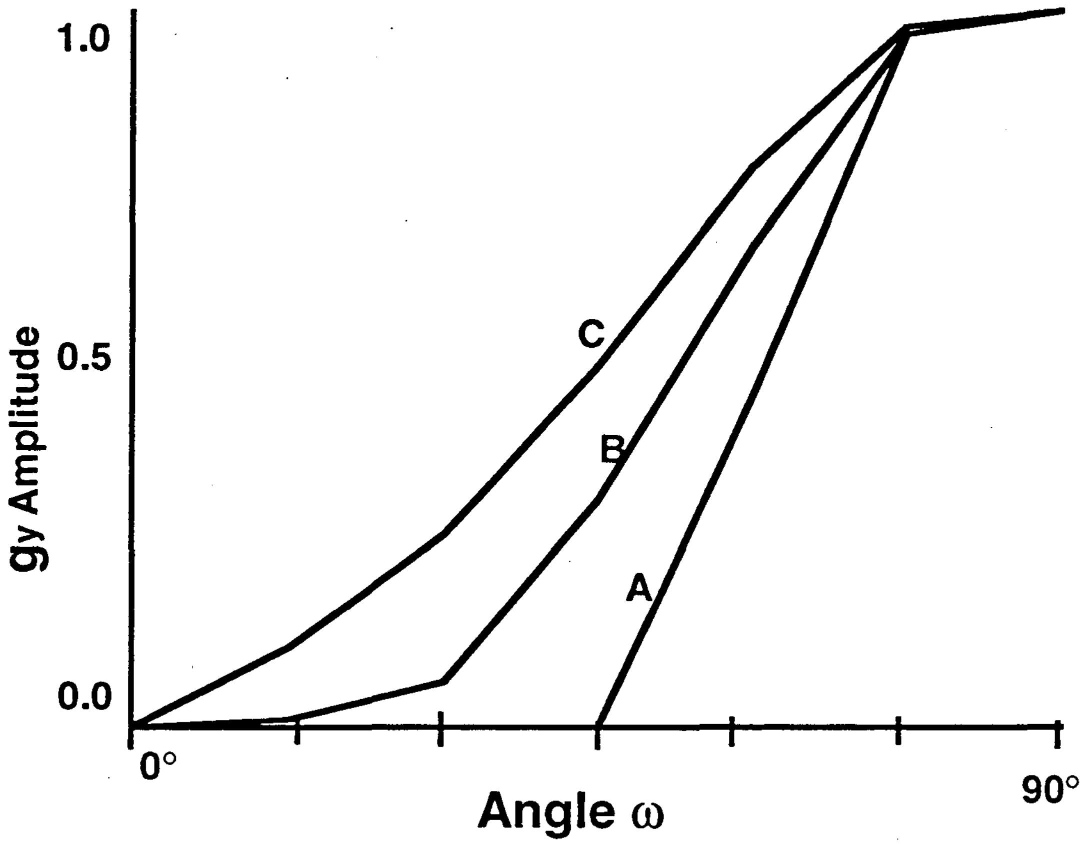

Figure 2.3: Plots of gy amplitude of simulations of cyt b559 vs. magnetic field angle ω for (A) Ω = 20°; (B) Ω = 30° and (C) Ω = 40°.

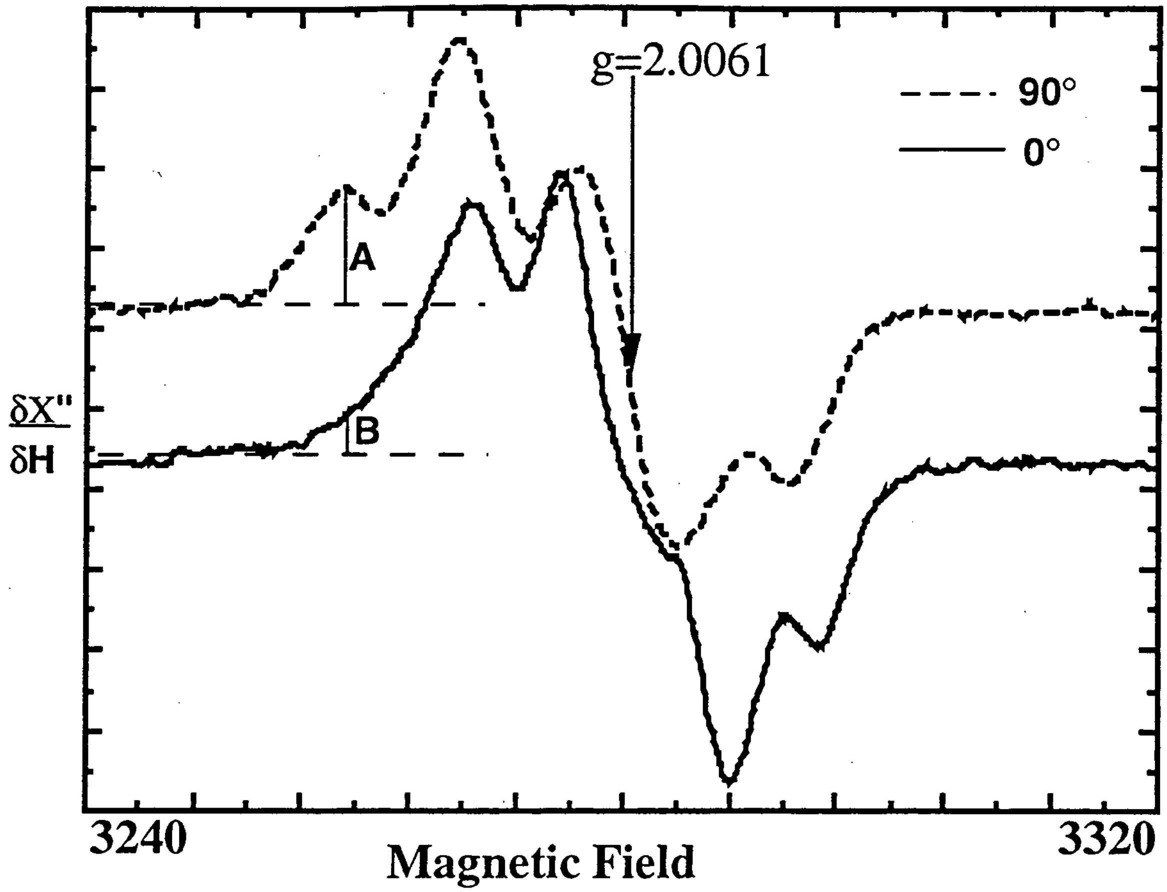

Figure 2.4: EPR spectra of Signal II at ω = 0° (____) and 90° (_ _) between the membrane normal and magnetic field. The ratio of the amplitude of the first peak at 90° (A) vs. 0° (B) is measured ("Signal II Ratio"). Instrument conditions: sample temperature 20 K, microwave power 50 μW, microwave frequency 9.215 GHz, magnetic field modulation frequency 100 kHz, modulation amplitude 2.5 G.

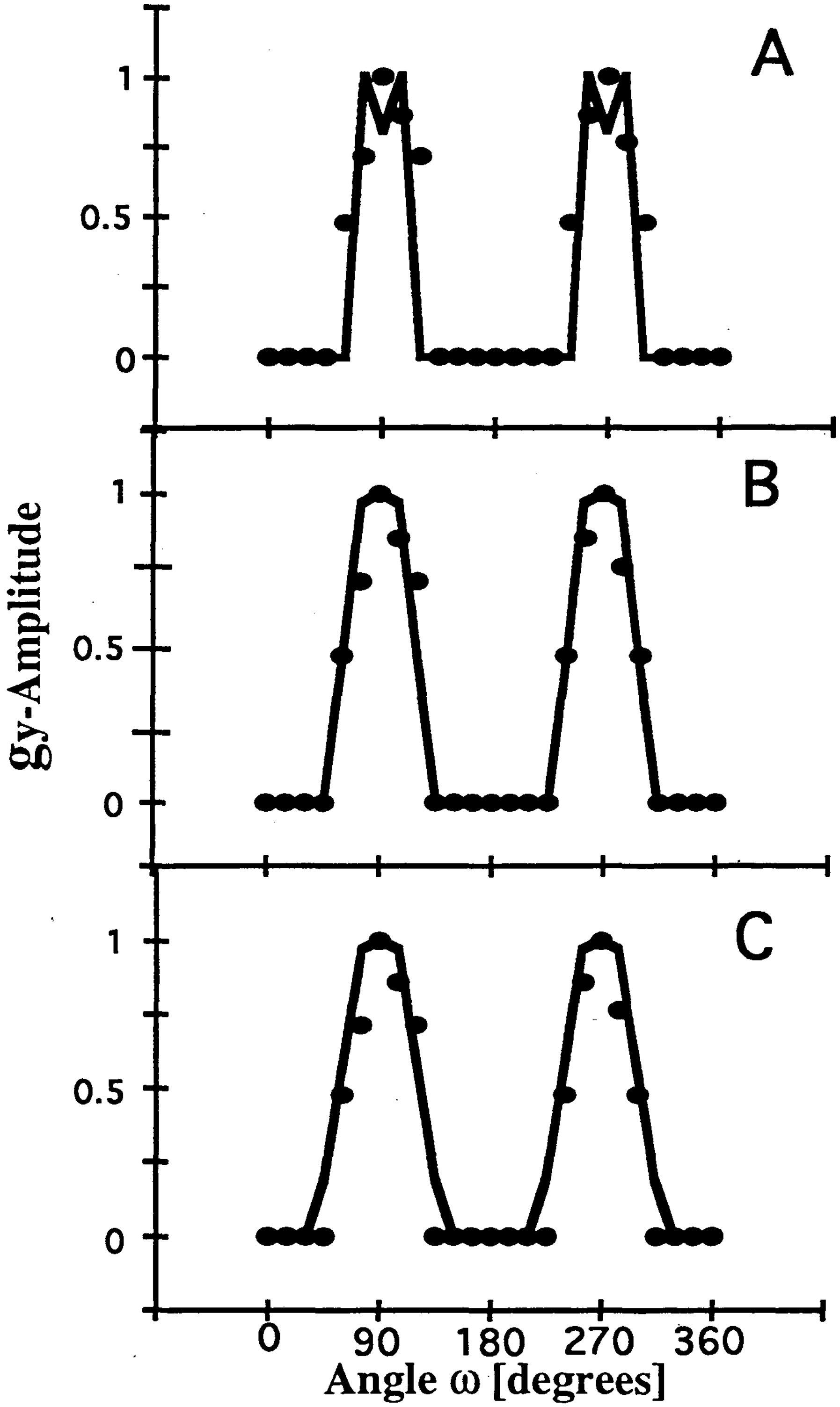

Figure 2.5: Comparison of the normalized height of gy peaks of cyt b559 measured with $\omega = 0°$ to 360°(points) with simulations over the same ω range (lines) at (A) 15°; (B) 20° and (C) 25°. A best fit was found for $\Omega = 20°$.

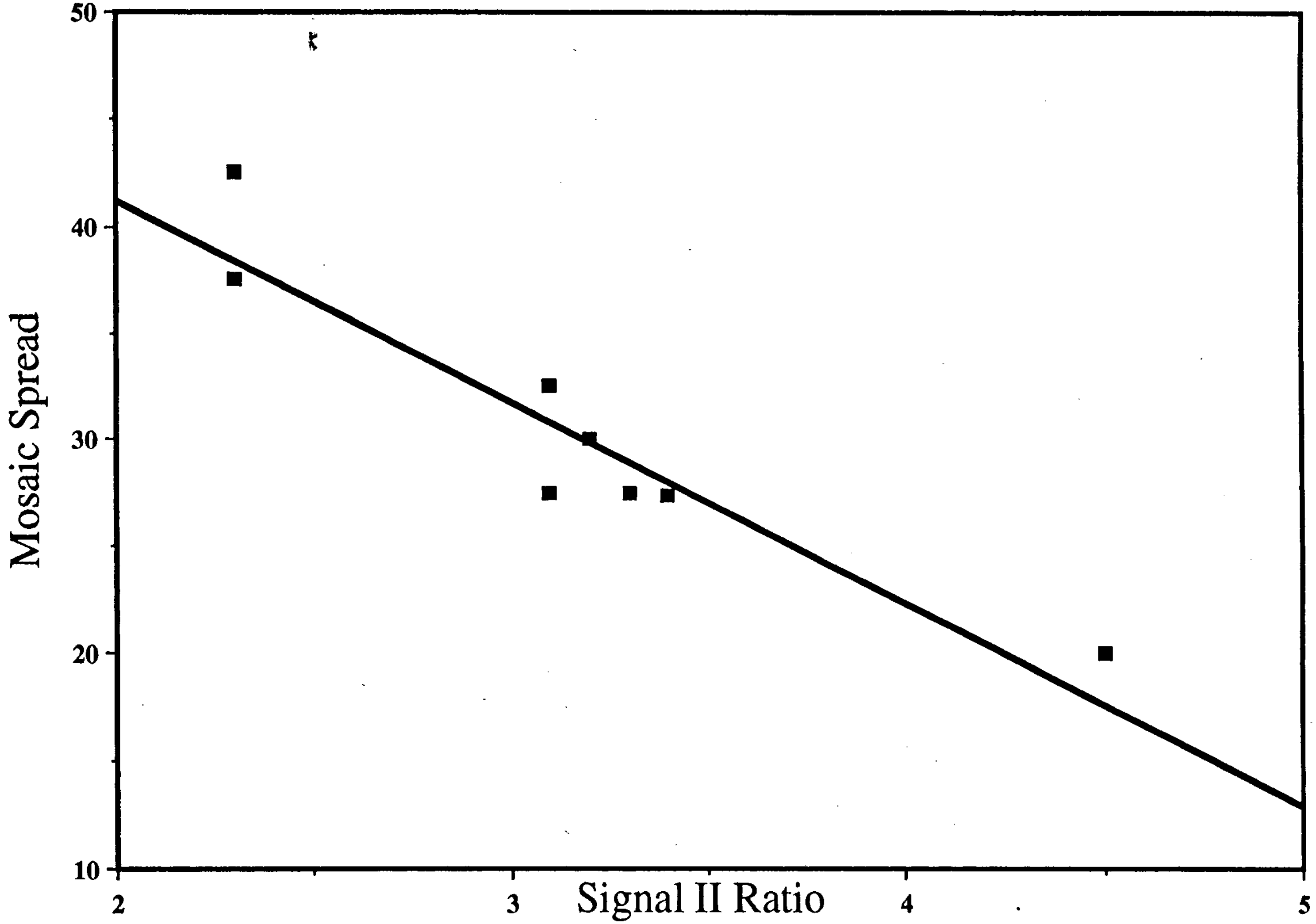

Figure 2.6: Plot of Signal II ratio vs. mosaic spread as derived from cyt b559 measurements for oriented PS II particles.

Chapter 3:

Oriented EXAFS: Studies of PS II in the S_2 state

Introduction

Oriented EXAFS (Extended X-ray Absorption Fine Structure) has been used to obtain structural information for membrane-bound proteins which cannot be obtained from EXAFS of unoriented samples (George et al., 1989; George et al., 1993; Mukerji et al., 1994; Dau et al., 1995). The angle resolution in these studies yields the angles of orientation of given absorber- backscatterer interactions with respect to the membrane normal, and can sometimes resolve vectors which are difficult to detect in a randomly oriented sample. Oriented X-ray Absorption Spectroscopy, as well as Electron Paramagnetic Resonance (EPR) of membrane-bound proteins, can be used to predict the three-dimensional structure of oriented membrane-bound prosthetic groups in proteins even before single crystals are available. They can also help to interpret x-ray crystallographic data.

Theory of Oriented EXAFS

In oriented EXAFS studies, samples which have been oriented (usually by drying) are measured at various angles θ between the membrane normal **N** and x-ray e-vector **E** (see Fig 3.1 for a diagram of the various angles involved in measurement and calculation, and Fig 3.2 for a diagram of an oriented ample and the setup for the oriented XAS experiment). For K-shell EXAFS, the intensity for a particular absorber-backscatterer vector **d** is proportional to $\cos^2\beta$, where β is the angle between the xray field vector **E** and the vector **d**. That is, a particular absorber-backscatterer interaction will be enhanced when β is close to the angle θ of the x-ray e-vector. The EXAFS intensity detected at a given angle θ, relative to the intensity which would be detected in an unoriented sample ($N_{apparent}/N_{isotropic}$) is given by the equation

$$F_{ab}(\theta) = \frac{3\int_{\Phi=0}^{\pi}(\frac{1}{2}\sin^2\theta\sin^2\Phi + \cos^2\theta\cos^2\Phi)P(\Phi)d\Phi}{\int_{\Phi=0}^{\pi}P(\Phi)d\Phi} \quad (3.1)$$

where $P(\Phi) = \sin\Phi \exp[(-\ln 2)(\Phi - \Phi_{ab})^2/\Omega^2]$ is the number of **d** vectors with orientation Φ, Φ_{ab} is the angle between the membrane normal and the absorber-backscatterer vector **d**, and Ω is the mosaic spread, or half-width of the gaussian distribution in Φ_{ab} (described in Chapter 2). A best fit of $N_{apparent}$ $(= F_{ab}(\theta)N_{isotropic})$ vs. θ gives the average orientation $<\Phi_{ab}>$ for a given vector. An average angle is obtained when a vector has two or more components which cannot be resolved due to distances which differ by less than the EXAFS resolution. The equation for the average angle $<\Phi ab>$ of two vectors (1 and 2) is

$$\cos^2<\Phi ab> = \{N_1\cos^2(\Phi_1) + N_2\cos^2(\Phi_2)\} / \{N_1 + N_2)\} \quad (3.2)$$

where $N_{(1,2)}$ is the number of indistinguishable backscatterers for a given vector and $\Phi_{(1,2)}$ is the angle for that vector. The fit to $F_{ab}(\theta)$ also gives a more reliable value for $N_{isotropic}$ than that obtained from unoriented data alone, since it is a global fit.

Materials and Methods

Sample preparation and characterization

PS II particles were prepared as previously described (Berthold et al., 1981). The membranes were resuspended in 50 mM MES, pH = 6.0 buffer containing 0.4 M sucrose and 5 mM $CaCl_2$ and pelleted by centrifugation at 4°C (39,000 g; 1h). One or two drops of the above buffer were added to the pellet, and the resulting paste was painted onto mylar tape. The PS II membranes were dried under a stream of pre-cooled N_2 gas at 4°C in the dark for approximately 1 h as previously described (Rutherford, 1985); however, EDTA was not added. This process was repeated 5-7 times to generate samples with sufficient concentration for x-ray absorption experiments. Orientation of the samples was assessed using X-band EPR spectroscopy performed with a Varian E-109 spectrometer, a standard

TE_{102} cavity and an Air Products liquid helium cryostat. S_2 state samples were prepared by illumination at 195 K for 5-10 min. The mosaic spread values were determined by comparison of EPR measurements of Cyt b_{559} at 15° intervals with simulations (Blum et al., 1978), as described in Chapter 2.

Data Collection and Analysis

X-ray absorption spectra were collected on beamline VII-3 at the Stanford Synchrotron Radiation Laboratory (SSRL). A diagram of the setup is shown in Fig 3.2. X-ray absorption spectra were measured by monitoring the fluorescence excitation spectrum using a 13 element Ge detector (Jaklevic et al., 1977; Cramer et al. 1988). Sample temperature was maintained at 10 K using an Oxford Instruments CF1204 liquid helium flow cryostat. Simultaneous measurement of the x-ray absorption spectrum of $KMnO_4$ provided the energy calibration (Goodin, et al., 1979). The multilayer samples were rotated and spectra were measured as a function of the angle θ between the x-ray **E**-vector and the membrane normal.

Data were treated as previously described (Yachandra et al., 1986; Guiles et al., 1990). A two-domain spline fit to data from ca. 6600 eV to 7100 eV was employed for subtraction of a low frequency background from the data. For a given sample measured at different angles, the EXAFS oscillations were normalized to the same fraction of the edge jump, and identical values were chosen for E_0, the photoionization threshold energy. Uniformity of data analysis is also maintained at other steps, including the transformation of data to *k*-space.

A square windowing function was applied to the Fourier transforms, and back-transformed data were fit to phase and amplitude scattering functions calculated using a curved-wave formalism (McKale et al., 1988). Fits were performed on the back-transformed isolate of the second and third Fourier peaks. The EXAFS function, $\chi(k)$, for each orientation was analyzed by curve-fitting to equation 3.3:

$$\chi(k)=\sum_{b=1}^{n} \frac{N_b F_{ab}(\theta) A_{ab}(k,R_{ab})}{kR_{ab}^2} \exp(-2\,\sigma_{ab}^2 k^2)\sin(2k R_{ab}+\alpha_{ab}(k,R_{ab})) \tag{3.3}$$

where $A_{ab}(k,R_{ab})$ and $\alpha_{ab}(k,R_{ab})$ represent the EXAFS amplitude and phase-shift functions, N_b, the apparent number of b-type backscattering atoms at a mean distance R_{ab} from the absorber atom a, and the wavevector $k = [(2m_e/h^2)(E - E_o)]^{1/2}$, in which m_e is the electron mass, and h is Planck's constant. The damping effect caused by static and thermal disorder is expressed by σ, the Debye-Waller factor. Fits to this equation were done for back-transformed isolates by varying the four fit parameters R_{ab}, N_b $(=F_{ab}(\theta)N_{isotropic})$, $-2\sigma^2$ and ΔE_o.

Error Analysis and Calculation of Vector Angle

The normalized error sum, ϕ, (sum of squared deviations between measured and calculated values) is given by the following equation:

$$\phi = \sum_{i}^{N}(1/s_i^2)(\chi^{exptl}(k_i) - \chi^{theor}(k_i))^2 \tag{3.4}$$

where N is the number of data points and s_i is defined as

$$1/s_i = k_i^3 / \sum_{j}^{N} k_j^3 |\chi_j^{exptl}(k_j)| \tag{3.4a}$$

The ε^2 error is a measure of the 'goodness' of the fit which takes into account the number of free-running fit parameters (p) and the number of independent data points (N_{ind}), as well as the error function ϕ and the total number of data points, $Npts$:

$$\varepsilon^2 = [N_{ind}/(N_{ind} - p)]Npts^{-1}\phi \tag{3.5}$$

The number of independent data points N_{ind} is estimated to be equal to $2\Delta k\Delta R/\pi$, where Δk is the k-range of the data used and ΔR is the width of the Fourier-filtered peak (for further details on equation. 3.5 see Binsted et al., 1992). A positive value for ε^2 indicates that the fit is not underdetermined, because the number of free parameters does not exceed the number of independent data points. Using equations 3.4 and 3.5, best fit values for the four above fit parameters were determined at each orientation. Then the vectors and isotropic coordination numbers were calculated by a best fit of $F_{ab}(\theta)N_{isotropic}$ vs. θ to the data.

Fits to equation 3.1 were done using Mathematica (@ 1991 Wolfram Research Inc.) First, the data points N_b ($=F_{ab}(\theta)\ N_{isotropic}$) vs. θ are plotted, and fit to $\Phi = 0°$, 10°, 20°,...90°. The Φ value which results in the lowest error value for this fit is selected as Φ_{best}. Then fits are done to $\Phi_{best} \pm 10°$ in 2.5° intervals. Plots of the fit angle Φ vs. error are fit to a fourth order polynomial, and the Φ angle corresponding to the minimum error in the plot is chosen as the vector angle Φ_{ab}. The error bars in are determined by the values for which the fit error doubles. $N_{isotropic}$ is determined as the value of N at the magic angle, 54.75°, on the plot of equation 3.1 using the final angle Φ_{ab}.

Results

In Fig 3.3, the EXAFS of oriented PS II in the S_2 state are compared at 10° (bottom) and 75° (top). This sample was well oriented, with a mosaic spread of approximately 20°. The dichroism is most apparent at about 11 Å^{-1}, where the peak height is significantly greater at 10° than at 75°. A monochromator glitch at about 11.5 Å^{-1} has been removed from the data.

The dichroism in these data becomes more apparent in the Fourier transform (see Fig 3.4). Three main peaks (I - III) are seen; the other peaks are not reproducible and are due to noise in the data. After correcting for phase R = R' + Δ where Δ is about 0.5 Å, these peaks are at ~2.0 Å (peak I), 2.7 Å (peak II), and 3.3 Å (peak III) . Peak III is the most dichroic, and has greater amplitude at 10° than at 75°. Differences are also present in the second peak, although they are more subtle. The second peak is slightly larger at 75°

than at 10°; an effect which is more pronounced in other samples (Mukerji et al., 1994). There is also a shoulder on the left side of this peak which shows up at 10°. In some samples this shoulder joins the first and second peaks, or appears as a small peak between peaks I and II. This shoulder has also been seen in other EXAFS studies of PS-II (Penner-Hahn et al., 1990).

Peak II

Fig 3.5 depicts fits to isolates of the second EXAFS peak at 10° (top) and at 75° (bottom). The fit parameters are shown in Table 3.1. When the values for $N_{apparent}$ are fit to equation 3.1, a polar plot results (Fig 3.7A). The average angle $<\Phi_{ab}>$ for this vector is 59.0 ± 1.8°. It is known from other studies (Liang et al., 1994; Dau et al., 1995) that there are two distinct 2.7 Å vectors; this angle therefore represents an average. Resolution of these two vectors using EXAFS studies of ammonia-treated PS II will be discussed in Chapter 4. The global fit for the coordination number ($N_{isotropic}$) is 0.98 ± 0.06; or four interactions per four Mn, which is quite consistent with the two di-μ-oxo bridged moieties proposed in the model discussed in Chapter 1.

Peak III

Fits to the isolates of the third EXAFS peak are seen in Fig 3.6, for 10° (top) and 75° (bottom). The results are tabulated in Table 3.1. These fits are from 5 to 12 $Å^{-1}$ to reduce contributions from low-Z backscatterers. The resulting polar plot in Fig 3.7B yields an average angle of 43.8 ± 0.8° for this vector. The global coordination number for this vector ($N_{isotropic}$) was 0.41 ± 0.02, or two Mn - Mn interactions at this distance. This is consistent with the presence of one mono-μ-oxo and mono- or di-carboxylato bridged moiety per tetramer (Vincent et al., 1987; Wieghardt et al., 1983, 1985; Sheats et al., 1987). Inclusion of a second shell of Mn-Ca decreased the fit error by a factor of 2 to 3, depending on the data set, but the results were not consistent enough to confirm the requirement for this shell. Contribution of a Mn-Ca vector to the third peak has been confirmed by EXAFS of PS II in which Sr has replaced Ca (Latimer et al., 1995; Sauer et al., 1992; Yachandra et al. 1992)

Discussion

Peak I

Peak I was not examined quantitatively in this study. However, after combination of these data with those from other samples, it was found that the data can be fit to two shells of Mn-O and/or Mn-N interactions at about 1.85Å and 1.97Å (Mukerji et al., 1994). This is consistent with the analysis of unoriented PS II samples (DeRose, 1990; McDermott et al, 1988; Yachandra et al., 1987), and probably arises from a combination of bridging O atoms which typically have Mn-O bond lengths of 1.8 to 1.9Å (Pecoraro, 1992; Wieghardt, 1989), and other Mn-N and/or O bonds. Due to the large number of interactions in this peak it is impossible to resolve any individual vectors.

Peak II

The number of interactions determined for the second peak (0.98 ± 0.6) is consistent with those found in most other EXAFS studies of PS II (Dau et al., 1995; DeRose, 1994; McDermott et al, 1988; Yachandra et al., 1987), and is probably due to two di-μ-oxo bridged Mn-Mn moieties. The average angle determined for this vector is close to that found by George et al., and is also in agreement as an average angle for the two vectors resolved in ammonia-treated PS II (Dau et al., 1995; and see chapter 4).

Results from these data plus those from other oriented S_2 samples (Mukerji et al, 1994) yield a coordination number of 1.0 ± 0.1 and an average angle of $60 \pm 4°$.

Presence of Cl

Fits to the second peak were improved by the inclusion of 1 Cl per 4 Mn as a second shell, especially at 10°. The distance for this interaction is 2.3 Å, typical of Mn-Cl bonds (Wieghardt et al., 1989). Earlier EXAFS studies have found the data to be consistent with this interaction as well (George et al. 1989), but it is difficult to say conclusively that Cl must be included in the fit. The possibility of a Mn-Cl bond will be studied further by measuring the EXAFS of oriented PS II in which Br has replaced Cl, enhancing this interaction (see Chapter 5).

Peak III

The number of interactions for the third peak is in good agreement with studies of randomly oriented PS II (Dau et al., 1995; DeRose, 1994; McDermott et al, 1988; Yachandra et al., 1987), and is consistent with the presence of a mono-μ-oxo and mono- or di-carboxylato Mn-Mn bridge. Results of this data set plus others (Mukerji et al., 1994) yield $N_{isotropic} = 0.44 \pm 0.7$, and $\langle \Phi_{ab} \rangle = 43 \pm 10°$. In an earlier study, an angle of 0° was found for this Mn-Mn vector (George et al., 1989). This probably owes to the fact that at 90° they detected no third peak above the noise level. The geometry of detection makes signal-to-noise very poor at angles near 90°, making the third peak, which is small in amplitude even in unoriented samples, difficult to resolve at high angles. In this study, over twice as many scans were taken at 75° vs. 10° (35 vs. 17) to obtain good data quality.

Presence of Ca

It is possible that a Mn-Ca interaction at about 3.3 - 3.5 Å also contributes to the third peak. This is implied in EXAFS studies of Ca-depleted PS II, in which the third peak is reduced or nonexistent, and EXAFS of PS II in which Sr has replaced Ca (Latimer, 1995; Sauer et al., 1992; Yachandra et al., 1993). In the Fourier transform of the EXAFS of Sr-replaced PS II, the intensity of the third peak increases, presumably because Sr is a better backscatterer than Ca. Thus, the angle determined for this vector is probably an average for the Mn-Mn and Mn-Ca interactions. These two vectors can possibly be resolved with EXAFS of oriented Sr-treated PS II.

Summary and Model for the Mn Tetramer.

The data in this study are consistent with the model for the Mn tetramer depicted in Fig 3.7. The two 2.7 Å Mn-Mn vectors form an average angle of 59°, and the 3.3 Å Mn-Mn vector forms an average angle of 44° with respect to the membrane normal. These angles are 60° and 43°, respectively, when other data sets are included (Mukerji et al., 1994). It is important to note that each vector represents a cone of possible orientations about the membrane normal. Other structures are possible, such as one like that in Fig 3.7 but with the two 2.7 Å vectors aligned trans to the membrane normal, or a 3.3 Å Mn-Mn bridge followed by two consecutive 2.7 Å bridges. The possible conformations called the "butterfly" (Brudvig & Crabtree, 1986) and "cubane" structures (Christou & Vincent, 1987) are ruled out by our observation that there are only four Mn-Mn interactions at 2.7 Å per tetramer. Further resolution of the structure with oriented EXAFS may be possible with studies of oriented Br-treated and Sr-treated PS II.

References

Berthold, D. A.; Babcock, G. T. & Yocum, C. F. (1981) *FEBS Lett. 134* , 231-234.

Binsted, N.; Strange, R. W. & Hasnain, S. S. (1992) *Biochemistry 31*, 12117-12125.

Blum, H.; Salerno, J. C. & Leigh, J. S., Jr. (1978) *J. Magnetic Resonance 30*, 385-391.

Brudvig, G. W. & Crabtree, R. H. (1986) *Proc. Natl. Acad. Sci. U. S. A. 83*, 4586-4588.

Christou, G. & Vincent, J. B. (1987) *Biochim. Biophys. Acta 895*, 259-265.

Cramer, S. P.; Tench, O.; Yocum, M. & George, G. N. (1988) *Nucl. Instrum. Methods Phys. Res. A 226*, 586-591.

Dau, H.; Andrews, J.; Yachandra, V. K.; Roelofs, T. A.; Latimer, M. J.; Liang, W.; Sauer, K. & Klein, M. P. (1995) *Biochemistry 34*, 5274-5287.

DeRose, V. J. (1990) *Ph.D. Thesis, University of California, Berkeley.* Lawrence Berkeley Laboratory Report: LBL-30077.

DeRose, V. J.; Mukerji, I.; Latimer, M. J.; Yachandra, V. K.; Sauer, K. & Klein, M. P. (1994) *J. Am. Chem. Soc. 116*, 1335-1341.

George, G. N., Prince, R. C., & Cramer, S. P. (1989) *Science 243*, 789-791.

George, G. N.; Cramer, S. P.; Frey, T. G. & Prince, R. C. (1993) *Biochim. Biophys. Acta 1142*, 240-252.

Goodin, D. B.; Falk, K. E.; Wydrzynski, T. & Klein, M. P. (1979) in *6th Annual Stanford Synchrotron Radiation Laboratory Users Group Meeting*, SSRL Report No. 79/05, 10-11.

Guiles, R. D.; Yachandra, V. K.; McDermott, A. E.; Cole, J. L.; Dexheimer, S. L.; Britt, R. D.; Sauer, K. & Klein, M. P. (1990) *Biochemistry 29*, 486-496.

Jaklevic, J.; Kirby, J. A.; Klein, M. P.; Robertson, A. S.; Brown, G. & Eisenberger, P. (1977) *Solid State Commun. 23*, 679-682.

Latimer, M. J.; DeRose, V. J.; Mukerji, I.; Yachandra, V. K.; Sauer, K. & Klein, M. P. (1995) *Biochemistry*, in press.

Liang, W.; Latimer, M. J.; Dau, H.; Roelofs, T. A.; Yachandra, V. K.; Sauer, K. & Klein, M. P. (1994) *Biochemistry 33,* 4923-4932.

McDermott, A. E.; Yachandra, V. K.; Guiles, R. D.; Cole, J. L.; Dexheimer, S. L.; Britt, R. D.; Sauer, K. & Klein, M. P. (1988) *Biochemistry 27,* 4021-4031.

McKale, A. G.; Veal, B. W.; Paulikas, A. P.; Chan, S. -K. & Knapp, G. S. (1988) *J. Am. Chem. Soc. 110*, 3763-3768.

Mukerji, I.; Andrews, J. C.; DeRose, V. J.; Latimer, M. J.; Yachandra, V. K.; Sauer, K. & Klein, M. P. (1994) *Biochemistry 33,* 9712-9721.

Pecoraro, V. L. (1992) in *Manganese Redox Enzymes* (Pecoraro, V. L., Ed.) VCH Publishers, New York, 197-231.

Penner-Hahn, J. E.; Fronko, R. M.; Pecoraro, V. L.; Yocum, C. F.; Betts, S. D. & Bowlby, N. R. (1990) *J. Am. Chem. Soc. 112*, 2549-2557.

Rutherford, A. W. (1985) *Biochim. Biophys. Acta 807*, 189-201.

Sauer, K.; Yachandra, V. K.; Britt, R. D. & Klein, M. P. (1992) in *Manganese Redox Enzymes* (Pecoraro, V. L., Ed.) VCH Publishers, New York, 141-175.

Sheats, J. E.; Czernuszewicz, R. S.; Dismukes, G. C.; Rheingold, A. L.; Petrouleas, V.; Stubbe, J.; Armstrong, W. H.; Beer, R. H. & Lippard, S. (1987) *J. Amer. Chem. Soc. 109*, 1435-1444.

Vincent, J. B.; Christmas, C.; Huffman, J. C.; Christou, G.; Chang, H. -R. & Hendrickson, D. N. (1987) *J. Chem. Soc. Chem. Commun. 1987*, 236-238.

Wieghardt, K.; Bossek, U. & Gebert, W. (1983) *Angew. Chem. Intl. Ed. Engl. 22*, 328.

Wieghardt, K.; Bossek, U.; Ventur, D. & Weiss, J. (1985) *J. Chem. Soc. Chem. Commun. 1985*, 347-349.

Wieghardt, K. (1989) *Angew. Chem. Int. Ed. Engl. 28*, 1153-1172.

Yachandra, V. K.; Guiles, R. D.; McDermott, A. E.; Britt, R. D.; Dexheimer, S. L.; Sauer, K. & Klein, M. P. (1986) *Biochim. Biophys. Acta 850,* 324-332.

Yachandra, V. K.; Guiles, R. D.; McDermott, A. E.; Cole, J. L.; Britt, R. D.; Dexheimer, S. L.; Sauer, K. & Klein, M. P. (1987) *Biochemistry 26*, 5974-5981.

Yachandra, V. K.; DeRose, V. J.; Latimer, M. J.; Mukerji, I.; Sauer, K.; & Klein, M. P. (1993) *Science 260*, 675-679.

Table 3.1: Mn EXAFS curve-fitting parameters for oriented PS II membrane preparations in the illuminated S_2 state.

Angle[a]	R(Å)	F(θ)N	$-2\sigma^2$ (Å^2)	$\Phi(x10^3)$[c]	$\varepsilon^2(x10^5)$[d]
Second Peak					
10°	2.71	0.76	-0.003	.656	1.13
54.7°[b]	2.72	0.94	-0.003	.494	.869
75°	2.72	1.09	-0.007	.299	.516
Third Peak					
10°	3.30	0.49	-0.003	.213	43.9
54.7[b]	3.34	0.40	-0.004	.148	32.6
75°	3.32	0.38	-0.008	.185	38.0

[a]Angle between the membrane normal and the x-ray electric field vector. [b]Mean values for isotropic S_2-state samples. The EXAFS data of isotropic samples should be identical to the data of oriented samples recorded with an angle of 54.7°. [c]Fit error as defined in equation 3.4. [d]Reduced chi-squared error as defined in equation 3.5.

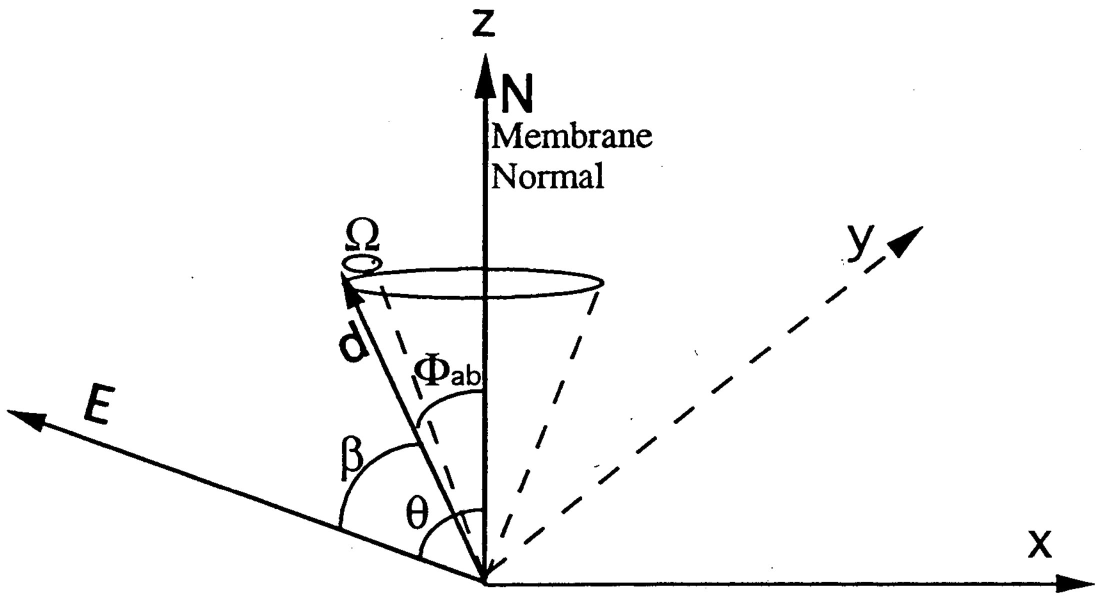

Figure 3.1: Angles used for oriented EXAFS samples. Φ_{ab} is the angle between the membrane normal **N** and absorber-backscatterer vector **d**. The cone around **d** represents the half-width of the gaussian distribution in Φ_{ab}, or mosaic spread, Ω. The angle Φ_{ab} describes a cone of possible orientations about the membrane normal. β is the angle between **d** and the xray e-vector **E**, and θ is the angle between **N** and **E**.

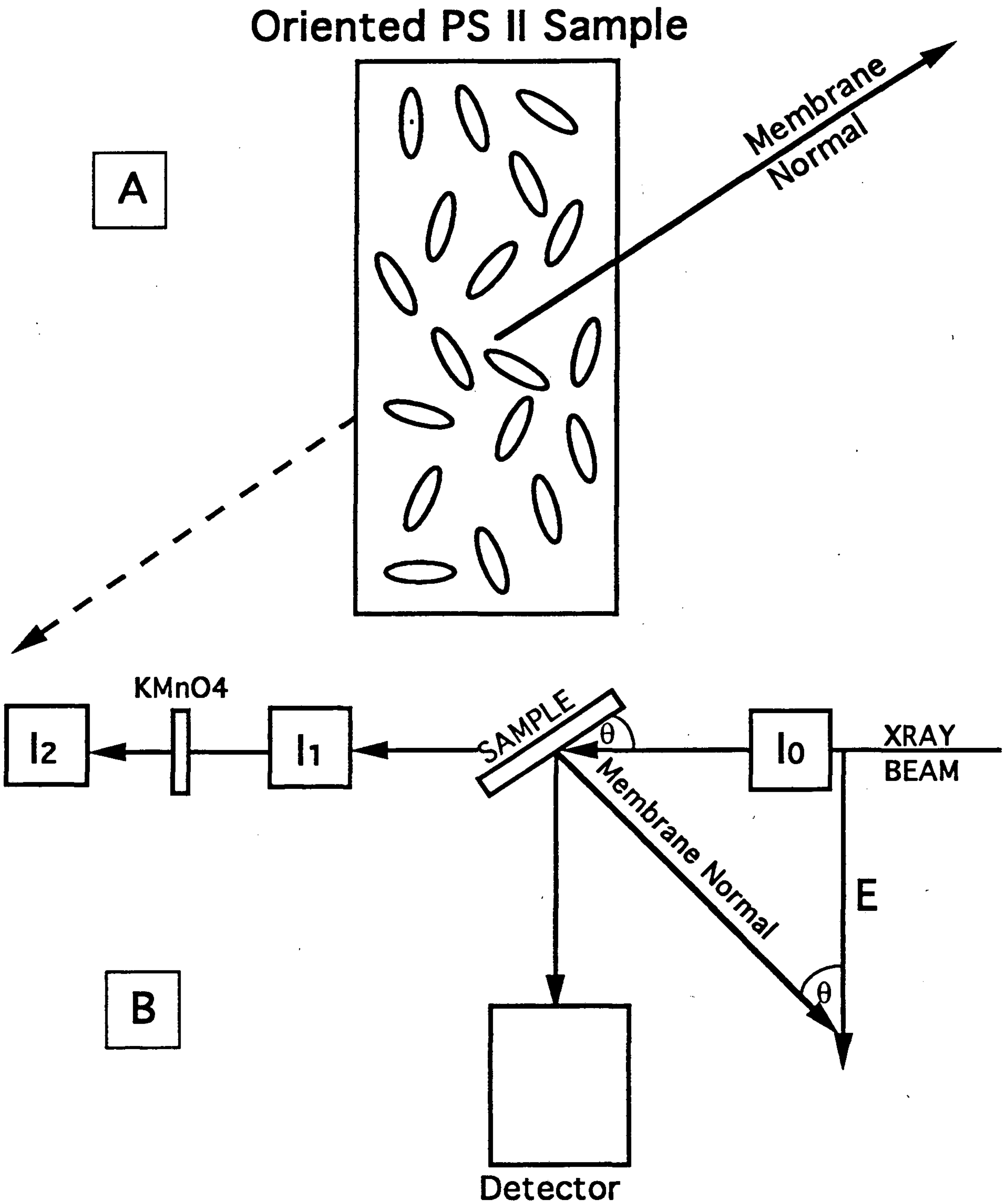

Figure 3.2: (A) Representation of an oriented PS II sample. The membrane normal of the PS II particles is prependicular to the plane in which they are painted. (B) Setup for XAS of an oriented sample. The angle θ between the sample and x-ray beam (the same as the angle between the membrane normal and x-ray **E**-vector) can be varied, thus selecting for vectors at different angles with respect to the membrane normal.

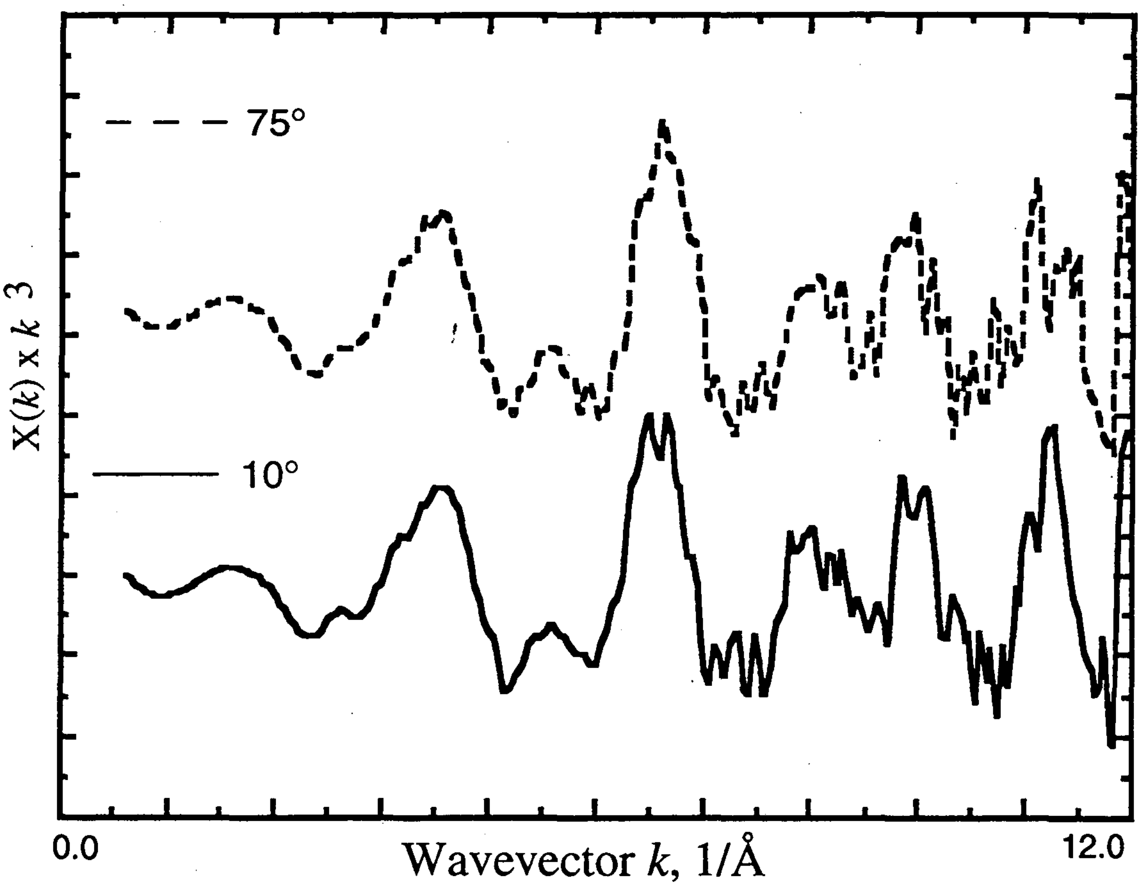

Figure 3.3: *k*-space Mn EXAFS of oriented control S2, 10° (___) and 75° (_ _). Data are weighted by *k* cubed.

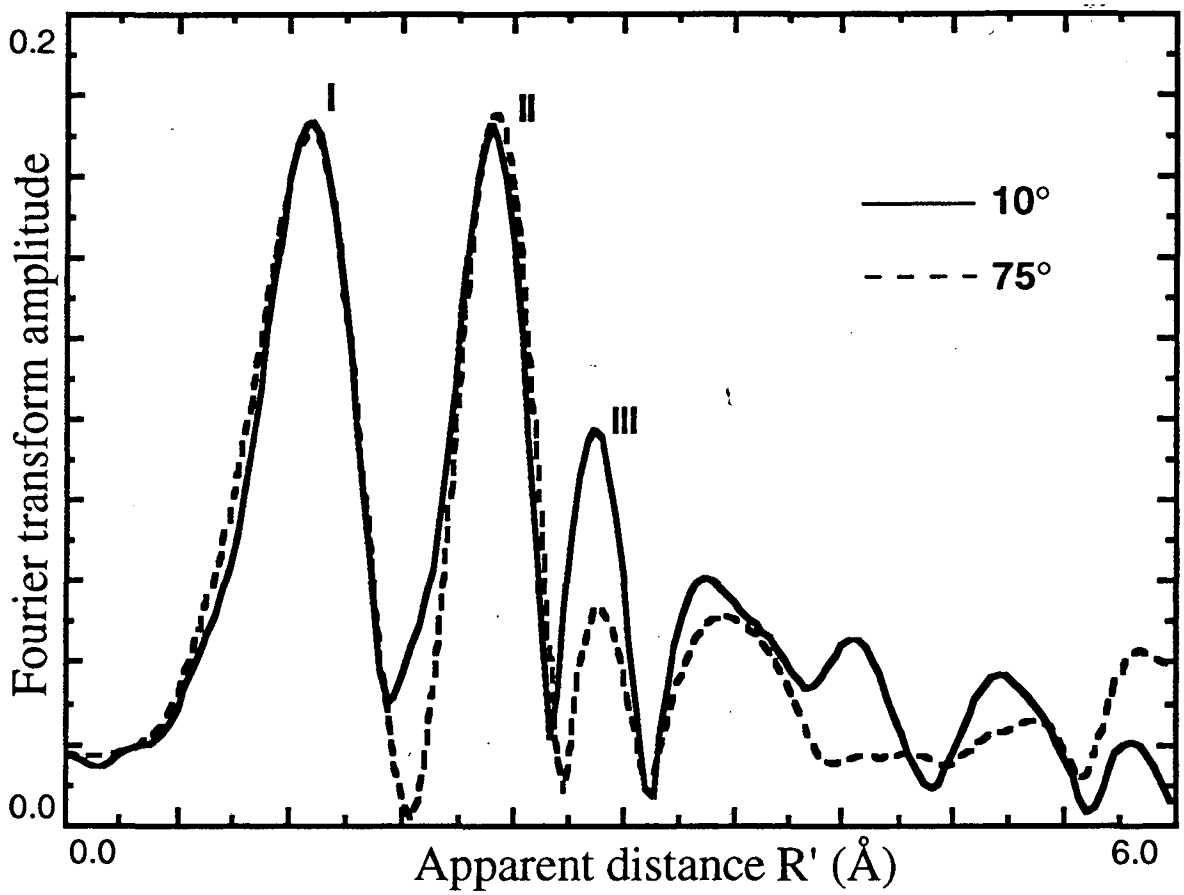

Figure 3.4: Fourier transforms of Mn EXAFS of Control PS II with the membrane normal oriented at 10° (__) and 75° (_ _) with respect to the x-ray **E**-vector.

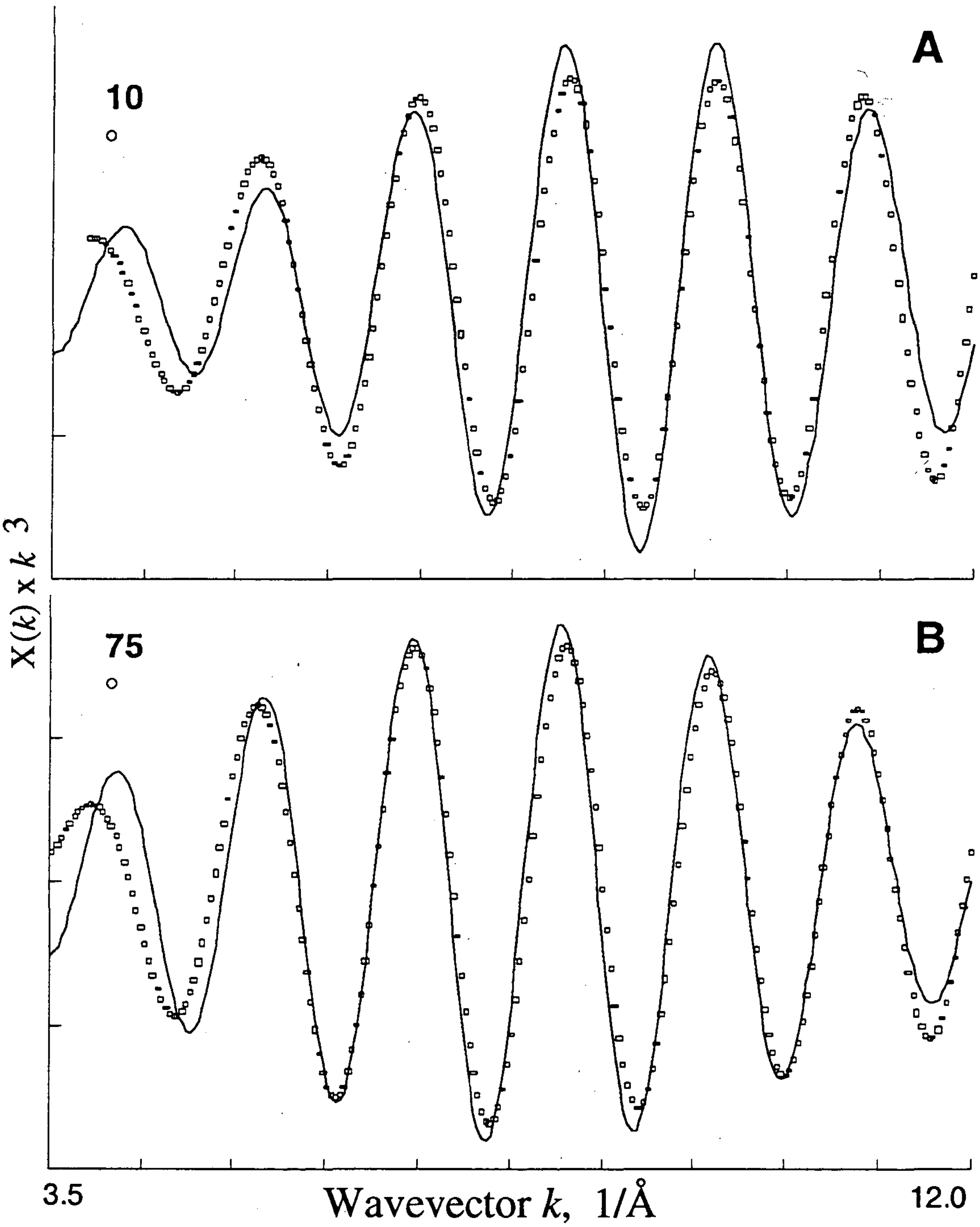

Figure 3.5: Fits of EXAFS isolates for S2, peak II. Samples are oriented at 10° (A) and 75° (B).

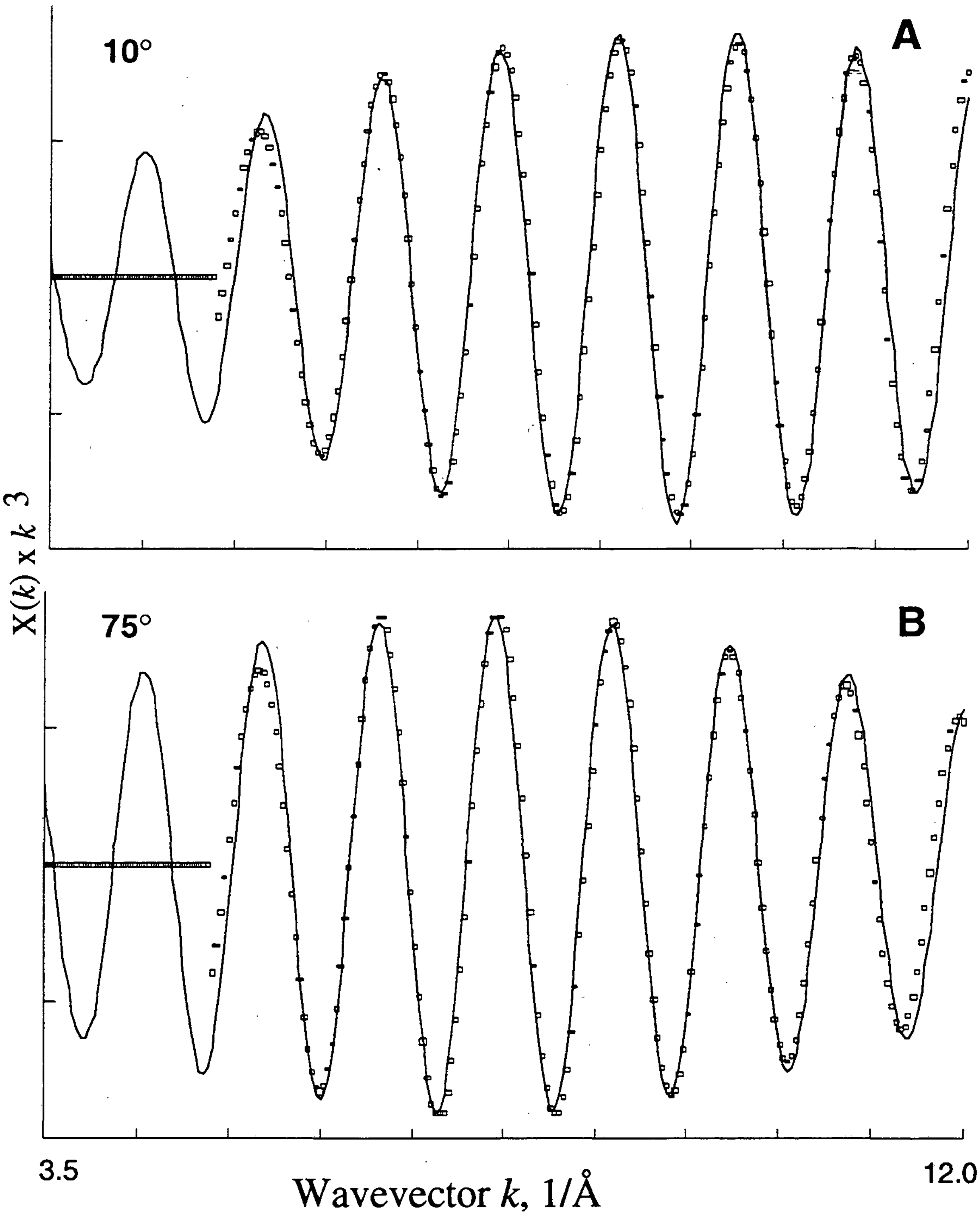

Figure 3.6: Fits of EXAFS isolates for control S2, peak III.
Samples are oriented at 10° (A) and 75° (B).

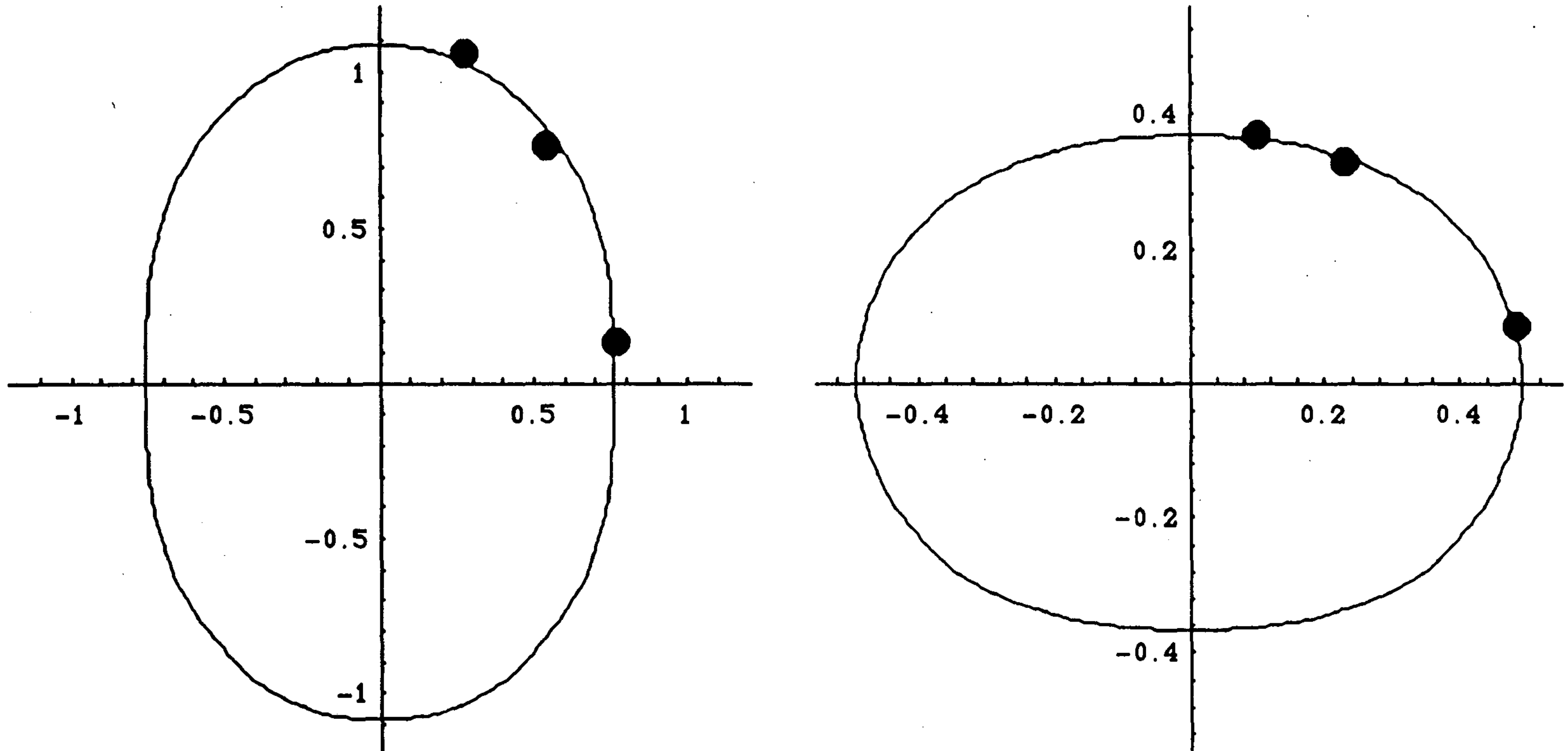

A. Second Peak

$<\Phi> = 59.0 \pm 1.8°$

$Nisotropic = 0.98 \pm 0.06$

B. Third Peak

$\Phi = 43.8 \pm 0.8°$

$Nisotropic = 0.41 \pm 0.02$

Figure 3.7: Polar plots of *Napparent* (=*Fab(θ)Nisotropic*) vs. *θ* for control PS II, S2 state. Plots are best fits to equation 3.1 for (A): peak II, 2.7 Å Mn-Mn, and (B): peak III, 3.3 Å Mn-Mn. The data point at 54.7° is taken from EXAFS data for a randomly oriented preparation.

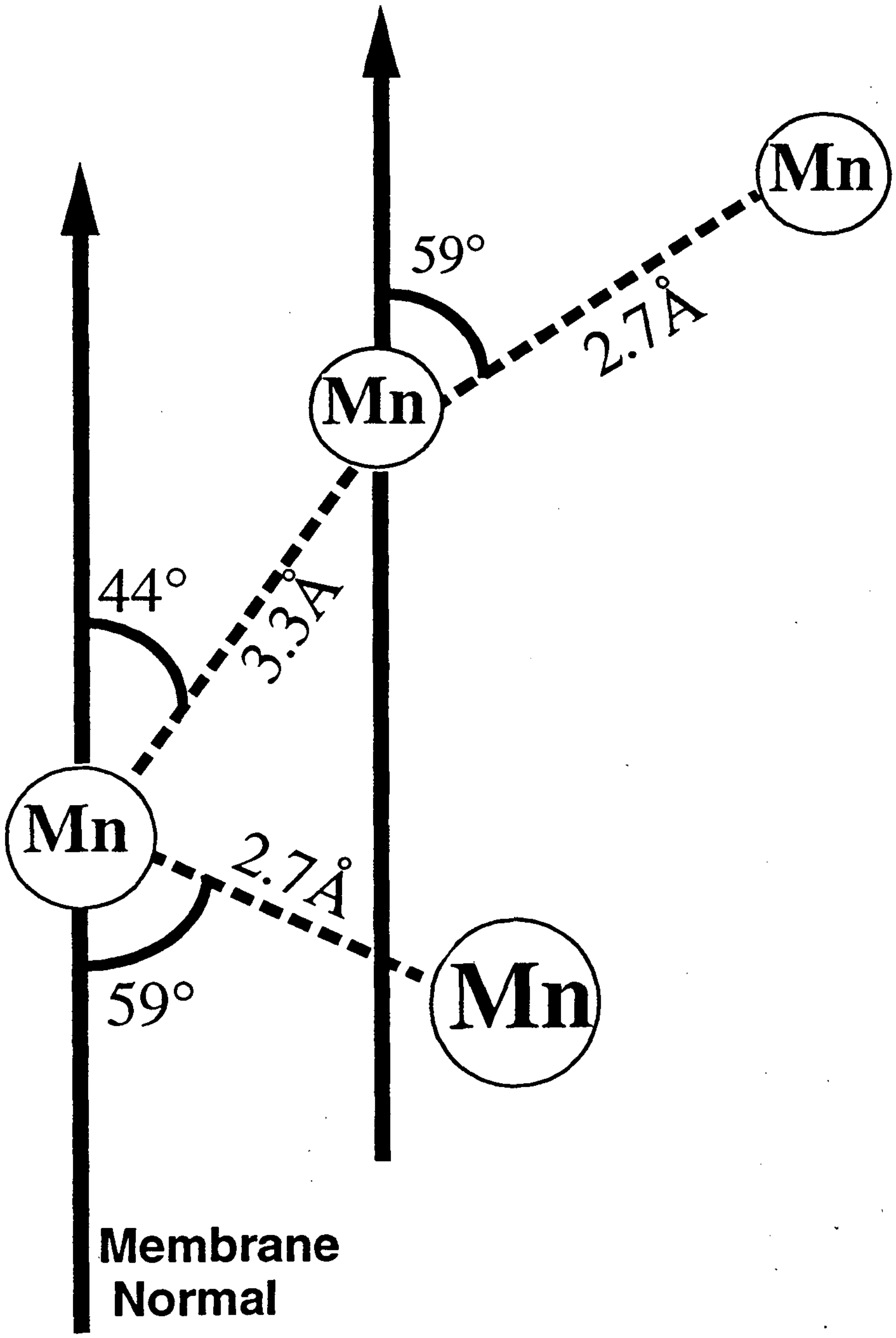

Figure 3.8: Proposed model for the Mn tetramer oriented within the membrane. Note that the vector measurement of 59°, and probably that of 44° as well, represent average values for at least two vectors.

Chapter 4:

Structural Changes in PS II as a Result of Treatment with Ammonia: EPR and X-ray Absorption Spectroscopy studies

Introduction

Amines inhibit oxygen evolution, probably as competitors for the water-binding site. Therefore the study of ammonia-treated PS II may yield insight into the mechanism of water binding in the OEC. Studies of amine-treated PSII have been recently reviewed (Debus 1992). The amines may act as Lewis bases to bind with Mn, a Lewis acid. There are two binding sites for amines: site 1, which competes with Cl^-, and site 2 which exhibits no Cl^- competition and binds only ammonia, not the larger amines (Sandusky & Yocum, 1984; 1986). This small, sterically hindered site is thought to be the binding location for water in the oxygen evolution cycle. The binding of ammonia to site 1 (which is not necessarily located on Mn) stabilizes the g=4 EPR signal relative to the g=2 multiline signal (Andréasson et al. 1988, Beck & Brudvig 1986a). The binding of NH_3 to site 2 does not occur immediately on illumination at 195 K; the sample must be "annealed" at 293 K to bind the NH_3 (Beck et al. 1986b; Britt et al., 1989). This binding to site 2 of the S_2 state alters the spacing of the multiline signal, reducing it from 87.5 to 67.5 G (Beck & Brudvig, 1986), indicating that the binding of ammonia affects the magnetic properties of the Mn complex. In 1975 flash studies were used to determine that NH_3 binds to the S_2 and S_3 states but not to the S_1 state, and also that the redox potentials of the S_2 and S_3 states are altered by NH_3 (Velthuys, 1975). Later it was found that weak binding of NH_3 to the S_1 state also occurs, although only to a small extent compared with binding to the S_2 state (Andréasson et al., 1988). Britt et al. (1989) found that there is an ammonia-derived species directly coordinated to the manganese. Their proposal is that there is a small amount of NH_3 bound to Mn in the S_1 state, but it is in competition with the solvent, H_2O. Upon oxidation of Mn(III) to Mn(IV) during the S_1 to S_2 transition, the increased electron affinity of the Mn allows deprotonation of the weakly bound NH_3 to form a strongly bound NH_2 amido bridge, which blocks ligation of H_2O and thereby inhibits oxygen evolution.

When the ammonia sample is oriented, the g=4.1 signal shows hyperfine splittings at 0° (membrane normal with respect to the magnetic field), which manifest as sixteen partially resolved hyperfine transitions 36 G apart (Kim et al., 1990; 1992). The resolution of the hyperfine coupling of the g=4.1 signal is greatly reduced at 45° and is barely apparent at 90°. It was earlier suggested that the Mn complex was a monomer plus trimer, and the monomer gave rise to the g=4.1 signal (Pecoraro, 1988; Hansson & Wydrzynski, 1990). However, the hyperfine coupling pattern in the g=4.1 signal of oriented ammonia-treated PS II refutes this possibility (Kim et al., 1990; 1992).

The g=2 multiline (stabilized with PPBQ) also exhibits orientation dependence, indicating that there is anisotropy in the g-tensor. A spin Hamiltonian has been developed (Kusunoki 1992) which has successfully simulated the EPR spectra of the normal (S=1/2) S_2 multiline signal, the oriented NH_3-treated (S=5/2) g=4 signal, and the normal (S=l) S_1 signal detected by Dexheimer using parallel polarization EPR (Dexheimer & Klein, 1992). This study gives further evidence of the tetramer conformation and spin states of the Mn complex, and corroborates ligation of an amine derivative to Mn.

Materials and Methods

Preparation of PS II Membranes for X-ray Absorption Measurements

PS II membrane particles were prepared by the method of Berthold et al. (1981). For NH_3 treatment, the PS II membrane pellet was washed first in 40 mM Hepes (pH 7.5) / 50 mM NaCl / 0.4 M sucrose and then in 40 mM Hepes (pH 7.5) / 5 mM NaCl / 0.4 M sucrose, each time followed by centrifugation for 15 min at 38000 g. The PS II electron acceptor PPBQ (30 mM in ethanol) was added to the pellet of the last centrifugation step resulting in a final PPBQ concentration of about 0.8 mM, and NH_4Cl solution (2 M, adjusted with NaOH to pH 7.5) was added to give a final NH_4Cl concentration of approximately 100 mM (Kim et al., 1992).

For randomly oriented samples, the suspension was transferred directly to x-ray sample holders and frozen in liquid nitrogen. The x-ray samples prepared as described above were predominantly in the S_1-state, because they were fully dark adapted. To establish the S_2-state, the x-ray samples were illuminated for 8 min at 195 K (Brudvig et al., 1983). To create the state which is associated with the ammonia-modified EPR multiline signal (Beck & Brudvig, 1986), the ammonia-treated samples were illuminated at 195 K and annealed by exposing them for 60 s to a stream of nitrogen gas at about 4 °C (Kim et al., 1992); after this annealing procedure the x-ray samples were quickly frozen in liquid nitrogen.

Preparation of Oriented PS II Membranes

The ammonia-treated PS II membrane suspension was painted onto mylar tape and dried for 20 min under a gentle stream of nitrogen gas in the dark at 4 °C as described in Chapter 3. However, only three layers were painted, spaced 20 minutes apart. Longer drying times resulted in the release of Mn(II). The structural integrity (absence of free manganese), functional states (S_1, S_2, ammonia-modified S_2) and orientation of all x-ray samples were routinely verified by means of EPR measurements. The mosaic spread of these samples was determined by measurement of the tyrosine D^+ signal and cytochrome b_{559} as described in Chapter 2, and was found to be 20-25°.

X-ray Absorption Measurements

The x-ray absorption spectra were recorded at the Stanford Synchrotron Radiation Laboratory (U.S.A.) on wiggler beam lines IV-2 (for EXAFS spectra) and VII-3 (for edge spectra) using Si<111> and Si<220> double-crystal monochromators, respectively. For all x-ray edge spectra, the obtained energy resolution was 1.8 ± 0.2 eV. EXAFS data collection, analysis and determination of vectors was performed as described in Chapter 3, with the exception that the theoretical phase and amplitude functions used to fit the EXAFS were generated using a model for the OEC based on the model presented in Yachandra et al. (1993) and the FEFF 5 program written by Rehr et al. (1992).

The FEFF 5 simulation of EXAFS differs from other curved-wave formalisms (e.g. Teo & Lee (1979); EXCURV (Binsted et al. 1986); McKale et al. 1988). It includes multiple scattering, a mean free path term, and a more accurate E0 (= Vint(E) - iΓ/2) in which iΓ/2 is the core-hole lifetime and Vint(E) is the interstitial potential. Most importantly, it includes system-dependent chemical effects, because a unique interstitial potential Vint(E) is calculated for the absorbing atom and each chemically unique backscatterer.

Analysis of Oriented EXAFS Data

The EXAFS intensity detected at a given angle θ, (George et al. 1989,1993) relative to the intensity which would be detected in an unoriented sample ($N_{apparent}/N_{isotropic}$) is given by the equation

$$F_{ab}(\theta) = \frac{3\int_{\Phi=0}^{\pi}(\frac{1}{2}\sin^2\theta\sin^2\Phi + \cos^2\theta\cos^2\Phi)P(\Phi)d\Phi}{\int_{\Phi=0}^{\pi}P(\Phi)d\Phi} \quad (4.1)$$

where $P(\Phi) = \sin\Phi\exp[(-\ln 2)(\Phi - \Phi_{ab})^2/\Omega^2]$ is the number of **d** vectors with orientation Φ, Φ_{ab} is the angle between the membrane normal and the absorber-backscatterer vector **d**, and Ω is the mosaic spread, or half-width of the gaussian distribution in Φ_{ab} (described in Chapter 2). A best fit of *Napparent* (= $F_{ab}(\theta)$*Nisotropic*) vs. θ gives the average orientation $<\Phi_{ab}>$ for a given vector. An average angle is obtained when a vector has two or more components which cannot be resolved due to distances which vary less than the EXAFS resolution. The equation for the average angle $<\Phi ab>$ of two vectors (1 and 2) (George et al. 1993) is

$$\cos^2<\Phi ab> = \{N_1\cos^2(\Phi_1) + N_2\cos^2(\Phi_2)\} / \{N_1 + N_2)\} \quad (4.2)$$

where $N_{(1,2)}$ is the number of indistinguishable backscatterers for a given vector and $\Phi_{(1,2)}$ is the angle for that vector. The fit to $F_{ab}(\theta)$ also gives a more reliable value for $N_{isotropic}$ than that obtained from unoriented data alone, since it is a global fit.

Results

EPR Spectra

Light minus dark EPR spectra of typical ammonia-treated samples are shown in Fig 4.1. After illumination at 195 K the spectrum is much like that of native PS II, although some g=4.1 signal is seen (Fig 4.1A) due to binding of ammonia to site 1 (Andréasson 1988; Beck & Brudvig, 1986). After annealing for 60 s at 4°C the multiline changes to the typical ammonia-treated form (Fig 4.1B), spaced 67.5 G apart (Beck & Brudvig, 1986). The spectrum of annealed samples is washed out in the low-field region, and much more even in the high field region after annealing, and more g=4.1 signal is seen than before annealing.

Mn K-edge Data

Mn K-edges of S_1, S_2 and S_2 annealed samples each show the same general shape in the pre-edge region (see Fig 4.2 and Dau et al., 1995), which indicates that the symmetry of the Mn complex is not significantly changed upon the binding of ammonia. Edge positions as determined by measurement of the zero-crossing of the second derivative of the spectra are 6552.58 ± 0.14 eV for S_1, 6553.45 ± 0.17 eV for S_2, and 6553.63 ± 0.05 eV for S_2 annealed samples.

EXAFS of Oriented NH_3-Treated PS II

The *k*-space data of ammonia-treated PS II are shown in Fig 4.3. The peaks at approximately 9 $Å^{-1}$ and 10 $Å^{-1}$ are less resolved than the analogous peaks in native oriented samples (see Fig 3.2). There is some damping in the peak at about 11$Å^{-1}$ as well, compared with native samples. Dichroism is seen in the last peak, which has greater amplitude at 10° than at 70°.

The Fourier transforms of the ammonia data at 10° vs. 70° are shown in Fig 4.4. Less dichroism is seen than in the native samples (compare with Fig 3.3 and Mukerji et al 1994), especially for peaks II and III. The Fourier transforms of the ammonia-treated PS

II, compared with those of native oriented PS II, are shown in Fig 4.5 at 10° (A) and 70° (B). At both angles, the second peak is greater in the native sample than in the ammonia-treated PS II, and the first and second peaks are broader than in native PS II. The third peak is considerably lower in the ammonia sample at 10° than in the control sample. At 70° the third peaks of ammonia-treated and native PS II have approximately the same amplitude, but that of the ammonia-treated PS II is broader.

Analysis of the Second Fourier Transform Peak

Isolates of the second peak are shown in Fig 4.6. At both 10° (Fig 4.6A) and 70° (Fig 4.6B), the ammonia sample (solid line) shows more damping than the native samples (dotted line) at high *k*. This is an indication that the reduced amplitude of the second peak of the ammonia samples relative to that of the native samples is not due to a decrease in the number of backscatterers contributing to that peak, but to damping of the peak. Damping can be due to greater general disorder in the peak, but can also arise due to destructive interference of two partial waves comprising the peak. This would be the case if there were two interactions contributing to this peak with different bond lengths.

The results of fits to the second peak are shown in Table 4.1. First, fits were done to one shell of Mn-Mn backscatterers at about 2.73 Å. The Debye-Waller factors, allowed to minimize to the best fit value, are higher at higher angles (0.0061-0.0077 $Å^2$) than at lower angles (0.0033-0.0055 $Å^2$). These Debye-Waller factors are higher than those seen for fits of the second Fourier transform peak in oriented native PS II. Those were 0.0015-0.003 $Å^2$ at 10°, and 0.0025-0.0035 $Å^2$ at 75° in the data from oriented native PS II (see Table 3.1 and Mukerji et al., 1994. Note that Debye-Waller factors there are listed as $-2\sigma^2$). The fits improve, as reflected in the ϕ and ε^2 values (defined in equations 3.4 and 3.5), upon addition of a second shell of Mn-Mn backscatters at 2.86 Å. When a two-shell Mn-Mn fit was attempted with the second peak of native PS II, no improvement in the fit error was seen. In these two-shell fits to ammonia-treated PS II, the Debye-Waller factor is also substantially lower for the two-shell fits than for the one-shell fits. Typical one-shell and two-shell fits to the second peak isolate are shown in Fig 4.7. The two-shell fit is a better match to the data over the whole *k*-range. These data are indicative that the binding of ammonia to the Mn center of PS II results in the increase in the Mn-Mn distance between one of the two di-μ-oxo bridged binuclear units, from approximately 2.73 Å to 2.86 Å. The two shells present in the fit in Fig 4.7B are presented separately in Fig 4.8. It is apparent that because the two shells are out of phase, they will exhibit interference and attenuate the second peak.

Fits of *Napparent* vs. θ to equation 4.1 were done to determine the angle of the two separate vectors in the second Fourier transform peak of ammonia-treated PS II. For the 2.73 Å vector, an angle of 53.9 ± 4.9° was obtained, and *Nisotropic* was 0.78 ± 0.11. For the 2.86 Å vector, an angle of 60.7 ± 4.5° and *Nisotropic* of 0.54 ± 0.09 were obtained. The angle for the 2.86 Å vector is different from that of 67 ± 3° reported by Dau et al. (1995) from fits to these data, although they are within the error range of each other. In the Dau et al study, curved wave theoretical amplitude and phase functions from McKale et al. (1988) were used to fit the data, whereas FEFF 5 (Rehr et al. 1992) is being used to fit the data in this study. This is not the reason for the difference in the angles, however. In this study ΔE_0 for the second shell was fixed to be equal to that of the first shell, a practice which has been found to be valid in fitting EXAFS of model compound data (O'Day et al. 1994). When these same data are fit with McKale amplitude and phase functions with ΔE_0 fixed for the second shell, an angle of 61° is obtained for the 2.86 Å vector.

The coordination number for the 2.73 Å vector is higher than expected for the model of two di-μ-oxo bridged binuclear Mn-Mn units, one of which is elongated upon the binding of ammonia. For this model, each vector would have an isotropic coordination number of 0.5, or two interactions per four Mn. The higher coordination number for the 2.73 Å vector could be due to the fact that not all of the Mn centers were affected by the ammonia treatment, or that not all of the centers were advanced to the S_2 state. In those untreated centers both vectors would have lengths of 2.73 Å, and when added to PS II in which one binuclear unit has bound ammonia, the coordination number for the 2.73 Å vector would be higher than that for the 2.86 Å vector.

Analysis of the Third Fourier Transform Peak

The third Fourier transform peak of EXAFS of ammonia-treated PS II has been analyzed in conjunction with the second peak. The third peak is quite small compared with the first and second, and is therefore much closer to the noise level of the data. It was also difficult to separate from the second peak in some of the data sets. Fits of the second and third peaks together were done by fixing the coordination numbers and Debye-Waller factors found from fits of the second peak alone (see Table 4.1). The distance R, coordination number N, and Debye-Waller factor for the third shell were free parameters for these fits, as well as R for the first two shells. The ΔE_0 value for shells 2 and 3 was fixed to be equal to that of the first shell. Results of fits to three shells of data, that is (1) Mn-Mn at 2.73 Å, (2) Mn-Mn at 2.86 Å, and (3) Mn-Mn at 3.3 Å are listed in Table 4.2.

Upon fitting of *Napparent* vs. θ for these data to equation 4.1, an angle of 41.0 ± 6.4° is found, and *Nisotropic* is equal to 0.76 ± .11 (see Fig 4.10). The angle of 41° is in agreement with that found by Mukerji et al. (1994) for the third peak of the EXAFS of oriented native PS II. This confirms that ammonia treatment has not significantly changed the structure of the oxygen evolving complex. The coordination number of 0.75 is an indication that the angle of 41° represents an average for at least two backscatterers. Based on the model in Fig 1.4, a coordination number of 0.5 is expected for the Mn-Mn interaction at 3.3 Å. There may be another interaction in the third peak with a coordination number of 0.25, or one per four Mn, resulting in a total coordination number of 0.75. A likely candidate for this second interaction in the third peak is Ca. Evidence for a Mn-Ca interaction at about 3.4 Å has been found in studies of PS II in which Sr has replaced Ca (Latimer 1995, Yachandra 1992).

Discussion

The structure of ammonia-treated PS II is not changed dramatically compared with that of native PS II. The EPR multiline signal before annealing of the ammonia samples is like that of native PS II. The pre-edges of the x-ray absorption edge data, which are very sensitive to symmetry changes (Kusunoki et al. 1990; Shulman 1976), have the same energy and shape as those of native PS II (Dau et al. 1995). The edge energies for the S_1 and S_2 states of 6552.6 and 6553.5 eV, respectively, are consistent with those of 6551.7 and 6553.4 eV for flashed S_1 and S_2 (Andrews et al. 1995; Liang 1994b), and with those of 6552.2 and 6553.3 for PS II which has been illuminated at 140 K and annealed at 200 K, resulting in a normal multiline signal (Liang 1994a). All of the above edge energies were determined by the zero-crossing of the second derivative of the edge spectrum. MacLachlan et al. (1994) found edge energies for ammonia-treated PS II of 6550.6 eV for S_1, 6551.5 eV for S_2, and 6552.5 eV for S_2 annealed samples. These edge energies were determined as the first inflection point of the rising edge. They are lower in energy than those reported here, possibly due to the different method of determination, or perhaps because the treatment of PS II with ammonia can cause the release of Mn(II) from the oxygen evolving complex (Beck et al., 1989). The dark EPR spectra from these samples of MacLachlan et al. (1994) indicate that Mn(II) may be present.

Another indication that the structure of PS II is not greatly changed by treatment with ammonia is that the vector angles for peaks II and III are in agreement with those from oriented native PS II (Mukerji et al. 1994). The average angle for the two vectors from the second peak in this work, calculated using equation 4.2, is 57°. This is within the error range of the average angle of $60 \pm 7°$ as reported by Mukerji et al. (1994). The average angle for peak III of $41 \pm 6°$ is in agreement with that of $43 \pm 10°$ reported by Mukerji et al.

Based on the above agreement of the data from ammonia-treated PS II with data from native PS II, we can say that the changes seen in the second EXAFS peak are due to the binding of ammonia, and are not due to major structural or symmetry changes. The binding of ammonia increases the Mn-Mn distance in one of the 2.7Å binuclear units to 2.86 Å, probably by replacement of one of the bridging oxygens with an amido bridge (Britt et al. 1989). Although it has been suggested that this could be a non-substrate replacement of a bridging oxygen (Rutherford et al. 1992), studies of amine inhibition of oxygen evolution (Sandusky & Yocum 1984; 1986) are suggestive that the ammonia binding site could be the small, sterically hindered, water binding site not accessible to other amines.

Heterogeneity of the two 2.7 Å Mn-Mn vectors in the OEC has been found by others. Two distances were required to fit the second EXAFS peak of PS II in the S_2 state produced upon illumination at 140 K, characterized by an EPR signal at g=4.1 (Liang et al. 1994a). Treatment of PS II with fluoride also produces heterogeneity in the second peak (DeRose 1995). Guiles et al. (1990) found heterogeneity in the second peak of EXAFS of PS II in a chemically induced S_3 state. EXAFS of PS II in a flash-induced S_3 state also have shown reduction in the height of the second Fourier transform peak (Liang, W., private communication), which may be due to heterogeneity in the second peak.

It has been suggested that water does not bind to the OEC until at least the S_3 state (Brudvig & Crabtree 1986; Vincent & Christou 1987) and possibly not until the S_4 state (Ghanotakis & Yocum 1990). Because amines are stronger Lewis bases than H_2O, ammonia is able to bind to PS II in the S_2 state. This reaction does require some thermal energy, however, as it does not occur until the sample is annealed at 4° C.

It has been suggested that one of the Mn-Mn binuclear units of the OEC is more active than the other, and is the site of most of the chemical activity during the oxygen evolution cycle. In their study of oriented native PS II, Mukerji et al. (1994) saw a decrease in the length of the 2.7 Å average vector upon the S_1 to S_2 transition in the data taken at 80°. They also detected changes in the *k*-space data that were more pronounced at 80° than at 10° upon the S_1 to S_2 transition. They were unable to resolve separate vectors for the second peak, presumably because they were very close in length, but based on the above facts they proposed that Mn in the 2.7 Å vector which was closer to 80° was oxidized during the S_1 to S_2 transition. This may be the more active binuclear unit of the two 2.7 Å Mn-Mn di-μ-oxo bridged centers. Ammonia treatment changes the vector that is closer to 80° of the two, which is further evidence that this moiety may be a more chemically active Mn-Mn binuclear unit than that at 10°.

Fig 4.11 shows a basic model of the oxygen evolving complex based on the model of Yachandra et al. (1993), with vector angles from this work. It must be emphasized that each of these vectors represents a cone of possible orientations about the membrane normal, and other conformations are possible. Bound ammonia is shown as an amido bridge, as suggested by Britt et al. (1989). Because no evidence for symmetry changes in ammonia-treated PS II were seen, the angles in this model should be equal to those in native PS II. Using an energy minimization routine and geometric calculations, Dau et al. (1995) found this conformation to be the most likely for the OEC based on current data. Further resolution of the 3.3 Å vector may be obtained by studies of oriented PS II in which Sr has replaced Ca.

References

Andréasson, L.-E.; Hansson, Ö. & von Schenck, K. (1988) *Biochim. Biophys. Acta 936*, 351-360.

Andrews, J. C.; Cinco, R.; Dau, H.; Latimer, M. J.; Liang, W.; Roelofs, T. A.; Rompel, A.; Sauer, K.; Yachandra, V. K. & Klein, M. P. (1995) *Physica B 208 & 209*, 657-659.

Beck, W. F. & Brudvig, G. W. (1986a) *Biochemistry 25,* 6749-6486.

Beck, W. F.; DePaula, J. C. & Brudvig, G. W. (1986b) *J. Am. Chem. Soc. 108*, 4018-4022.

Beck, W. F.; Sears, J.; Brudvig, G. W.; Kuwaliec, R. J. & Crabtree, R. H. (1989) *Tetrahedron Lett. 45*, 4903-4911.

Berthold, D. A.; Babcock, G. T. & Yocum, C. F. (1981) *FEBS Lett. 134*, 231-234.

Binsted, N.; Gusman, S. J.; Campbell, J. W. (1986) *EXCURV; SERC Daresbury Laboratory*; Daresbury, Warrington, U. K.

Britt, R. D.; Zimmerman, J.-L.; Sauer, K. & Klein, M. P.. (1989) *J. Am. Chem. Soc. 111,* 3522-3532.

Brudvig, G. W.; Casey, J. L. & Sauer, K. (1983) *Biochim. Biophys. Acta 723*, 366-371.

Brudvig, G. W. & Crabtree, R. H. (1986) *Proc. Natl. Acad. Sci. USA 83*, 4586-4599.

Debus, R. J. (1992) *Biochim. Biophys. Acta 1012*, 269-352.

DeRose, V. J.; Mukerji, I.; Latimer, M. J.; Yachandra, V. K.; Sauer, K. & Klein, M. P. (1994) *J. Am. Chem. Soc. 116*, 5239-5249.

DeRose, V. J.; Latimer, M. J.; Zimmerman, J.-L.; Mukerji, I.; Yachandra, V. K.; Sauer, K. & Klein, M. P. (1995) *Chemical Physics 194*, 443-459.

Dexheimer, S. L. & Klein, M. P. (1992) *J. Am. Chem. Soc. 114,* 2821-2826.

George, G. N.; Prince, R. C. & Cramer, S. P. (1989) *Science 243*, 789-791.

George, G. N.; Cramer, S. P.; Frey, T. G. & Prince, R. C. (1993) *Biochim. Biophys. Acta 1142*, 240-252.

Ghanotakis, D. F. & Yocum, C. F. (1990) *Annu. Rev. Plant Physiol. Plant Mol. Bio. 41*, 255-276.

Guiles, R. D.; Zimmerman, J.-L.; McDermott, S. E.; Yachandra, V. K.; Cole, J. L.; Dexheimer, S. L.; Britt, R. D.; Wieghardt, K.; Bossek, U.; Sauer, K. & Klein, M. P. (1990) *Biochemistry 29*, 471-485.

Hansson, Ö. & Wydrzynski, T. (1990) *Photosynth. Res. 23*, 131-162.

Kim, D. H.; Britt, R. D.; Klein, M. P. & Sauer, K. (1990) *J. Am. Chem. Soc. 112*, 9389-9391.

Kim, D. H.; Britt, R. D.; Klein, M. P. & Sauer, K. (1992) *Biochemistry 31*, 541-547.

Kusunoki, M.; Ono, T.; Matsushita, T.; Oyanagi, H. & Inoue, Y. (1990) *J. Biochem. (Tokyo) 108*, 560-567.

Kusunoki, M. (1992) in *Research in Photosynthesis, Vol. 2* (Murata, N., Ed.) Kluwer Academic Publishers, Dordrecht, 297-300.

Latimer, M. J.; DeRose, V. J.; Mukerji, I.; Yachandra, V. K.; Sauer, K. & Klein, M. P. (1995) *Biochemistry*, in press.

Liang, W.; Latimer, M. J.; Dau, H.; Roelofs, T. A.; Yachandra, V. K.; Sauer, K. & Klein, M. P. (1994a) *Biochemistry 33*, 4923-4932.

Liang, W. (1994b) Ph.D. Dissertation, University of California, Berkeley, CA; Lawrence Berkeley Laboratory Report LBL-36632.

MacLachlan, D. J.; Nugent, J. H. A. & Evans, M. C. W. (1994) *Biochim. Biophys. Acta 1185*, 103-111.

McKale, A. G.; Veal, B. W.; Paulikas, A. P.; Chan, S.-K. & Knapp, G. S. (1988) *J. Am. Chem. Soc. 110*, 3763-3768.

O'Day, P. A.; Rehr, J. J.; Zabinsky, S. I. & Brown, G. E., Jr. (1994) *J. Am. Chem. Soc. 116*, 2938-2949.

Pecoraro, V. L. (1988) *Photochem. Photobiol. 48*, 249-264.

Rehr, J. J.; Albers, R. C. & Zabinsky, S. I. (1992) *Phys. Rev. Lett. 69*, 3937-3400.

Rutherford, A. W.; Zimmerman, J.-L. & Boussac, A. (1992) in *The Photosystems: Structure, Function and Molecular Biology* (Barber, J., Ed.), Elsevier, Amsterdam, 179-229.

Sandusky, P. O. & Yocum, C. F. (1984) *Biochim. Biophys. Acta. 766*, 603-611.

Sandusky, P. O. & Yocum, C. F. (1986) *Biochim. Biophys. Acta. 849*, 85-93.

Shulman, R. G.; Yafet, Y.; Eiseberger, P. & Blumberg, W. E. (1976) *Proc. Natl. Acad. Sci. U.S.A. 73*, 1384-1388.

Teo, B.-K. & Lee, P. A. (1979) *J. Am. Chem. Soc. 101*, 2815-2832.

Velthuys, B. R. (1975) *Biochim. Biophys. Acta 396*, 392-401.

Vincent, J. B. & Christou, G. (1986) *FEBS Lett. 207*, 250-252.

Yachandra, V. K.; DeRose, V. J.; Latimer, M. J.; Mukerji, I.; Sauer, K. & Klein, M. P. (1993) *Science 260*, 675-679.

Table 4.1 Fits to the second peak of oriented annealed ammonia-treated PS II

One-Shell Fits: Mn-Mn

Angle	R1(Å)	N1	σ^2(Å^2)	ΔE_0	ϕ (x 10^3)^a	ε^2(x 10^5)^a
10°						
A	2.74	1.21	.0055	-15.	.310	.370
B	2.72	1.06	.0039	-19.	.404	.491
C	2.71	0.700	.0033	-19.	.328	.394
54.75°^{b}						
D	2.73	1.34	.0068	-17.	.509	.649
70°						
E	2.76	1.52	.0061	-15.	.311	.377
80°						
F	2.74	1.50	.0068	-19.	.394	.473

Two-Shell Fits:^{c} (1) Mn-Mn at 2.73 Å; (2) Mn-Mn at 2.86 Å

Angle	R1	R2	N1	N2	ΔE_0^{d}	ϕ (x 10^3)^a	ε^2(x10^5)^a
10°							
A	2.73	2.86	.742	.473	-11.	.153	.305
B	2.72	2.85	.805	.433	-15.	.250	.509
C	2.72	2.86	.594	.293	-13.	.171	.342
54.75°^{b}							
D	2.71	2.85	.737	.542	-13.	.258	.549
70°							
E	2.74	2.87	.847	.589	-11.	.147	.298
80°							
F	2.72	2.86	.781	.592	-15.	.196	.392

[a]Best fit parameters as defined in equations 3.4 and 3.5. [b]Data at 54.75° are an average of two data sets of unoriented samples. [c]Debye-Waller factors were fixed for both shells at 0.0005. [d]ΔE_0 for the second shell was fixed to be equal to that of the first shell.

Table 4.2 Fits to peaks II and III of oriented annealed ammonia-treated PS II
Three shells: (1) Mn-Mn at 2.73 Å; (2) Mn-Mn at 2.86 Å; (3) Mn-Mn at 3.3 Å[a]

Angle	R1	R2	R3	N3	$\sigma^2(3)$	ΔE_0[b]	ϕ (x 10^3)[c]	ε^2(x 10^5)[c]
10°								
A	2.73	2.86	3.34	1.08	.0072	-10.3	.187	.192
B	2.72	2.86	3.31	.814	.0084	-13.1	.303	.317
C	2.74	2.89	3.34	.986	.012	-9.9	.077	.083
54.75°[d]								
D	2.72	2.86	3.32	.808	.0091	-10.1	.269	.280
70°								
E	2.75	2.88	3.35	.640	.0044	-9.4	.155	.162
80°								
F	2.74	2.88	3.34	.629	.0051	-11.1	.278	.302

[a]Coordination numbers and σ^2 (=0.0005) for shells 1 and 2 are fixed to their values from Table 4.1. [b]ΔE_0 values for shells 2 and 3 were fixed to be equal to that of the first shell. [c]Best fit parameters as defined in equations 3.4 and 3.5. [d]Data at 54.75° are an average of two data sets of unoriented samples.

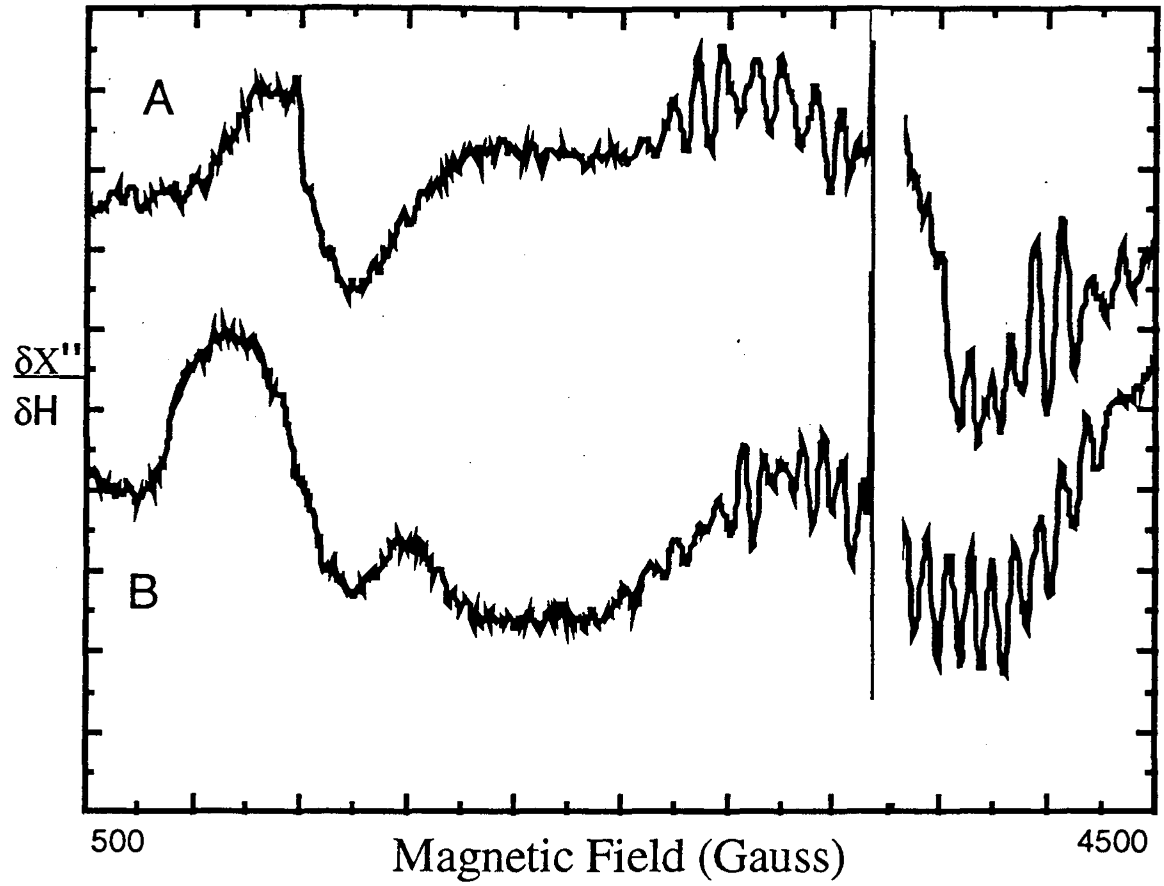

Figure 4.1: LIght minus dark EPR spectra of ammonia-treated PSII (A): after illumination at 195 K and (B): after annealing 60 s at 4°C. Instrument parameters: sample temperature 20 K, microwave power 30 mW, microwave frequency 9.215 GHz, magnetic field modulation frequency 100 kHz, modulation amplitude 32 G.

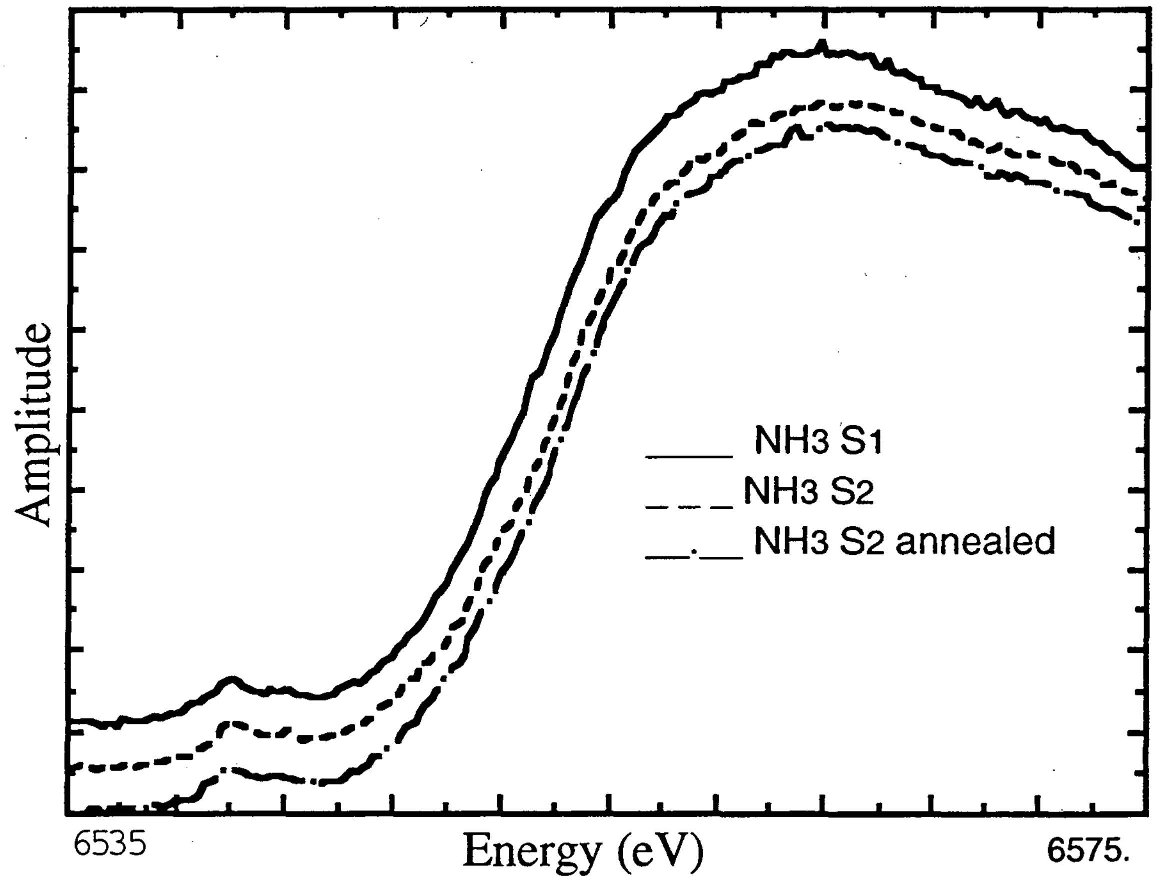

Figure 4.2: Mn K-edges of ammonia-treated PS II in the (___) S1 state; (_ _) S2 state; and (_._) S2 annealed state.

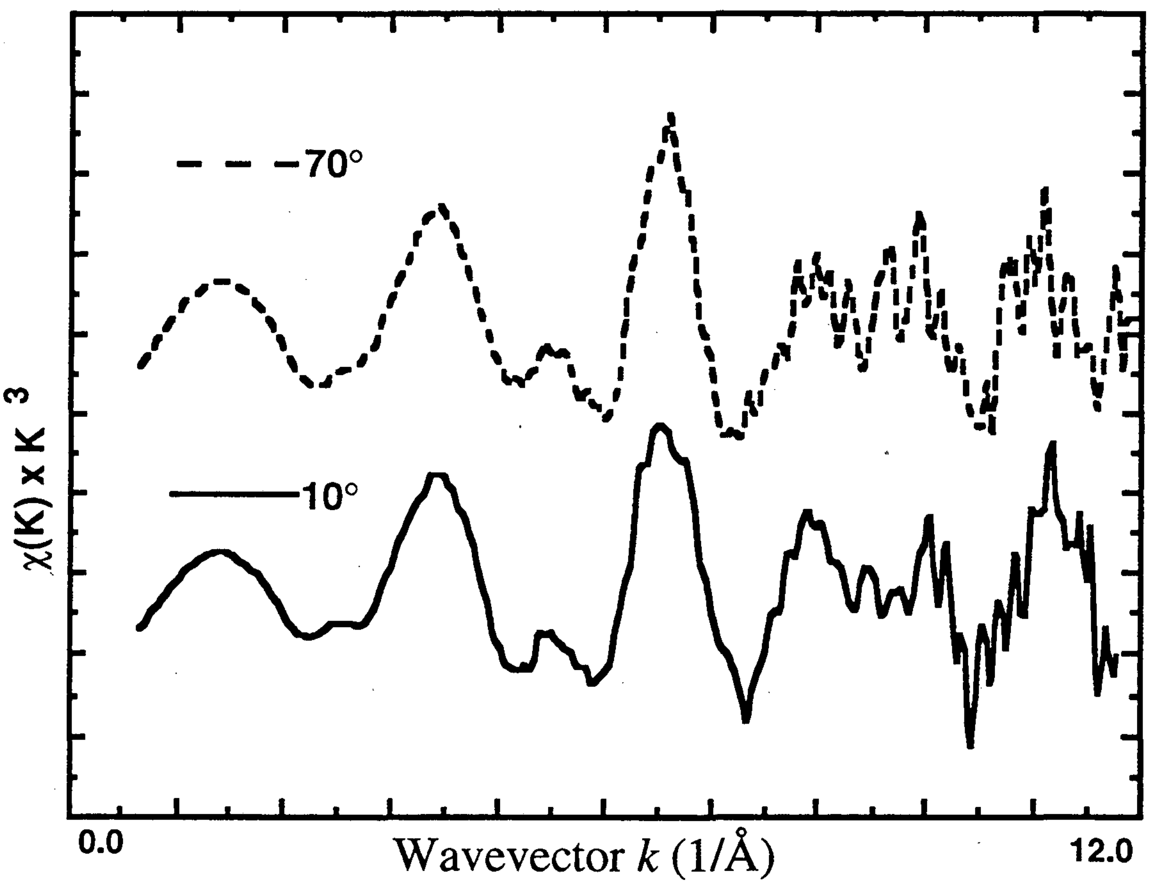

Figure 4.3: *k*-space of oriented annealed ammonia-treated PS II at (___) 10° and (_ _) 70° of the membrane normal with respect ot the x-ray e-field vector. Data are weighted by *k* cubed.

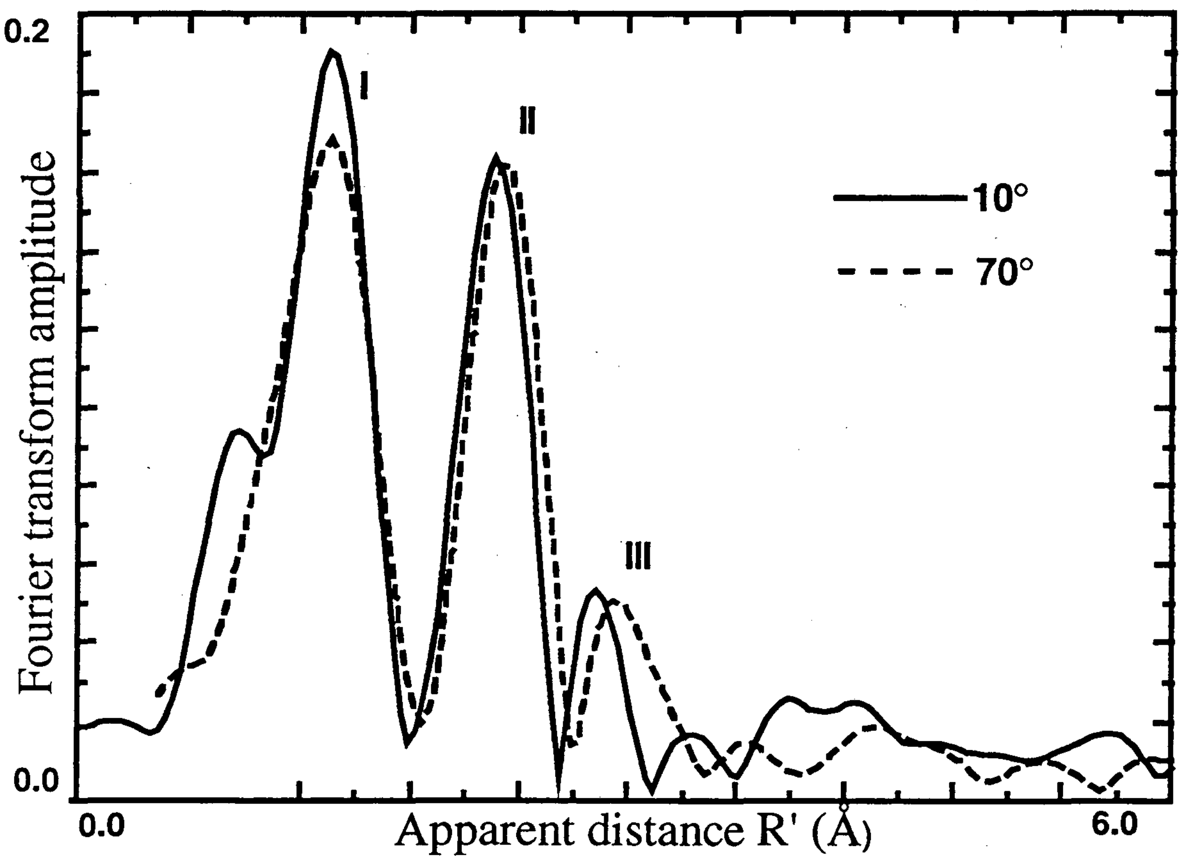

Figure 4.4: Fourier transforms of Mn EXAFS of oriented ammonia-treated PS II at 10° (___) and 70° (_ _).

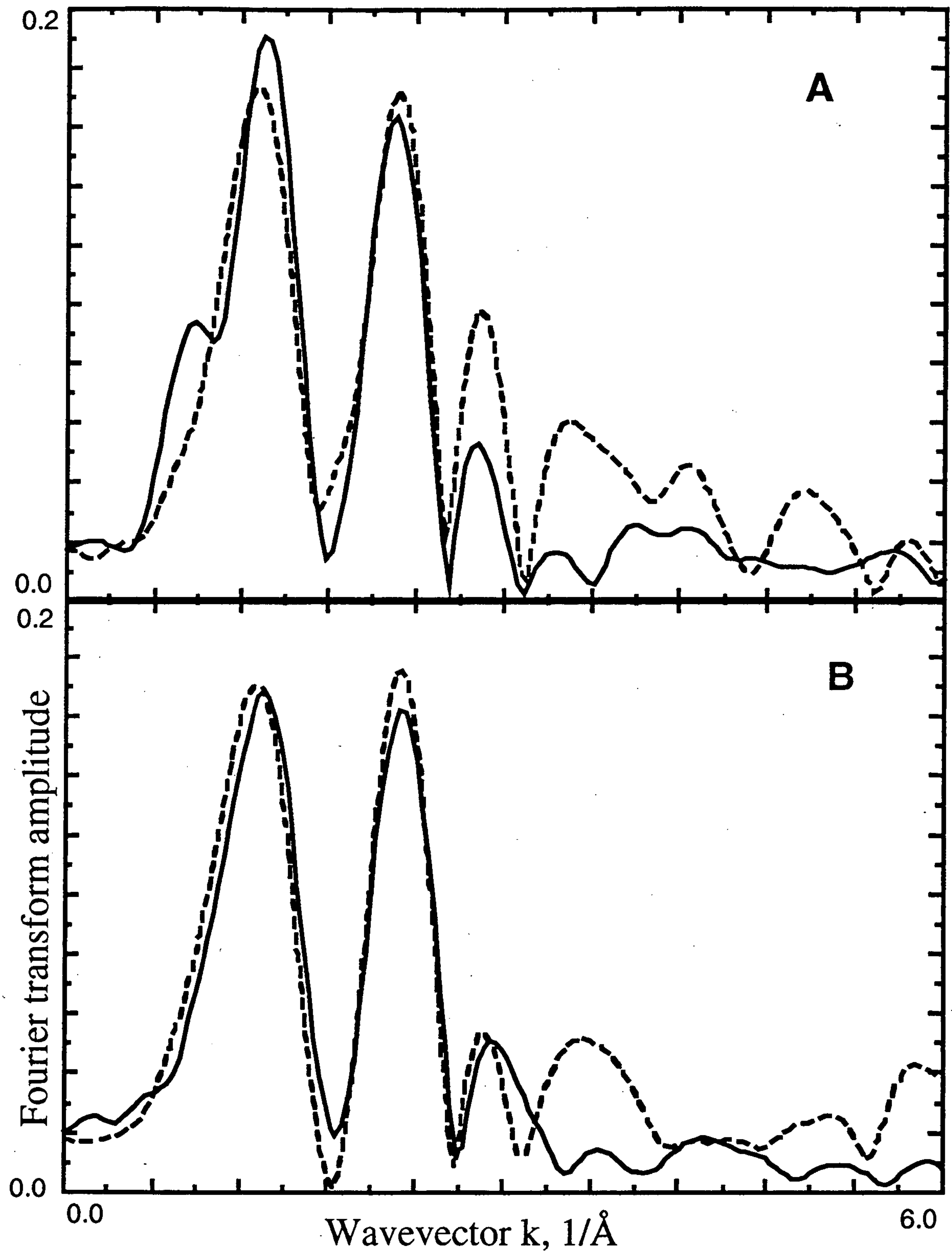

Figure 4.5: Fourier transforms of ammonia-treated PS II (___) vs. native PS II (_ _).
A: 10° B: 70°

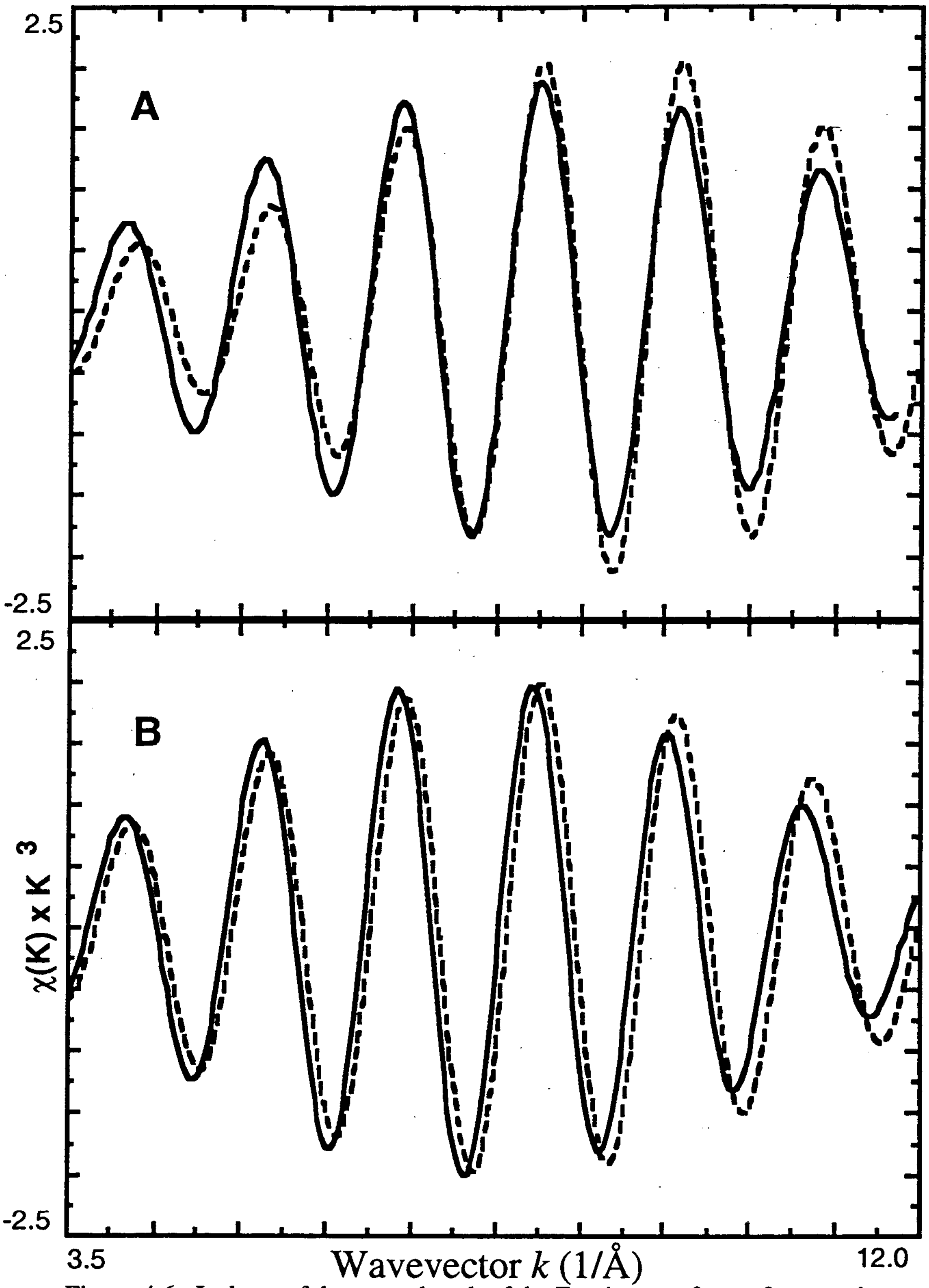

Figure 4.6: Isolates of the second peak of the Fourier transform of ammonia-treated PS II (____) and native PS II (_ _). A: 10° B: 70°

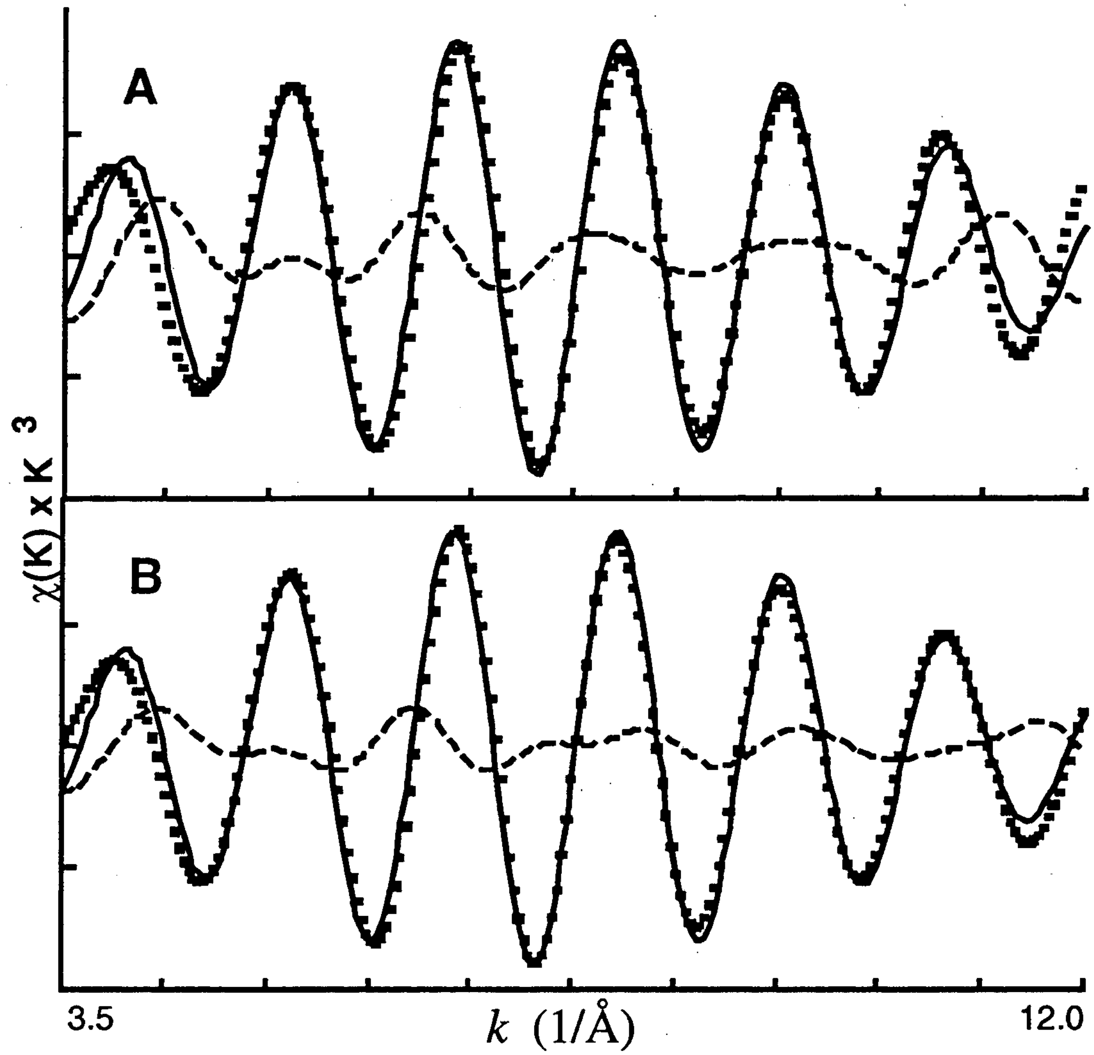

Figure 4.7: Fits to isolate of the second peak of ammonia-treated PS II, 70°.
A: one-shell fit ; B: two-shell fit. Dotted line is plot of fit residual. .

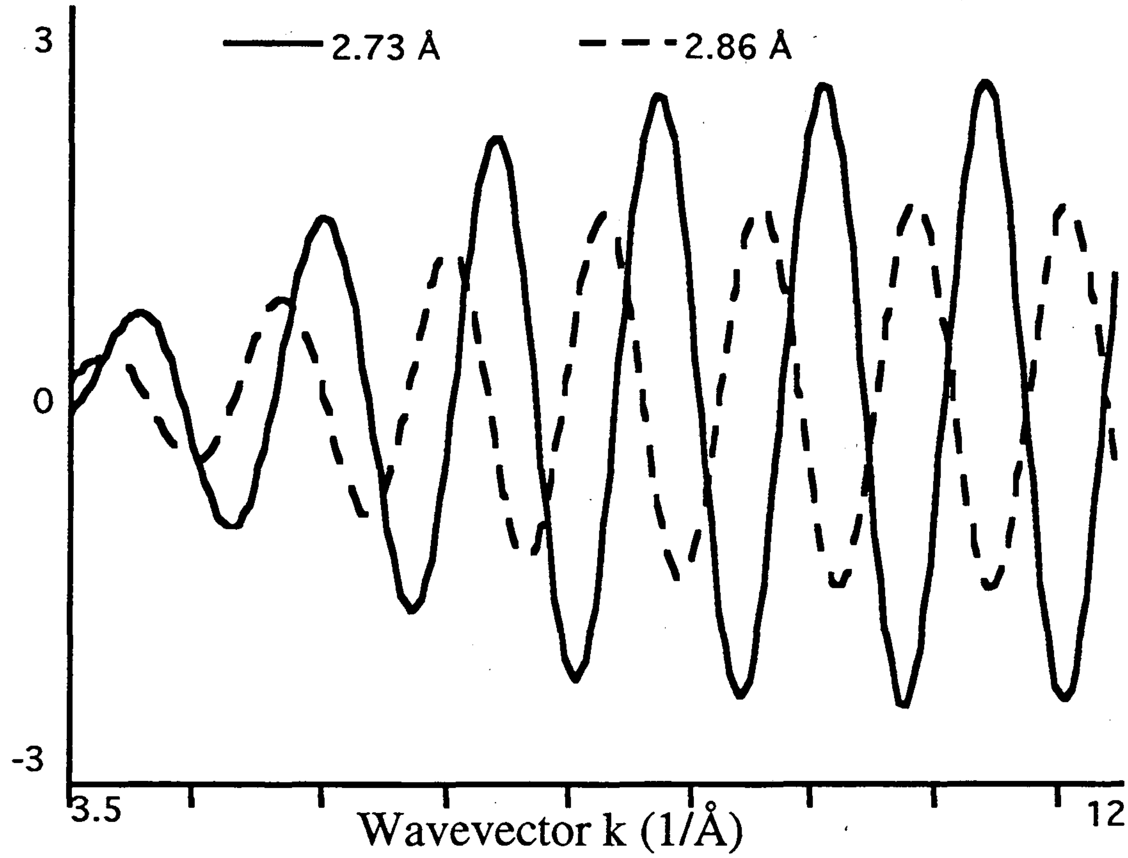

Figure 4.8: Separate shells of 2.73 Å (___) and 2.86 Å (_ _) for fit to isolate of the second Fourier transform peak of ammonia-treated PS II, 70°.

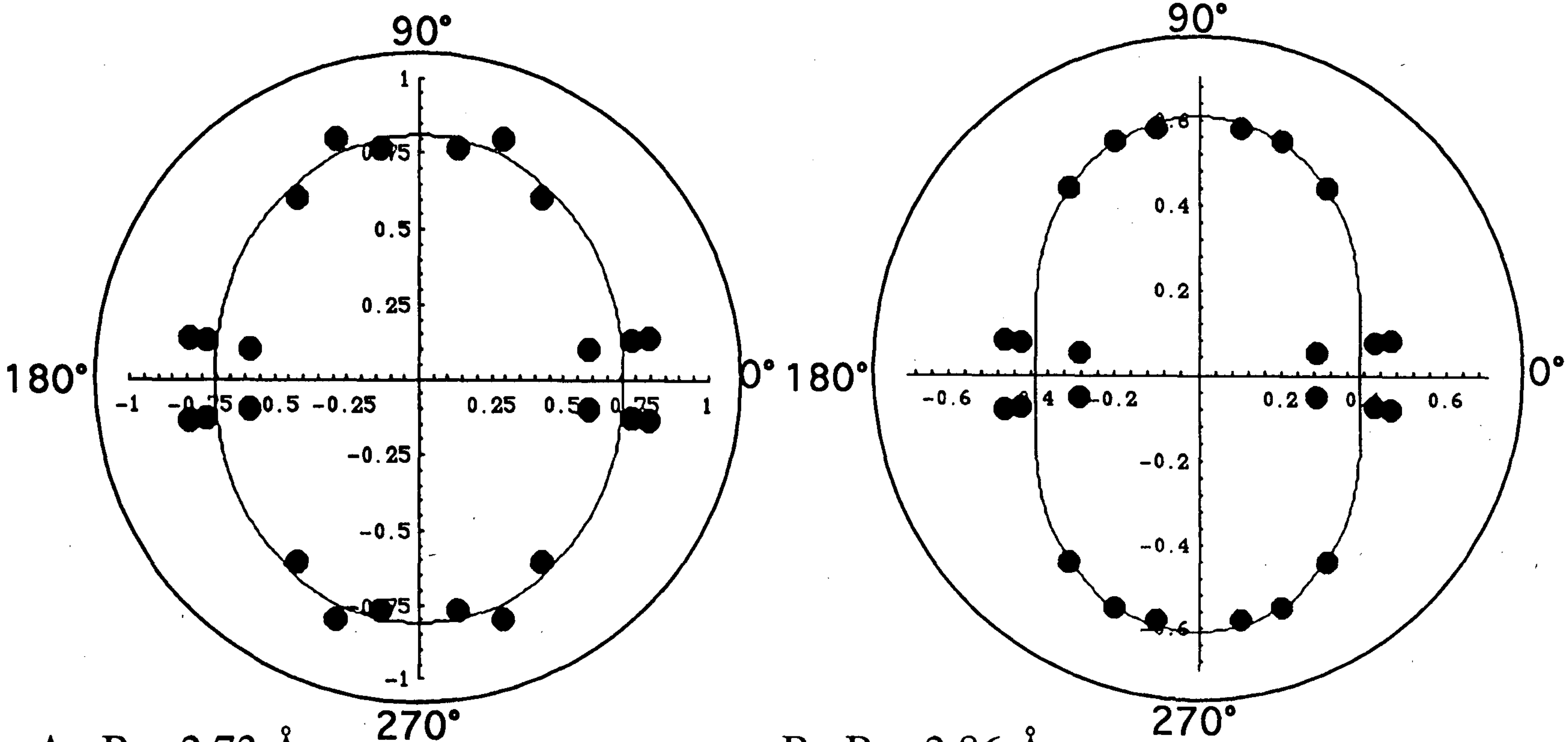

A: R = 2.73 Å
$<\Phi> = 53.9 \pm 4.9°$
$\textit{Nisotropic} = 0.78 \pm .11$

B: R = 2.86 Å
$<\Phi> = 60.7 \pm 4.5°$
$\textit{Nisotropic} = 0.54 \pm .09$

Figure 4.9: Fits of Napparent(θ) to equation 4.1 for the second peak of ammonia-treated PS II. Original data in the first quadrant is mirrored into quadrants 2 -4.

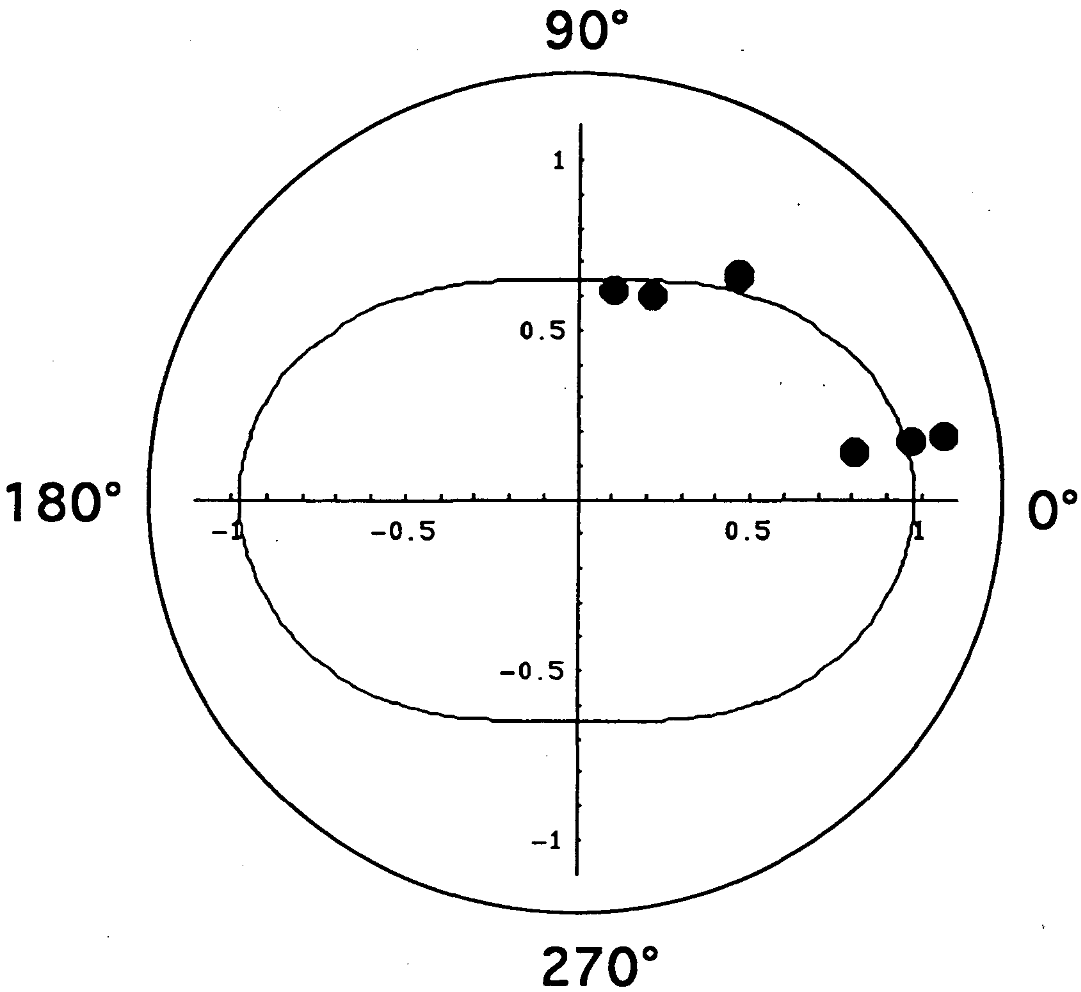

Third peak: R=3.3 Å
$<\Phi> = 41.0 \pm 6.4°$
Nisotropic $= 0.76 \pm .11$

Figure 4.10: Fits of Napparent (θ) to equation 4.1 for the third peak of ammonia-treated PS II.

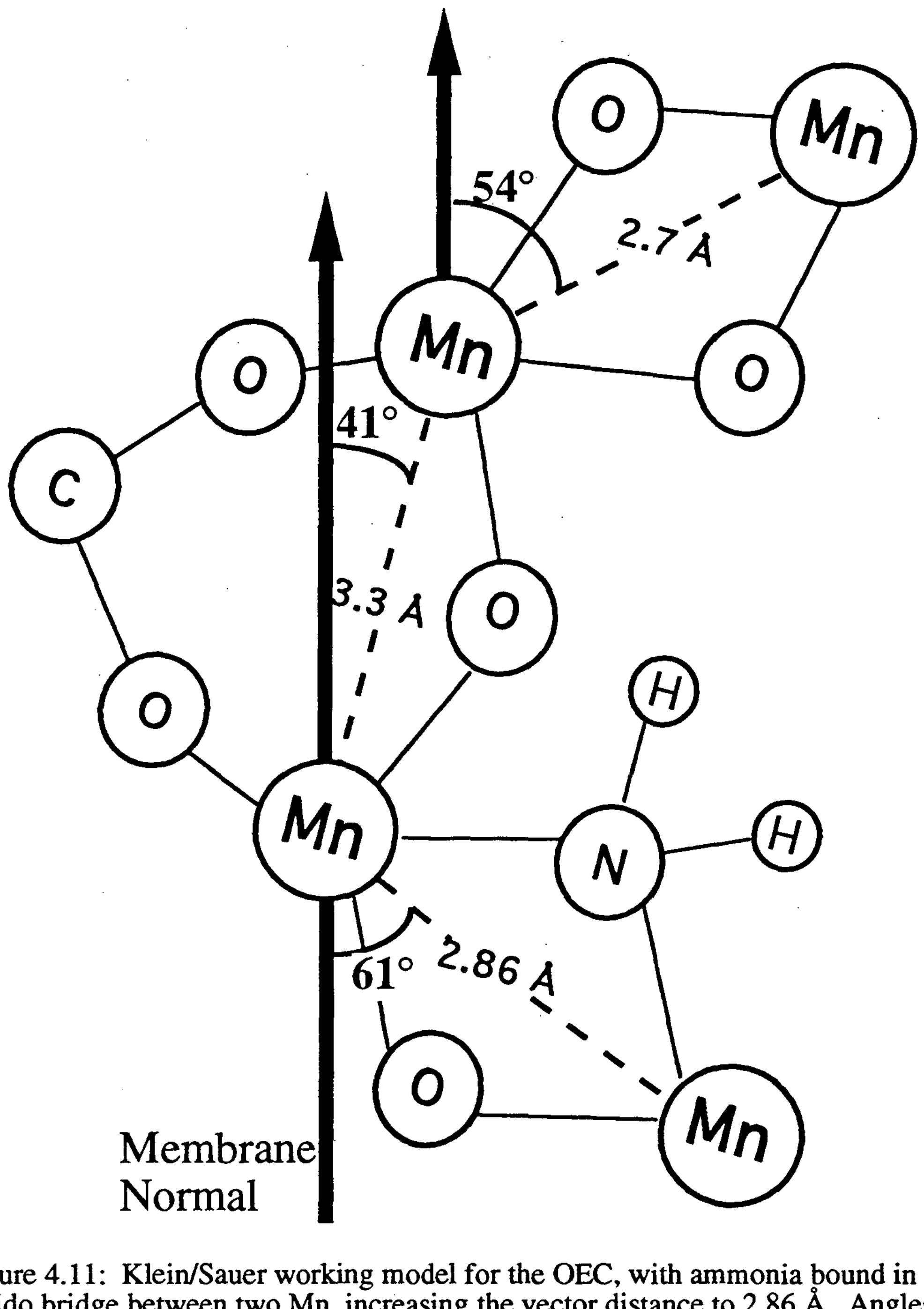

Figure 4.11: Klein/Sauer working model for the OEC, with ammonia bound in an amido bridge between two Mn, increasing the vector distance to 2.86 Å. Angles with respect to the membrane normal are 41° for the Mn-Mn 3.3 Å vector (probably an average of the Mn-Mn interaction at 3.3 Å and another interaction), 54° for the Mn-Mn 2.73 Å vector, and 61° for the Mn-Mn 2.86 Å vector. The arrangement of these components may be different from that drawn.

Chapter 5:

Studies of Halide Binding to Mn: Cl K-edge and Mn EXAFS of Mn-Cl Model Compounds, and Mn EXAFS of Oriented Br-Treated Photosystem II

Introduction

Background on the Role and Presence of Chloride in PS II

As early as 1944, it was found that chloride (Cl^-) is an essential cofactor for oxygen evolution in photosystem II (PS II). Warburg & Lüttgens (1944) found that chloride reactivated oxygen evolution activity in water-washed broken chloroplasts. After a period of contradictory results (Arnon & Whatley 1959; Clendenning & Ehrmentraut 1950) the finding of Warburg & Lüttgens was confirmed by Bové et al. (1963), who proposed that Cl^- may act as an electron carrier in the water oxidation process. Izawa et al. (1969) found that chloride accelerated the Hill reaction (O_2 evolution in the presence of an external electron acceptor) over a wide pH range in EDTA-treated spinach chloroplasts. They also found that Cl^- was required specifically for the oxidation of water. Kelly & Izawa (1978) found that O_2 evolution was almost completely inhibited in the absence of Cl^-.

Depletion of chloride is thought to create a lesion in the electron transport between the oxygen evolving complex (OEC) and Z, a tyrosine radical (Itoh et al., 1984; Theg et al., 1984). Cl^- can be replaced by various anions, in the order $Cl^- \geq Br^- > NO_3^- \geq I^- \geq HCOO^- \geq HCO_3^- > F^-$, with F^- replacement resulting in almost complete inhibition of O_2 evolution (Critchley et al., 1982). Replacement of Cl^- with Br^- restores normal oxygen evolution activity (Ono et al., 1987; Haddy & Vänngård, 1990; Kelly & Izawa, 1978; Yachandra et al., 1986), and replacement with I^- results in ~50% of normal activity (Rashid & Homann, 1992). It is known that Cl^- requirements are dependent on the presence of the 23 kDa protein associated with PS II. Critchley et al. (1984) have shown that after removal of the 17 and 23 kDa proteins and depletion of Cl^-, re-addition of the 23 kDa protein resulted in a 50-fold less requirement for Cl^- (2.5 mM vs. 100 mM) to regain full O_2 evolution activity.

Several roles have been proposed for chloride: (1) ligation to Mn, taking an active role in the advance of the Mn complex through the various S-states in the Kok cycle (Wydrzynski & Sauer 1980) (2) a structural role, anchoring the OEC in an active conformation in the protein matrix (Johnson et al., 1983) (3) facilitation of protonation / deprotonation events which occur during the Kok cycle (Homann, 1985) (4) neutralization of the positive charges which accrue on the Mn atoms (Dismukes, 1986; Govindjee, 1984).

Ono et al. (1986) have shown that PS II particles which have been depleted of chloride do not have an EPR multiline signal in the S_2 state . There is, however, a large signal at g = 4.1, indicating that some sort of S_2 state is formed. They found that the S_2 state can be formed in the absence of chloride, and subsequent addition of chloride after illumination results in an EPR multiline signal. However, in this case the OEC can no longer advance to higher S-states. It has also been found that, in the absence of chloride, the OEC can accumulate oxidizing equivalents (Muallem et al,. 1981) but there is no oxygen evolution. A total of three charge separations are thought to be facilitated by electron donors: first by the Mn complex during the S_1-S_2 transition, and subsequently by cyt b_{559} and Z (Itoh et al., 1984; Theg et al., 1984).

Oxygen evolution can be inhibited by some compounds which compete with the chloride binding site; e.g. fluoride (Sandusky & Yocum, 1986) and primary amines (Sandusky & Yocum, 1983; 1984; 1986). When PS II is substituted with fluoride, no multiline signal is seen in the S_2 state. There is a signal at g=4.1, however, similar to that seen in chloride-depleted PS II, but narrower by about 50 G (Beck & Brudvig 1988; Casey & Sauer, 1984). A signal at g=2 appears at concentrations of fluoride > 20 mM (DeRose et al. 1995) which is proposed to be due to a radical interacting with the Mn cluster.

Kinetic studies of inhibition of oxygen evolution in PS II done by Sandusky & Yocum (1984; 1986) have shown that primary amines also compete for the chloride binding site. They found that ammonia is an exception: in addition to binding at a chloride - competitive site, it also binds at a site which is not competitive with chloride. This second ammonia-binding site is thought to be the small sterically hindered location of water binding (Radmer & Ollinger, 1983). The degree to which the amines can inhibit oxygen evolution is directly related to their nucleophilicity (Sandusky & Yocum 1986). This implies that they bind as Lewis bases to a metal; i.e. that they are bound to Mn in an oxidation state ≥ Mn(II).

From the results of fluoride and amine replacement of chloride in PS II, it is known that the chloride binding site is electrophilic. It has been proposed by some (Bové et al., 1963; Sandusky & Yocum, 1983; 1984) that chlorine is a bridging ligand between two Mn atoms, since large soft nucleophiles activate the OEC (Cl^-, Br^-, I^-) and small, hard nucleophiles inhibit (amines, OH^-, F^-). Dismukes et al. (1988) have proposed a model in which chlorine binds to two Mn atoms as a bridging ligand. However, EXAFS studies and simulations of Br - replaced PS II indicate that there is a possibility of at most one chlorine ligand per four Mn (DeRose, 1990; Yachandra 1993). Also, in studies of oriented native PS II, George et al. (1989) found that they could not rule out the presence of 1 Cl per 4 Mn, but the interaction was so small that the requirement for Cl was not conclusive. This evidence makes a bridging conformation highly unlikely.

It is difficult to verify that chlorine may be a ligand to Mn. The fact that replacement of Cl^- by F^- changes the EPR signal (Casey & Sauer 1984; DeRose 1990,1995) and EXAFS (DeRose et al. 1995) indicates that the halide binding site is very close to Mn. Continuous-wave and pulsed EPR studies have shown no change when Cl^- is replaced with Br^- (Boussac, 1995; DeRose 1990; Homann 1988; Ono et al. 1986; Yachandra et al. 1993). However, based on simulations, the couplings are predicted to be indistinguishable by pulsed EPR (Reijerse et al. 1987; Wang et al. 1992). EXAFS of Br - replaced PS II were inconclusive as well (DeRose 1990; Yachandra et al. 1993). It may be possible to enhance the EXAFS of the Mn-Cl interaction with studies of <u>oriented</u> Br-treated PS II. Bromine has a significantly different backscattering amplitude function than chlorine (see Fig. 5.1) which enhances the interaction, especially at high *k* values. Oriented XAS has the advantage that it can select for vectors at or near a particular angle. By orienting the PS II membranes and varying the angle between the X-ray **e**-vector and the membrane normal of the sample, it may be possible to select for the particular Mn - halide vector(s) among the many other vectors.

Background on the Properties of Halides

Table 5.1 lists various properties of halides. The ionic radii, covalent radii and polarizability of the Group VII elements increase and electronegativity decreases as we go down the periodic table from F to I. For all of these properties, the values for Br are closer to Cl than F is to Cl, or Br is to I. Because the similarity in properties between Cl and Br, it is probable that PS II in which Br^- has replaced Cl^- stays very close to its native form. It has been found in Mn-halide model compounds that replacement of Cl with Br does not significantly alter the structure or magnetic properties of the complex (Wang et al. 1992). EPR spectra and oxygen evolution values for Br-treated PS II are indistinguishable from those of native PS II, in this work and others (DeRose 1990), in agreement with this proposal. Thus, with such a replacement one can hope to enhance the Mn-halide interaction without disturbing the OEC.

Examination of a series of Mn-halide model compounds (see table 5.1) reveals that bond lengths for terminal Mn-Cl bonds range from 2.12 to 2.61 Å, and for bridging Mn-Cl bonds they range from 2.61 to 2.77 Å. Mn-Br terminal and bridging bond lengths range from 2.47 - 2.73 Å and 2.60 - 2.85 Å, respectively. Some of the longer bond distances are seen for Mn(III) - halide bonds due to Jahn-Teller distortion.

Background on ligand X-ray absorption spectroscopy

A method which can be used to explore ligand-metal bonding is ligand XAS. Hedman et al. (1990) performed Cl K-edge studies of $CuCl_4^{-2}$ in which they found that the pre-edge feature gave information on the degree of covalency in the Cl-metal bond.

They proposed that the pre-edge feature in the Cl K-edge spectrum is due to a forbidden 1s to 3d transition, which becomes allowed due to mixing of ligand p-orbitals with metal d-orbitals (Cu in this case). The pre-edge feature is not present when chlorine is not ligated to a transition metal. Since the pre-edge feature is well separated from the main inflection point, contamination with some free chloride will not interfere with observing the pre-edge feature. In a related study at the S K-edge of plastocyanin Shadle et al. (1993) showed that the pre-edge feature due to the S ligated to Cu is observable despite the presence of two other types of S interactions in the protein. Ligand XAS has also been used to investigate halide-metal binding in Cu(II), Ni(II), Co(II), Fe(II) and Fe(III) complexes (Shadle et al. 1995), and in photographic materials (Smith et al. 1994).

In order to investigate possible ligation of Mn to the OEC, it is helpful to know more about the nature of halide bonding to Mn. Therefore, in this study we will look at Mn K-edge EXAFS and Cl K-edges of several Mn-halide model compounds, as well as Mn EXAFS results of oriented Br-treated PS II. With these methods we will explore the nature of the halide site in PS II.

Materials and Methods

Model compounds containing both Mn and Cl were obtained from the laboratories of George Christou at Indiana University and Vincent Pecoraro at the University of Michigan, Ann Arbor.

The preparation of PS II from spinach was done with a modified procedure of Berthold et al. (1981). In this modified procedure, the incubation in Triton was done for 15 min rather than 30 min. It was found that these slightly more intact PS II preparations were less subject to degradation after treatment with fluoride.

Treatment of PS II to replace Cl^- with F^- and Br^-

To replace the chloride in PS II with bromide, a series of wash steps were done, all in buffers with 400 mM sucrose and 50 mM MES adjusted to pH 6.0. The first two washes were in successively lower chloride concentrations: first in 5 mM $CaCl_2$ and 20 mM $MgSO_4$ (to keep ionic strength constant), and second in 1 mM $CaCl_2$ and 24 mM $MgSO_4$. Replacement of Cl^- with F^- was accomplished by three washes in 50 mM NaF. Replacement of F^- with Br^- was accomplished by washing first in 30 mM NaBr, 5 mM $CaBr_2$ and 5 mM $MgBr_2$, then in 1 mM $CaBr_2$ and 5 mM $MgBr_2$. The Mg^{+2} was helpful in allowing stacking of the membranes during the orientation procedure. To avoid release of Mn^{+2}, the F^- washes were done as thoroughly and quickly as possible. After the washes in F^- buffer, Cl control samples were made alongside the Br samples by washing in 30 mM NaCl, 5 mM $CaCl_2$ and 5 mM $MgCl_2$, then in 1 mM $CaCl_2$ and 5 mM $MgCl_2$. Oxygen evolution and EPR signals were monitored during this process to verify replacement of the Cl^-. F^-treated PS II had O_2 activity and EPR MLS height of 10-15% of the original samples. Replacement of fluoride with bromide resulted in O_2 activities and EPR MLS of 90-100% of the original.

Orientation of Samples

Br-treated samples were oriented by painting of thin layers onto mylar tape, as described by Rutherford (1985). Orientation of samples was checked by looking at the EPR spectra of Signal II in the dark at 0° and 90° (see Chapter 2), and mosaic spread was verified by comparison of the cyt b_{559} EPR signal measured from 0° - 360° with simulations (Blum et al. 1978).

Mn EXAFS data collection and analysis

Mn EXAFS data collection was done as described in Chapter 3, on beamline 7-3 at SSRL and on beamline X-9B at NSLS, using a Si <220> monochromator. Mn K-edges of Br samples required a mirror to reduce the amount of harmonics, to avoid attenuation of the Mn EXAFS by absorption by Br at half the energy of the Br K-edge (13.47 keV). This effect results in a dip in the Mn EXAFS at about 6735 eV due to absorption of the second harmonic by Br. The in-hutch mirror used on beamline 7-3 at SSRL was designed and built by Latimer et al. (1995). There is a built-in mirror after the monochromator at beamline X-9B at NSLS. Mn K-edge EXAFS of PS II and model compounds were run at 10 ± 1 K.

EXAFS data analysis and background correction was done as described in chapter 3. For consistency in data analysis, a constant E_0 value of 6563.0 eV was used for all Br and control samples, regardless of orientation. Fitting was done with theoretical phase and amplitude functions prepared with FEFF 5 (Rehr et al. 1992), as described in chapter 4. For model compounds and PS II, a window of R = 1.0 to 4.0 Å (the first four Fourier transform peaks or so) was used for comparison of the main features, and for fits of the model compound data. For PS II, fits were done to isolates using various windows, but fits to back transforms of Fourier peaks II and III together (R = 1.8 to 3.9 Å) are shown. Error analysis was done using the equations of Binsted et al. (1992) as described in chapter 3. When fitting to more than one shell of backscatterers, a single value for ΔE_0 was used. This has been shown to be an appropriate method for fitting multiple shells using FEFF 5 (O'Day et al. 1994).

Collection of Cl K-edge data

Collection of Cl K-edge data was done on beamline 6-2 at SSRL, with a setup as described by Hedman et al. (1988) and Shadle (1994a). A 54-pole wiggler magnet was used, with a Pt-coated focusing mirror and a Si<111> crystal monochromator. A He flight path was used to avoid attenuation of the low-energy beam by N_2 and O_2. The sample chamber was enclosed in He as well, with thin polypropylene windows between the flight path and sample box, and between the sample box and detector. Collection with a Lytle detector (Stern et al. 1976) was done at room temperature. A small amount of model compound was ground and put onto mylar tape. The compounds were run at successively lower concentrations until a constant spectrum was obtained, to avoid loss of resolution due to self-absorption of the sample. Scans were run from 2710 to 3100 eV, with a step size of 0.08 eV from 2810 to 2850 eV to obtain good resolution in the pre-edge and edge regions. Simultaneous collection of a standard compound for calibration was not possible, as very little beam is transmitted through the samples and mylar tape. Therefore samples of $(Et_4N)_2MnCl_4$ were collected between measurements of other model compounds. The pre-edge position of $MnCl_4^{-2}$ was calibrated with thiosulfate, which has a pre-edge energy of 2472.02 eV (Shadle 1994). The thiosulfate sample was run when the beamline was set up for use with sulfur immediately after measurement of the Cl samples. After correction for the thiosulfate standard, the $MnCl_4^{-2}$ pre-edge position was determined to be at 2824.80 eV, and this value was used to correct the edge positions of the Cl compounds. Background removal and normalization of the Cl K-edge spectra were done as described in chapter 3. Pre-edge positions were determined as the zero-crossing of the first derivative in the pre-edge region. Edge inflection points were calculated as the maximum of the first derivative of the spectrum.

Results

Cl K-edges of Mn-Cl Model Compounds

Cl K-edges were run on a variety of model compounds. Figure 5.2 shows the Cl K-edges of (A) KCl; (B) $NaClO_3$; and (C) $NaClO_4$, and their edge inflection point energies are listed in Table 5.2. A successively higher edge energy position is seen as the oxidation state of Cl increases from -1 for KCl (2826.01 eV), to +5 in ClO_3^- (2830.99 eV), to +7 in ClO_4^- (2835.05 eV). Increases in amplitude are also seen as the oxidation state increases, due to the greater number of hole states. The edge energy positions are different from those found by Shadle (1994a), (edges were 2824.8, 2830.5 and 2833.7, respectively). These differences should not be due to self-absorbance, because in both studies successively thinner samples were prepared and measured until the spectra remained constant. Differences are seen in the edge shape as well as edge position, and more features are resolved in the present work. Another compound containing free chloride, $MnCl_2 \cdot 2H_2O$, has the same edge position as KCl. (Figure not shown, edge positions listed in Table 5.2).

Figure 5.3 shows the Cl K-edges for three compounds which have the same Mn-Salpn [SALPN = 1,3 bis(salicylideneiminato)propane] basic structure (see Fig 5.3a). In compound I (Fig 5.3b), Mn(III)(5-Cl Salpn), Cl is bound to the 5-position on the phenyl ring (Larson et al. 1991). A large peak is seen in the edge at 2825.52 eV, probably due to a 1s to 3p transition of Cl mixed with the π system of the phenyl ring. Because this is an allowed transition, the amplitude is high. This feature is seen in the Cl K-edges of other compounds in which Cl is bound to a phenyl ring, one of which is shown in Figure 5.4(D). The edge feature in the latter spectrum is at 2825.56 eV, very close to the energy of the feature in Fig 5.3b for compound I.

In compound II, Mn(III)Cl Salpn (Pecoraro & Butler 1986), Cl is bound to Mn(III), parallel to the Mn-Salpn (approximate) plane. A small pre-edge peak is seen at 2823.26 eV, and the edge inflection point is at 2825.81 eV. The small pre-edge feature is due to a forbidden 1s-3d transition, seen due to mixing of Mn 3d orbitals with Cl 3p orbitals. For compound III, Mn(IV)Cl_2Salpn (Pecoraro, V. L., unpublished work), there are two Cl atoms bound to Mn(IV), one above and one below the Mn-Salpn plane. Two pre-edge features are present at 2820.67 and 2822.81 eV, due to these two distinct covalent interactions. The edge energy for this compound is at 2824.74 eV. This edge position, which is lower than that of compound II, indicates that the effective charge on the Cl in the Mn(IV) compound (compound III) is less than that for the Cl in the Mn(III) compound (compound II). For a single Cl bound to Mn(IV), we would expect to see a higher edge energy than for a single Cl bound to Mn(III) due to additional electron withdrawal by Mn in the higher oxidation state. In the case of two Cl atoms bound to Mn(IV), however, the electron donation is split between two Cl, and thus the edge energy for the Mn(IV)Cl_2 compound is lower than that for the Mn(III)Cl compound.

The edge inflection point of Cl bound to a phenyl ring, as seen in compound I of Fig 5.3b and compound D of Fig 5.4 (noted in Table 5.2), is 2824.8 eV. This is lower than that seen for Cl bound to Mn, for example in compounds A, B and C in Fig 5.4 (2826

- 2827 eV). This is because the phenyl ring is an electron-rich environment, and the Cl does not donate much electron density to the ring. Cl bound to a metal in a high oxidation state, Mn(III) in the case of compounds A, B, and C, donates more electrons to the electron-poor metal environment, and the higher Cl effective charge is reflected in the higher edge energy.

The Cl K-edges of a series of cubic Mn-Cl compounds are shown in Fig 5.4. The core structure of these compounds, a distorted cubane with a μ_3-Cl-bridge to 3 Mn(III) with a fourth Mn(IV) atom at the apex, is shown in Fig 5.5A. Compound A of Fig 5.4, $Mn_4O_3Cl(O_2CMe)_3(dbm)_3$ [dbm = dibenzoylmethane] (Wang et al. 1991) has 3 pre-edges, at 2821.21, 2822.48, and 2823.92 eV. These 3 features are due to the Cl bridging interactions with 3 different Mn(III) atoms. Compound B, $Mn_4O_3Cl_4(O_2CMe)_6(py)_3$ [py = pyridine] (Wemple et al. 1993a), has a μ_3 bridging Cl plus 3 terminal Cl ligands (see Fig 5.5B for the core structure). In the Cl K-edge of this compound (Fig 5.4B) there are three pre-edge peaks as in compound A, but there is an increase in the amplitude of the first pre-edge peak relative to the second and third pre-edge peaks, due to the addition of terminal Cl-Mn interactions. The peak positions are given in Table 5.2. The terminal Cl ligand interactions have a pre-edge at a slightly lower energy than the first bridging pre-edge peak, as indicated by the slight decrease in energy of the first pre-edge peak from 2821.21 eV in compound A to 2821.12 in compound B. Shadle et al. (1994b) found that terminal ligands have less charge donation to a metal than bridging ligands; thus it is reasonable that the pre-edge transition due to the terminal ligands occurs at a lower energy than that for the bridging ligands. Compound C, $(Hpy)_3[Mn_4O_3Cl_7(O_2CMe)_3]$ (Schmitt et al. 1992) has 6 terminal Cl atoms, plus the μ_3 bridging Cl, much like the structure of compound B but with 2 Cl bound to each Mn(III) atom. It has 3 pre-edge peaks, and the first is further increased in amplitude relative to that of compounds B and A due to the contribution of additional terminal Cl ligands. The first pre-edge peak also has an even lower energy (2821.08 eV) than that of compound A or B, indicating a further contribution of the lower-energy Cl-Mn terminal ligand contribution. Compound D, $Mn_4O_3Cl_4(O_2CPh$-3,$5Cl_2)_3(py)_3$ (Wemple et al. 1993a) has one μ_3 bridging and 3 terminal Cl as in compound B, with the addition of 2 Cl bound to each of the phenyl rings. As seen in Fig 5.3 (compound I) and mentioned above, the Cl-phenyl π interaction produces a 1s-3p transition with high amplitude at about 2825 eV. The three pre-edge features are similar to those of compound B, although the feature at highest energy is hidden by the large 1s-π^* transition.

Mn EXAFS of Mn-Cl Model Compounds

The *k*-space data of the Mn EXAFS for the three model compounds shown in Fig 5.5 are shown in Fig 5.6, with *k*-space data from PS II from spinach in the S_2 state shown for comparison (Fig 5.6D). The first compound, shown in Fig 5.6A, $Mn_4O_2Cl_2(O_2CPh$-3,$5F_2)_6(py)_4$, (Wemple et al. 1993b) (sometimes called the butterfly; core structure shown in Fig 5.5C), is distinctly different from PS II, as all the peaks are different in amplitude and position. This is verified in the Fourier transform (Fig 5.7A), which shows a third peak much larger than that for PS II (Fig 5.7D). This is due to the eight Mn-Mn interactions at about 3.3 Å in this compound, vs. two in the Klein-Sauer model for PS II. Fits to this compound are useful for this project because, for the four Mn present, there are only two terminal Cl ligands. This is twice the ratio we expect for the OEC (1 per 4 Mn) but it is the closest available at this time. Fits to the back transform of R ≈ 1.0 to 4.0 Å for this compound are shown in Table 5.3. There are 9 Mn-O interactions at about 1.8 Å, and 9 N and/or O interactions at about 2.1 Å as seen in the crystal structure (Wemple et al. 1993b), and the fitting is improved when they are fit as two separate shells. The crystal structure distances are given in Table 5.3 as well. The fit error ϕ was 3.16×10^3 and ε^2 was 2.16×10^5 for a fit with a single Mn-O shell (not shown), vs. 1.73×10^3 and 1.37×10^5 for the two shells for the low-Z scatterers. In both cases, Mn-Mn at 2.8 Å and 3.3 Å were included as well. There is significant improvement in the fit error when we compare a fit to 4 shells (Mn-O at 1.9Å, Mn-O at 2.1 Å, Mn-Mn at 2.8 Å and Mn-Mn at

3.3 Å) vs. 5 (Mn-Cl added at 2.3 Å). The latter fit has fit parameters of 0.929 x10^3 and 0.799 x10^5, respectively, a significant improvement over the 4-shell fit parameters. This demonstrates that, even with a large number of Mn-Mn and Mn-O interactions, two Mn-Cl interactions are still significant, and are required for a good fit. The Mn-Cl interactions in this compound fit to 2.317 Å. This is ~0.03 Å higher than the 2.296 and 2.287 Å from the crystal structure data.

For the second compound, $Mn_4O_3Cl_4(O_2CPh\text{-}3,5Cl_2)_3(py)_3$ (core structure shown in Fig 5.5B), the *k*-space data (Fig 5.6B) and Fourier transform (Fig 5.7B) are also different from that for PS II. The Fourier transform shows a large second peak, wider than that of PS II, and the first peak is much smaller that than that for PS II. The fits for this compound (Table 5.3) improve from three shells (Mn-O at 1.9 Å, Mn-Mn at 2.8 Å and Mn-Mn at 3.2 Å) to four, with the addition of a shell of the 3 Mn-Cl bridging ligands at 2.6 Å. However, upon the addition of the three terminal Mn-Cl interactions at 2.1 Å, there is no improvement in the fit parameters over the four-shell fit. Inclusion of the 3 terminal Mn-Cl interactions as a fourth shell (fit not shown) did not improve the fit parameters over the 3-shell fit. Thus, in this case, the bridging Mn-Cl interactions contribute more to the EXAFS than the terminal Mn-Cl interactions, even though the coordination numbers are the same for both interactions. The Mn-Cl distances fit to ~2.58 Å for bridging Cl and 2.13 Å for terminal Cl ligands. These are lower than the distances from the crystal structure by about 0.05 and 0.1 Å, respectively.

The third compound, $Mn_4O_3Cl(O_2CMe)_3(py)_3$ (Fig 5.5A) has *k*-space data (Fig 5.6C) and Fourier transform (Fig 5.7C) which are the closest to PS II of the three model compounds, but the *k*-space peak positions are shifted to lower *k*, and the first two Fourier peaks are greater in amplitude than those of PS II. DeRose et al. (1995) found large differences in the *k*-space of this compound and that of PS II when back transforms of isolates from 1.8 Å to 3.5 Å were compared. A third peak was not resolved for this model compound in that work.

EPR and EXAFS of Br -treated PS II

In Figure 5.8, the *k*-space data of Mn EXAFS of Br-treated PS II are shown. The peaks at about 9 and 10 $Å^{-1}$ are slightly less resolved than those of native and Cl control oriented PS II (See Fig 3.3). Dichroism is seen in both Br and Cl samples, in these peak as well as in the peak at about 7 $Å^{-1}$: they are all greater in amplitude at 80° than at 10°. In Fig 5.9, back transforms of Fourier peaks 1 through 4 (R= 1.0 to 4.0 Å) are shown. Data from the Cl-treated control sample which was prepared from the same PS II preparation and went through the F^- washes and reconstitution is shown as a solid line, and data from Br-treated PS II is shown as a broken line. Differences are seen, but when differences from sample to sample (5 Br samples and 2 Cl samples) are taken into account, these changes are not significant. In Figure 5.10, the Fourier transforms of these data are shown. At 10° (Fig 5.10A) the Cl data (solid line) are quite similar to the Br data (broken line), but at 80° (Fig 5.10B) the Fourier transform peak amplitudes are greater for the Br sample than for the Cl sample. Again, there was variation among the samples and these differences are not significant.

In Fig 5.11, control Cl data taken at 80° are shown, plus simulations of Br data created by subtracting the partial wave for 0.25 (1 per 4 Mn) Cl at 2.2 Å (the partial waves for Cl and Br are at the bottom of the figure) and adding the partial wave for 0.25 Br at 2.6 Å (A), 2.7 Å (B), and 2.8 Å (C). ΔE_0 was taken as the same for the other shells of data (Mn-O at 1.8 Å, Mn-Mn at 2.7 Å and Mn-Mn at 3.3 Å). Differences are seen in the Br simulations vs. the Cl control data, especially in the region around 9 to 10 $Å^{-1}$. These differences vary significantly depending on the length R chosen for the Mn-Br interaction.

In Table 5.4, results of fits to peaks II and III (ΔR = 1.8 Å) of Br-treated and Cl control data are shown. Each isolate was first fit to two shells of Mn, with R starting at 2.73 A and 3.3 Å, respectively. These R values did not vary much among the fits. Debye-Waller factors for these shells were fixed at 0.0035 and 0.003 for these shells, respectively, based on a variety of fits of several types of isolates for these data and for other PS II data. Coordination numbers for these shells were fixed at 0.83 (10°) and 1.15 (80°) for the 2.7 Å Mn-Mn shell, and at 0.57 (10°) and 0.46 (80°) for the 3.3 Å Mn-Mn shell. These numbers are based on the average coordination numbers for oriented PS II (Mukerji et al. 1994) and were found to be similar for fits using either McKale tables (McKale et al. 1988) or FEFF 5 theoretical phase and amplitude functions. Fits were done from $k = 5.0$ Å to 12.0 $Å^{-1}$, to reduce the contributions from low-Z scatterers to the EXAFS.

Samples were run as sets, prepared from the same PS II preparation and Br/Cl treatments. These sets are BE2 and BE3; BG5, BG7 and CG12; and BJ5 and CJ3 (B as the first letter denotes a Br sample, C as first letter denotes a Cl control sample). The Cl control samples CG12 and CJ3 fit nicely to Cl at about 2.2 Å at both 10° and 80°, although the coordination numbers are low (0.08 and 0.11 at 10°, 0.13 and 0.11 at 80°). A coordination number of 0.25 is expected for 1 Mn-Cl interaction per 4 Mn in the OEC. One Cl sample fit to Br (CJ3 at 80°), but the coordination number is quite high (0.625) and ΔE_0 is significantly different from the two-shell fit (-6 vs. -18). Thus, this is not a consistent or physically reasonable fit.

Of the 10 Br sample fits, only four show better fits to Br than to Cl (BE2 and BJ5 at 10°; BE3 and BG5 at 80°). These have coordination numbers of 0.42 and 0.58 at 10°, and 0.21 and 0.26 at 80°. The coordination numbers for the poorer fits were lower. Nine out of the ten Br samples show an improvement in fit parameters with the addition of Cl as a third shell, relative to the fits with the two shells of Mn-Mn interactions. These coordination numbers are still smaller (0.05 to 0.16) than 0.25, at both near-extreme angles of 10° and 80°. With oriented samples it is not unreasonable to find coordination numbers lower than the actual coordination number at one extreme angle (e.g. at 80°), but in that case the numbers would be higher than the actual coordination number at the near-complimentary angle (e.g. at 10°).

A Fourth Fourier Transform Peak

A seen in Figure 5.10B, a fourth peak appears in the Fourier transforms of these data. This fourth peak was seen in several of the samples, and has been reported by others (Penner-Hahn et al. 1990). As for the peak at about 2 Å (best seen in Fig 5.10A, between peaks I and II), it was present when we simulated Mn EXAFS of our model (See Fig 1.4) using FEFF 5 with and without halide, and thus does not arise from a Mn-halide interaction. This peak was reported by Penner-Hahn et al. (1990) as well.

Discussion

Cl K-edges

Cl K-edge studies of Mn-Cl model compounds provide information on the nature of Mn-halide bonding. The presence of pre-edge features, due to forbidden 1s-3d transitions, indicates mixing of metal 3d orbitals with Cl 3p orbitals. The amplitude of the pre-edge features gives information on the degree of covalency between the metal and halide (Hedman et al. 1990), and the pre edge position is affected by the effective charge on the Cl and the energy of the metal orbitals involved in bonding (Shadle et al. 1993).

It is interesting that for the $Mn_4O_3Cl_{(n)}$ distorted cubane compounds whose Cl K-edges are shown in Fig 5.4, three distinct pre-edges are seen for the three Mn-μ_3-Cl bonds. In a series of LCAO Xα calculations of $Mn_4O_3Cl_7(O_2CEt)_3]^-$, Schmitt et al. (1992) found LCAOs of differing energies involved in these interactions. They found Mn(III) d_{yz} (16.0% charge density) plus μ_3-Cl p_y (19.9%); Mn(III) d_{xy} (21.1%) plus μ_3-Cl p_x (21.1%); and Mn(III) d_{x2-y2} (10.2%) plus d_{zy} (22.5%) plus μ_3-Cl p_z (21.2%) molecular orbitals involved in the Mn(III)-Cl bridging interactions. The rest of the charge density was distributed evenly over the entire molecule. The pre-edge position is dependent on both the charge of the ligand and the energy of the metal orbital involved in bonding. Thus, although the effective charge on the bridging Cl is the same for all three interactions, the variation in the molecular orbital energy shifts the energy of the pre-edge feature. This is probably the reason for the two distinct pre-edge features in Mn(IV)Cl_2 Salpn (Fig 5.3) as well -- the Cl ligands are bonded in molecular orbitals of different energies.

The terminal and bridging Cl ligands are clearly distinguished in the Cl K-edges of the Mn-Cl model compounds in Fig 5.4. Differences in terminal vs. bridging ligands have been found in other ligand K-edge studies (Shadle et al. 1994). They found that bridging ligands had greater charge donation to the bonding metal, and a higher ligand covalent contribution to the metal HOMO. Thus, bridging ligands tend to have a higher pre-edge energy than terminal ligands. This is the case found in the bridging and terminal ligands in Fig 5.4: the bridging ligands have pre-edge features at 2821.2, 2822.5 and 2823.9 eV, and terminal ligands have a pre-edge feature at about 2821.0 eV.

Mn EXAFS of Mn-Cl Model Compounds

Fitting with simulations of the Mn EXAFS of $Mn_4O_2Cl_2(O_2CPh\text{-}3{,}5F_2)_6(py)_4$ has demonstrated that, even in the midst of many Mn-Mn and Mn-O contributions, inclusion of two Mn-Cl terminal interactions makes a significant improvement to the simulation of the EXAFS. This may not be the case for a single Mn-Cl interaction, although we will not know until a suitable model compound with 1 Cl per 4 Mn is made. In the case of the fitting of $Mn_4O_3Cl_4(O_2CPh\text{-}3{,}5Cl_2)_3(py)_3$, which has 3 bridging Mn-Cl interactions and 3 terminal interactions, the inclusion of the three bridging interactions improved the fit, whereas subsequent inclusion of the 3 terminal Mn-Cl interactions made little difference in the fit quality.

We have not yet seen a model compound with EXAFS like that of PS II. The EXAFS and Fourier transform of $Mn_4O_3Cl(O_2CMe)_3(dbm)_3$ were the closest to PS II of the compounds investigated in this work, but the peak positions of the *k*-space data, the amplitudes of the Fourier transform peaks, and the coordination numbers for the Mn-Mn interactions at 2.7 Å and 3.3 Å, are inconsistent with data from PS II.

EXAFS of Br-treated PS II

The fits to Br and Cl control data are difficult to interpret. Br fit to only 4 of 10 Br samples, but at distances close to 2.6 Å with reasonable coordination numbers for Br terminal ligation to Mn and fairly consistent dichroism (0.21 and 0.26 at 80°, and 0.42 and 0.58 at 10 °). However, 6 of the 10 Br samples did not fit better to Br than to Cl.

Cl fit to almost all of the samples (Br and Cl) at about 2.2 Å. The distances found are consistent with those seen in model compounds for terminal halide ligands. Fits to longer distances, equivalent to bridging interaction distances, were tried, but these fits did not improve the fit errors. Thus, if halide is indeed ligated to Mn in the OEC, based on these fitting distances we would predict that Cl is ligated as a terminal rather than a bridging ligand to Mn. This is in agreement with the work of DeRose (1990), in which small differences were found in the Mn EXAFS of Synechococcus grown with Br salts, compared with that of control Synechococcus. Simulations in that work indicated that in the case of a bridging Mn-halide interaction, greater differences would be seen in the EXAFS of the control vs. Br samples than those reported. As shown in Fig. 5.11, the differences between simulated Br and Cl control samples can still be subtle, even in oriented samples. There are no large differences which would stand out boldly above the signal to noise level found in EXAFS samples.

Subtle differences are seen in the *k*-space data and Fourier transforms of Cl-treated control PS II vs. Br data, but these are within the differences seen from sample to sample. Simulations of Br data created by subtraction of 0.25 Cl at 2.2 Å from Cl control data and subsequent addition of 0.25 Br at 2.6 Å, 2.7 Å and 2.8 Å show differences in the region of $k = 9$ to 10 $Å^{-1}$. These distances vary significantly as R for Br is changed. Because we do not know the exact nature of halide bonding in the OEC this distance, and therefore the Br EXAFS, is difficult to predict. If halide is bound as a terminal ligand to Mn, we would expect a Mn-Br distance of 2.6-2.7 Å in Br-treated PS II.

The fact that Cl effects an improvement in the fit parameters of almost all the samples, Br or Cl, can be interpreted as either (1) the Cl amplitude function is behaving as a "skeleton key" function, filling in for any deficiencies in the fit due to noise in the data or contributions from low-Z scatterers, or (2) we have not replaced all of the Cl in PS II with Br or (3) there are two halide sites, one of which is replaced by Br.

This last proposal may not be as likely because we should see better fits to Br in that case. Boussac et al. (1995) have proposed that there may be two sites for halide binding in the OEC. In their ESEEM studies, they saw differences for PS II washed with high salt concentrations and replaced with halide (NaBr or NaCl). These differences were close to the Larmor frequencies for Br and Cl, which indicated that halide was nearby, but not bound to Mn. They did not see Cl/Br differences after PS II was treated with high pH and sulfate. However, based on simulations, Cl/Br couplings are predicted to be indistinguishable with pulsed EPR (Reijerse & Keijzers 1987; Wang et al. 1992). They suggested that there may be two halide binding sites, one nearby the OEC but not bound to Mn, and one ligated to Mn, for which differences between Br and Cl would not be expected.

With regard to option (2), it is a significant question whether we have replaced Cl with Br in all of the OEC centers. In all of these preparation a large g=4 signal was seen after treatment with NaF, indicating that F had replaced Cl, and the MLS returned after treatment with Br with concurrent disappearance of the g=4 signal. Presumably, the halide responsible for these changes had indeed been replaced, but a small amount of Cl may remain. In a PS II sample with a concentration of 2 mg Chl/ml, as little as 10 μM Cl is still equivalent to one Cl per PS II, assuming 250 Chl per PS II. A better method for replacement of Cl with Br may be to remove all of the halide entirely by removal of the 17 and 23 kDa proteins with high pH treatment, and adding back a stoichiometric amount of Br, with an excess of halide-free proteins.

As for option (1), we can test this by fitting Mn-Br model compounds with both Cl and Br. Mn-Br model compound data were not available for this comparison.

Future Work

Our study of the bonding of halide to the OEC can be improved with XAS studies of model compounds closer to our model of PS II (see Fig 1.4). Two di-μ-oxo bridged Mn-Mn binuclear units, plus a Mn-Mn interaction at about 3.3 Å, possibly mono-μ-oxo bridged, are likely components of the OEC. The addition of one terminal Cl to these Mn will provide us with a way to determine whether bonding to one terminal Cl ligand per 4 Mn can be detected with EXAFS, and an indication as to whether our model is close to the correct structure for the OEC.

Fitting of oriented data may be improved by using the latest version of FEFF, FEFF 6. This version includes angle-dependent effects in XAS, and can be used to simulate oriented data specifically.

EXAFS of PS II treated with iodine is in progress in this laboratory, and with these preparations the Mn-halide interaction may be further enhanced by the inclusion of the large I scatterer, whose amplitude function is distinctly different from that of Cl. A disadvantage of the I-treated samples is that the MLS and O_2 evolution values are about 50% of that for PS II. This fact, plus the fact that the chemical properties of I are significantly different from those of Cl, indicates that in the I preparations the OEC may not be in its native form.

Another method which can be used to determine whether Cl is ligated to Mn in the OEC is XAS studies at the Cl or Br edge, with native PS II or Br - replaced PS II, respectively. If we were to see a pre-edge in the Cl K-edge of PS II, this would provide solid evidence that Cl is ligated to a metal. Early attempts of this experiment produced data too noisy to make a conclusion; plans are being drawn for a new cryostat to try again. For this study, special care must be taken to ensure that there is a single halide in the sample. The best method for this is to deplete PS II of the 17 and 23 kDa proteins, and replete with small amounts of halide. The edge inflection point of free halide is at about 2826 eV, whereas the pre-edges for Mn-Cl model compounds is about 2821 to 2824 eV; thus free halide is not expected to overshadow the pre-edge contributions.

As a control for the Cl K-edges of single-halide PS II, samples from which Mn had been removed could be run to eliminate the possibility of interaction of halide with another metal in PS II. In the event that halide is found to be ligated to Mn, changes in the Cl K-edge for PS II in different S-states may also give information as to the oxidation environment of the Mn to which it is bound and insight into the mechanism of oxygen evolution by the OEC.

References

Arnon, D. I. & Whatley, F. R. (1959) *Science 110*, 554-556.

Bashkin, J. S.; Chang, H.-R.; Streib, W. E.; Huffman, J. C.; Hendrickson, D. N. & Christou, G. (1987) *J. Am. Chem. Soc. 109*, 6502-6504.

Beck, W. F. & Brudvig, G. W. (1988) *Chem. Scripta 28A*, 93-98.

Berthold, D. A.; Babcock, G. T. & Yocum, C. F. (1981) *FEBS Lett. 134*, 231-234.

Binsted, N.; Strange, R. W. & Hasnain, S.S. (1992) *Biochemistry 31*, 12117-12125.

Blum, H.; Salerno, J. C. & Leigh, J. S., Jr. (1978) *J. Magn.Res.30*, 385-391.

Boussac, A. (1995) *Chem.Phys.194*, 409-418.

Bové, J.; Bové, M.; Whatley, F. R. & Arnon, D. I. (1963) *Z. Naturforsch. 18b*, 683-688.

Casey, J. L. & Sauer, K. (1984) *Biochim. Biophys. Acta 767,* 21-28.

Chang, H.-R.; Larson, S. K.; Boyd, P. D. W.; Pierpont, C. G. & Hendrickson, D. N. (1988) *J. Am. Chem. Soc. 110*, 4565-4576.

Clendenning, K. A. & Ehrmentraut, H. C. (1950) *Arch. Biochem. 29*, 387-403.

Critchley, C.; Baianu, I. C.; Govindjee & Gutowsky, H. S. (1982) *Biochim. Biophys. Acta 682,* 436-445.

Critchley, C.; Andersson, B.; Ryrie, I. J. & Anderson, J. H. (1984) *Biochim. Biophys. Acta 767*, 532-539.

Daugherty, P. A.; Glerup, J.; Goodson, P. A.; Hodgson, D. J.; Michelsen, K. (1991) *Acta Chemica Scandinavica 45*, 244-253.

DeRose, V. J. (1990) Ph.D. Dissertation, University of California, Berkeley. Lawrence Berkeley Laboratory Report # LBL-30077.

DeRose, V. J.; Mukerji, I.; Latimer, M. J.; Zimmerman, J.-L.; Mukerji, I.; Yachandra, V. K.; Sauer, K. & Klein, M. P. (1995) *Chem.Phys.194* 443-459.

Dismukes, G. C. (1986) *Photochem. Photobiol. 43*, 99-115.

Dismukes, G. C. (1988) *Chem. Scripta 28A*, 99-104.

Douglas, B. E.; McDaniel, D. H. & Alexander, J. J. (1983), *Concepts and Models of Inorganic Chemistry, Second Edition,* Wiley & Sons, New York.

George, G. N.; Prince, R. C. & Cramer, S. P. (1989) *Science 243*, 789-791.

George, G. N.; Cramer, S. P.; Frey, T. G. & Prince, R. C. (1993) *Biochim. Biophys. Acta 1142,* 240-252.

Goldberg, D. P.; Caneschi, A.; Delfs, C. D.; Sessoli, R. & Lippard, S. J. (1995) *J. Am. Chem. Soc. 117*, 5789-5800.

Gorter, S.; van Ingen Schenau, A. D. & Verschoor, G. C. (1974) *Acta Cryst. B 30*, 1867-1871.

Govindjee (1984) in *Advances in Photosynthesis Research, Vol I* (Sybesma, C., Ed.), The Hague, Nijhoff/Junk, pp. 227-238.

Haddy, A. & Vänngård, T. (1990) in *Current Research in Photosynthesis Vol. I* (Baltscheffsky, M., ed.), Kluwer, Dordrecht, pp. 753-756.

Hedman, B.; Hodgson, K. O. & Solomon, E. I. (1990) *J. Am. Chem. Soc. 112*, 1643-1645.

Hedman, B.; Frank, P.; Gheller, S. F.; Roe, A. L.; Newton, W. E. & Hodgson, K. O. (1988) *J. Am. Chem. Soc. 110*, 3798-3805.

Hendrickson, D. N.; Christou, G.; Schmitt, E. A.; Libby, E.; Bashkin, J. S.; Wang, S.; Tsai, H.-L.; Vincent, J. B.; Boyd, P. D. W.; Huffman, J. C.; Folting, K.; Li, Q. & Streib, W. (1992) *J. Am. Chem. Soc. 114*, 2455-2471.

Homann, P. H. (1985) *Biochim. Biophys. Acta 809,* 311-319.

Homann, P. H. (1988) *Photosynthes. Res. 15* (1988) 205-220.

Itoh, S.; Yerkes, C. T.; Koike, H.; Robinson, H. H. & Crofts, A. R. (1984) *Biochim. Biophys. Acta 766,* 612-622.

Izawa, S.; Heath, R. & Hind, G. (1969) *Biochim. Biophys. Acta 180*, 388-398.

Johnson, J.; Pfister, V. & Homann, P. (1983) *Biochim. Biophys. Acta 723,* 256-265.

Kelly, P. M. & Izawa, S. (1978) *Biochim. Biophys. Acta 502,* 198-210.

Larson, E. J. & Pecoraro, V. L. (1991) *J. Am. Chem. Soc. 113*, 3810-3818.

Latimer, M. J.; Rompel, A.; Underwood, J. H.; Yachandra, V. K. & Klein. M. P. (1995) *Rev. Sci. Instrum. 66*, 1843-1845.

Li, Q.; Vincent, J. B.; Libby, E.; Chang, H.-R.; Huffman, J. C.; Boyd, P. D. W.; Christou, G. & Hendrickson, D. N. (1988) *Angew. Chem. Int. Ed. Engl. 27*, 1731-1733.

McKale, A. G.; Veal, B. W.; Paulikas, A. P.; Chan, S.-K. & Knapp, G. S. (1988) J. Am. Chem. Soc. 110, 3763-3768.

Muallem, A.; Farineau, J.; Laine-Böszormenyi, M. & Izawa, S. (1981) in *Photosynthesis Vol. II* (Akoyunoglou, G., ed.), Balaban International Science Services, Philadelphia, pp. 435-443.

O'Day, P. A.; Rehr, J. J.; Zabinsky, S. I. & Brown, G. E., Jr. (1994) *J. Am. Chem. Soc. 116,* 2938-2949.

Ono, T.-A.; Nakayama, H.; Gleiter, H.; Inoue, Y. & Kawamori, A. (1987) *Arch. Biochem. Biophys. 256*, 618-624.

Ono, T.; Zimmerman, J.-L.; Inoue, Y. & Rutherford, A. W. (1986) *Biochim. Biophys. Acta 851,* 193-201.

Pecoraro, V. L. & Butler, W. M. (1986) *Acta Cryst. C 42*, 1151-1154.

Penner-Hahn, J. E.; Fronko, R. M.; Pecoraro, V. L.; Yocum, C. F.; Betts, S. D. & Bowlby, N. R. (1990) *J. Am. Chem. Soc. 112*, 2549-2557.

Phillips, F. L.; Shreeve, F. M. & Skapski, A. C. (1976) *Acta Cryst. B 32*, 687-692.

Radmer, R. & Ollinger, O. (1983) *FEBS Lett. 152,* 39-43.

Rashid, A. & Homann, P. H. (1992) *Biochim. Biophys. Acta 1101,* 303-310.

Reedijk, J.; Stork-Blaisse, B. A. & Verschoor, G. C. (1971) *Inorg. Chem. 10,* 2594-2599.

Rehr, J. J.; Albers, R. C. & Zabinsky, S. I. (1992) *Phys. Rev. Lett. 69*, 3937-3400.

Reijerse, E. J. & Keijzers, C. P. (1987) *J. Magn. Res. 71*, 83.

Rutherford, A. W. (1985) *Biochim. Biophys. Acta 807*, 189-201.

Sandusky, P. O. & Yocum, C. F. (1983) *FEBS Lett. 162*, 339-343.

Sandusky, P. O. & Yocum, C. F. (1984) *Biochim. Biophys. Acta 766,* 339-343.

Sandusky, P. O. & Yocum, C. F. (1986) *Biochim. Biophys. Acta 849,* 85-93.

Saygin, Ö. & Witt, H. T. (1984) *FEBS Lett. 176*, 83-87.

Saygin, Ö. & Witt, H. T. (1984) *FEBS Lett. 187,* 224-226.

Schmitt, E. A.; Noodleman, L.; Baerends, E. J. & Hendrickson, D. N. (1992) *J. Am. Chem. Soc. 114*, 6109-6119.

Shadle, S. E.; Penner-Hahn, J. E.; Schugar, H.; Hedman, B.; Hodgson, K. O. & Solomon, E. I. (1993) *J. Am. Chem. Soc. 115*, 767-776.

Shadle, S. (1994a) Ph.D. Dissertation, Stanford University, Stanford, Ca. Stanford Linear Accelerator Center publication # SLAC-449, SLAC/SSRL-0088, and UC-408.

Shadle, S. E.; Hedman, B.; Hodgson, K. O. & Solomon, E. I. (1994b) *Inorg. Chem. 33*, 4235-4244.

Shadle, S. E.; Hedman, B.; Hodgson, K. O. & Solomon, E. I. (1995) *J. Am. Chem. Soc. 117*, 2259-2272.

Smith, T. A.; DeWitt, J. G.; Hedman, B. & Hodgson, K. O. (1994) *J. Am. Chem. Soc. 116*, 3836-3847.

Stern, E. A.; Sayers, D. E. & Lytle, F. W. (1976) *Phys. Rev. Lett. 37*, 298-301.

Theg, S.; Jursinic, P. & Homann, P. (1984) *Biochim. Biophys. Acta 766,* 636-646.

Vincent, J. B.; Tsai, H.-L.; Blackman, A. G.; Wang, S.; Boyd, P. D. W.; Folting, K.; Huffman, J. C.; Lobkovsky, E. B.; Hendrickson, D. N. & Christou, G. (1993) *J. Am. Chem. Soc. 115*, 12353-12361.

Wang, S.; Folting, K.; Streib, W. E.; Schmitt, E. A.; McCusker, J. K.; Hendrickson, D. N. & Christou, G. (1991) *Angew. Chem. Int. Ed. Engl. 30,* 305-306.

Wang, S.; Tsai, H.-L.; Streib, W. E.; Christou, G. & Hendrickson, D. N. (1992) *J. Chem. Soc., Chem. Commun.*, 1427-1429.

Warburg, O. & Lüttgens, W. (1944) *Naturwissenschaften 301*, 40-43.

Warren, L. F. & Bennett, M. A. (1976) *Inorg. Chem. 15*, 3126-3140.

Wemple, M. W.; Tsai, H.-L.; Folting, K.; Hendrickson, D. N. & Christou, G. (1993a) *Inorg. Chem. 32*, 2025-2031.

Wemple, M. W.; Streib, W. E.; Huffman, J. C. & Christou, G. (1993) *J. Inorg. Biochem. 51*, 454.

Wydrzynski, T. & Sauer, K. (1980) *Biochim. Biophys. Acta 589,* 56-70.

Yachandra, V. K.; Guiles, R. D.; Sauer, K. & Klein, M. P. (1986) *Biochim. Biophys. Acta 850,* 333-342.

Yachandra, V. K.; DeRose, V. J.; Latimer, M. J.; Mukerji, I.; Sauer, K. & Klein, M. P. (1993) *Science 260*, 675-679.

Table 5.1

Physical Properties of Halides[a]

	F	Cl	Br	I
Ionic Radius (Å)	1.19	1.67	1.82	2.06
Covalent Radius(Å)	0.71	0.99	1.14	1.33
Electronegativity	4.0	3.0	2.8	2.5
Polarizability (cm^3/atom x10^{24})	1.04	3.66	4.77	7.10

Bond lengths (from model compounds)

	bridging (Å)	terminal (Å)	ref
Mn-Cl			
Mn(II)	2.763	2.348, 2.49	b
Mn(III)	2.766	2.491	b
Mn(II)		2.592, 2.594	c
Mn(III)		2.461	d
		2.381, 2.363, 2.201, 2.53, 2.34	d
Mn(III)	2.672	2.237	e
Mn(II)		2.525 axial	f
		2.392 equatorial	f
Mn(III)		2.526	g
Mn(III)	2.629	2.229	h
Mn(III)		2.515, 2.611 (JT Distortion)	i
		2.123, 2.269, 2.302	i
Mn(III)	2.641, 2.656, 2.655		j
Mn(III)	2.627	2.237	k
Mn(III)		2.266, 2.237, 2.236, 2.242	k
Mn(II)		2.502	l
Mn(III)		2.239	l
Mn(IV)		2.195	l
Mn(III)	2.608, 2.630, 2.633	2.251, 2.263, 2.264, 2.270, 2.280	m
Mn-Br			
Mn(II)		2.514	b
		2.727, 2.52, 2.49, 2.68, 2.72	n
	2.735, 2.731, 2.682, 2.840, 2.650, 2.850, 2.840, 2.831, 2.823, 2.610, 2.851, 2.812, 2.627, 2.596, 2.752, 2.664, 2.756, 2.690, 2.597, 2.851	2.470, 2.482, 2.521, 2.494	o
		2.689	g
Mn(III)	2.802, 2.807, 2.799		p

a Douglas et al. 1983
b Chang et al. 1988

c Gorter et al. 1974
d Pecoraro & Butler 1986
e Li et al. 1988
f Phillips et al. 1976
g Daugherty et al. 1991
h Wemple et al. 1993a
i Vincent et al. 1993
j Wang et al. 1991
k Hendrickson et al. 1992
l Warren & Bennett 1976
m Bashkin et al. 1987
n Reedijk et al. 1971
o Goldberg et al. 1995
p Wang et al. 1992

Table 5.2:

Pre-edge positions and Edge Inflection Points for Cl K-edges of model compounds

	pre-edge position(s) (eV)	edge (eV)
KCl		2826.01
ClO_3^-		2830.99
ClO_4^-		2835.05
$MnCl_2 \cdot 2H_2O$		2826.01
$MnCl_4^{-2}$	2824.82	2825.73
Mn(III) (5-Cl-salpn)		2824.82
Mn(III)salpn Cl	2823.26	2825.81
Mn(IV)salpn Cl_2	2820.67, 2822.81	2824.74
$Mn_4O_3Cl(O_2CMe)_3(dbm)_3$ (Mn(III)$_3$Mn(IV);bridging Cl)	2821.21, 2822.48, 2823.92	2826.34
$Mn_4O_3Cl_4(O_2CMe)_6(py)_3$ 1 bridging, 3 terminal	2821.12, 2822.48, 2823.92	2826.79
$(Hpy)_3[Mn_4O_3Cl_7(O_2CMe)_3]$ 1 bridging, 6 terminal	2821.08, 2822.48, 2823.84	2826.34
$Mn_4O_3Cl_4(O_2CPh\text{-}3,5Cl_2)_3(py)_3$ (2 CL on Ph ring)	2821.21, 2822.56	2824.82

Table 5.3:

Fits to Mn EXAFS of Mn-Cl Model Compounds

I. $Mn_4O_2Cl_2(O_2CPh\text{-}3,5F_2)_6(py)_4$

interaction	R (crystal structure)	R(Å)	N[a]	σ^2(Å^2)	ΔEo	φ[b]	ε^2 [c]
Mn-O	1.864-1.985	1.877	2.75	.0047	-20.0	1.73	1.37
Mn-O	2.010-2.184	2.124	2.75	.0104			
Mn-Mn	2.875	2.809	0.50	.0004			
Mn-Mn	3.418, 3.361, 3.314, 3.294	3.328	2.00	.0045			
Mn-O		1.894	2.75	.0084	-16.5	929	.799
Mn-O		2.408	2.75	.0131			
Mn-Mn		2.805	0.50	.0036			
Mn-Mn		3.348	2.00	.0050			
Mn-Cl	2.296,2.287	2.317	0.50	.0000			

II. $Mn_4O_3Cl_4(O_2CPh\text{-}3,5Cl_2)_3(py)_3$

interaction	R (crystal structure)	R(Å)	N[a]	σ^2(Å^2)	ΔEo	φ[b]	ε^2 [c]
Mn-O	1.857-2.134	1.886	3.00	.0127	-19.9	1.76	1.04
Mn-Mn	2.802	2.779	1.50	.0017			
Mn-Mn	3.260	3.242	1.50	.0030			
Mn-O		1.900	3.00	.0133	-18.7	.755	.484
Mn-Mn		2.785	1.50	.0050			
Mn-Mn		3.241	1.50	.0049			
Mn-Cl	2.629	2.570	0.75	.0000			
Mn-O		0.877	3.00	.0221	-17.5	.735	.492
Mn-Mn		2.788	1.50	.0051			
Mn-Mn		3.249	1.50	.0045			
Mn-Cl		2.577	0.75	.0000			
Mn-Cl	2.229	2.128	0.75	.0116			

III. $Mn_4O_3Cl(O_2CMe)_3(dbm)_3$

interaction	R (crystal structure)	R(Å)	N[a]	σ^2(Å^2)	ΔEo	φ[b]	ε^2 [c]
Mn-O	1.842-1.945	1.891	2.25	.0014	-12.5	.422	.248
Mn-Mn	2.798,2.797,2.793	2.807	1.50	.0027			
Mn-Mn	3.253,3.265,3.238	3.284	1.50	.0052			
Mn-O		1.895	2.25	.0018	-11.8	.185	.085
Mn-Mn		2.789	1.50	.0048			
Mn-Mn		3.279	1.50	.0057			
Mn-Cl	2.642,2.657,2.655	2.625	0.75	.0008			

[a]Coordination numbers for all model compounds are held constant at the crystal structure values. [b]Fit error values, written as x 10^3, defined in Materials and Methods. [c]Fit error values x 10^5, as defined in Materials and Methods.

Table 5.4

Fits to Fourier peaks II & III for Br-treated and Cl control PS II

A: Data taken at $\theta = 10°$

Sample			R(Å)	N	ΔE_0	ϕ^a	$\varepsilon^{2\,b}$
Br	BE2	Mn[c]			-17.3	1.055	1.027
		Cl[d]	2.13	.121	-15.2	.608	.984
		Br[e]	2.61	.415	-7.1	.406	.657
Br	BE3	Mn			-15.1	.165	.152
		Cl	2.16	.054	-14.6	.092	.141
		Br	2.28	.035	-13.6	.081	.123
		Br	2.56	.087	-14.0	.117	.178
Br	BG5	Mn			-10.4	.550	.511
		Cl	2.24	.133	-11.5	.172	.265
		Br	2.66	.028	-10.5	.515	.796
Br	BG7	Mn			-16.4	.569	.520
		Cl	2.20	.125	-16.3	.220	.334
		Br	2.62	.024	-16.5	.546	.826
Br	BJ5	Mn			-20	.743	.686
		Cl	2.16	.154	-18.8	.342	.525
		Br	2.64	.584	-6.2	.203	.312
Cl	CG12	Mn			-12.5	.289	.265
		Cl	2.19	.083	-12.2	.142	.217
		Br	2.59	.104	-11.3	.202	.308
Cl	CJ3	Mn			-16.1	.413	.379
		Cl	2.23	.111	-17.4	.172	.262
		Br	2.56	.000	-16.1	.413	.631

[a] Fit error values, written as x 10^3, defined in Materials and Methods.
[b] Fit error values x 10^5, as defined in Materials and Methods.
[c] For all samples, initially two shells of Mn were fit, with starting values of R= 2.73 and 3.3 Å, ΔE_0 = -10.0. N was fixed for these shells at 0.83 and 0.57, respectively, based on average coordination numbers for oriented native PS II. Debye-Waller factor were fixed at 0.0035 and 0.003 Å^2, respectively, for the two Mn shells, based on average values for many fits.
[d] For all Cl fits, a starting value of R=2.3 was used for Cl, and σ^2 was fixed at 0.0005Å^2.
[e] For all Br fits, a starting value of R=2.6 was used for Br, and σ^2 was fixed at 0.0005Å^2.

Table 5.4

Fits to Fourier peaks II & III for Br-treated and Cl control PS II

B: Data Taken at 80°

Sample			R(Å)	N	ΔE_0	ϕ [a]	ε^2 [b]
Br	BE2	Mn[c]			-17.3	.322	.296
		Cl[d]	2.14	.081	-16.5	.215	.328
		Br[e]	2.85	.089	-14.9	.272	.415
Br	BE3	Mn			-15.6	.379	.348
		Cl	2.13	.093	-14.7	.205	.313
		Br	2.59	.262	-10.9	.080	.123
Br	BG5	Mn			-14.5	.480	.443
		Cl	2.21	.157	-13.5	.244	.374
		Br	2.62	.211	-12.6	.181	.278
Br	BG7	Mn			-16.6	.301	.459
		Cl	2.20	.127	-15.6	.116	.177
		Br	2.61	.152	-14.8	.194	.295
Br	BJ5	Mn			-18.8	.518	.468
		Cl	2.22	.160	-18.3	.286	.428
		Br	2.62	.129	-18.0	.295	.443
Cl	CG12	Mn			-17.3	.363	.334
		Cl	2.19	.128	-16.1	.113	.173
		Br	2.58	.012	-17.1	.363	.554
Cl	CJ3	Mn			-18.4	.303	.279
		Cl	2.18	.111	-17.2	.152	.233
		Br	2.66	.625	-6.0	.111	.170

[a] Fit error values, written as x 10^3, defined in Materials and Methods.

[b] Fit error values x 10^5, as defined in Materials and Methods.

[c] For all samples, initially two shells of Mn were fit, with starting values of R= 2.73 and 3.3 Å, ΔE_0 = -10.0. N was fixed for these shells at 0.83 and 0.57, respectively, based on average coordination numbers for oriented native PS II. Debye-Waller factor were fixed at 0.0035 and 0.003, respectively, for the two Mn shells, based on average values for many fits.

[d] For all Cl fits, a starting value of R=2.3 was used for Cl, and σ^2 was fixed at 0.0005Å^2.

[e] For all Br fits, a starting value of R=2.6 was used for Br, and σ^2 was fixed at 0.0005Å^2.

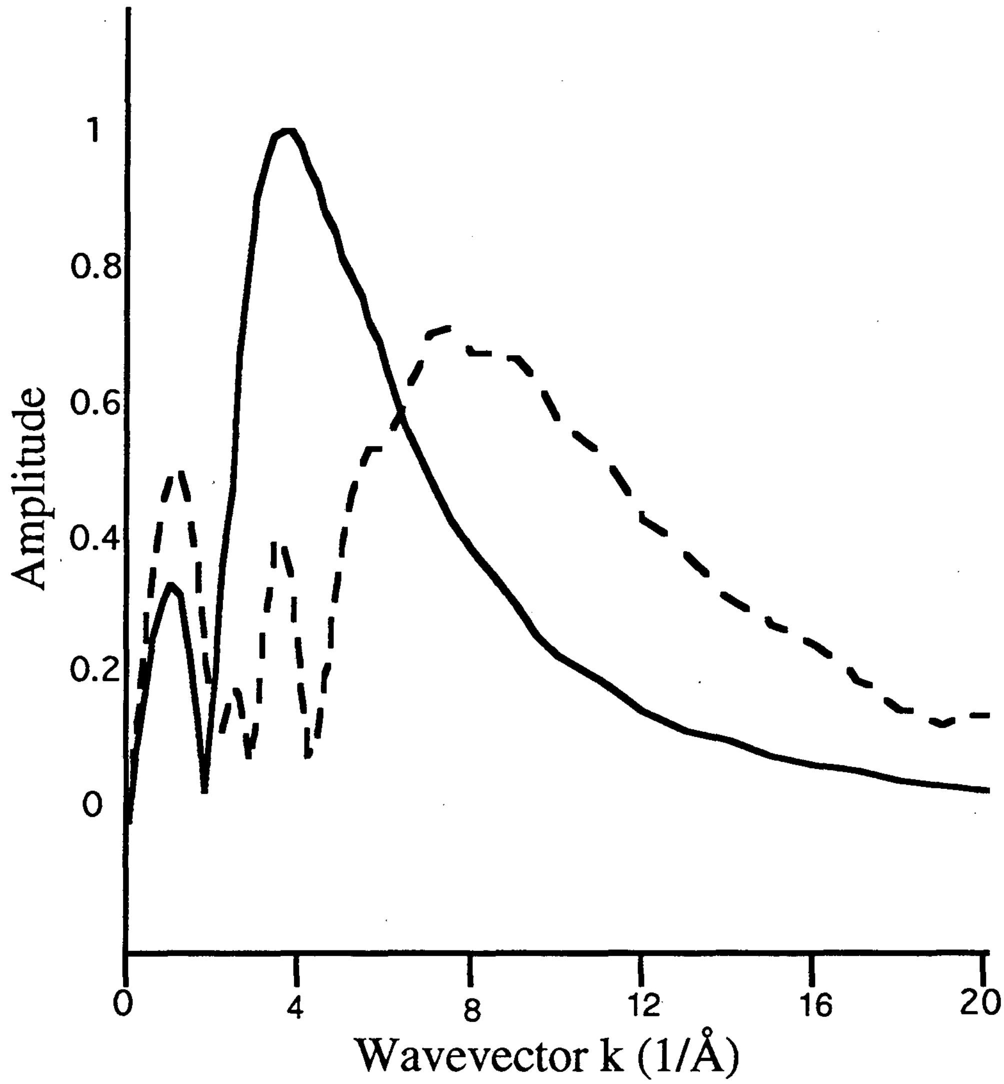

Figure 5.1: Theoretical Mn K-edge EXAFS amplitudes for Mn-Cl (___) and Mn-Br (_ _) created using FEFF 5.

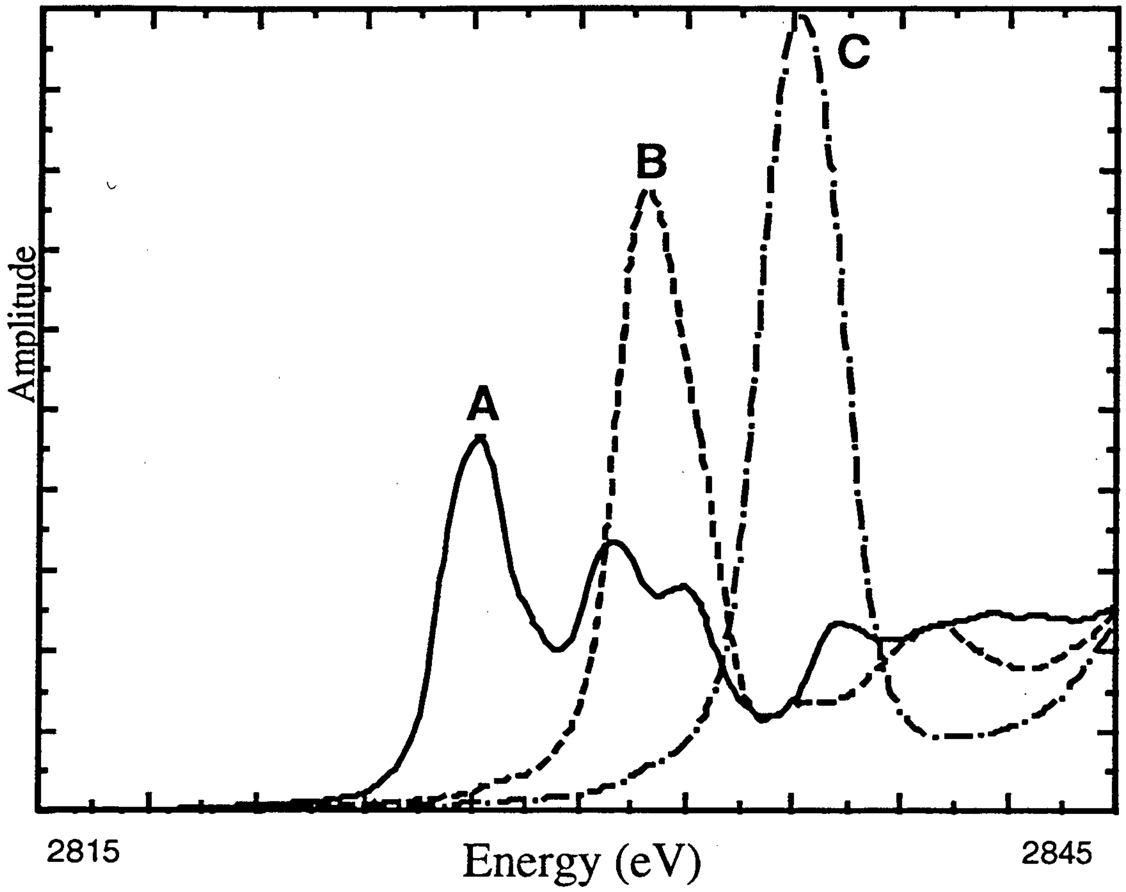

Figure 5.2: Cl K-edges for (A) KCl; (B) $NaClO_3$; (C) $NaClO_4$.

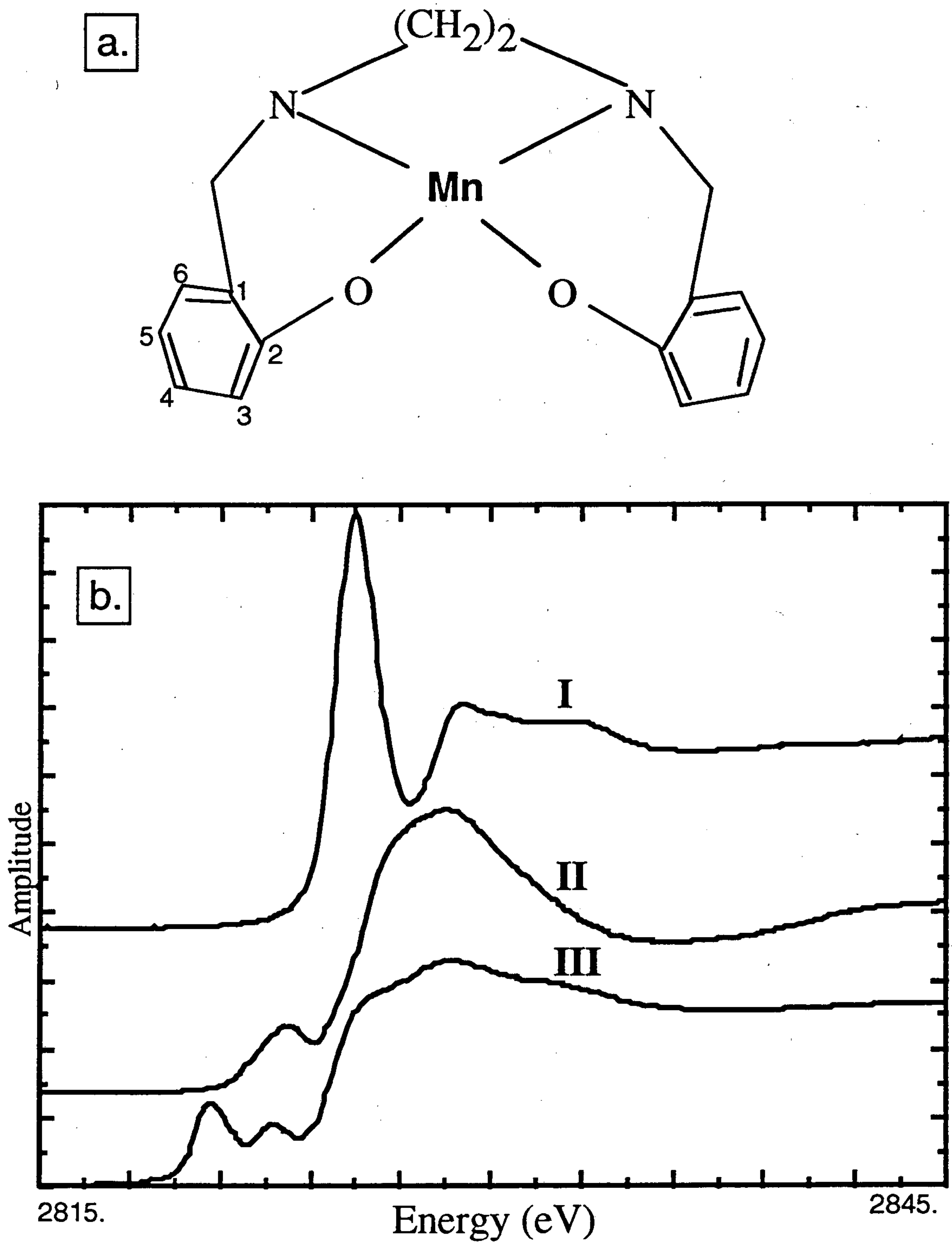

Figure 5.3: (a) Basic structure of Mn-Salpn model compounds (b) Cl K-edges of (I) Mn(III)(5-Cl Salpn) (no Mn-Cl ligand); (II) Mn(III)Cl Salpn (one Mn-Cl ligand); (III) Mn(IV) Cl_2 Salpn (two Mn-Cl ligands).

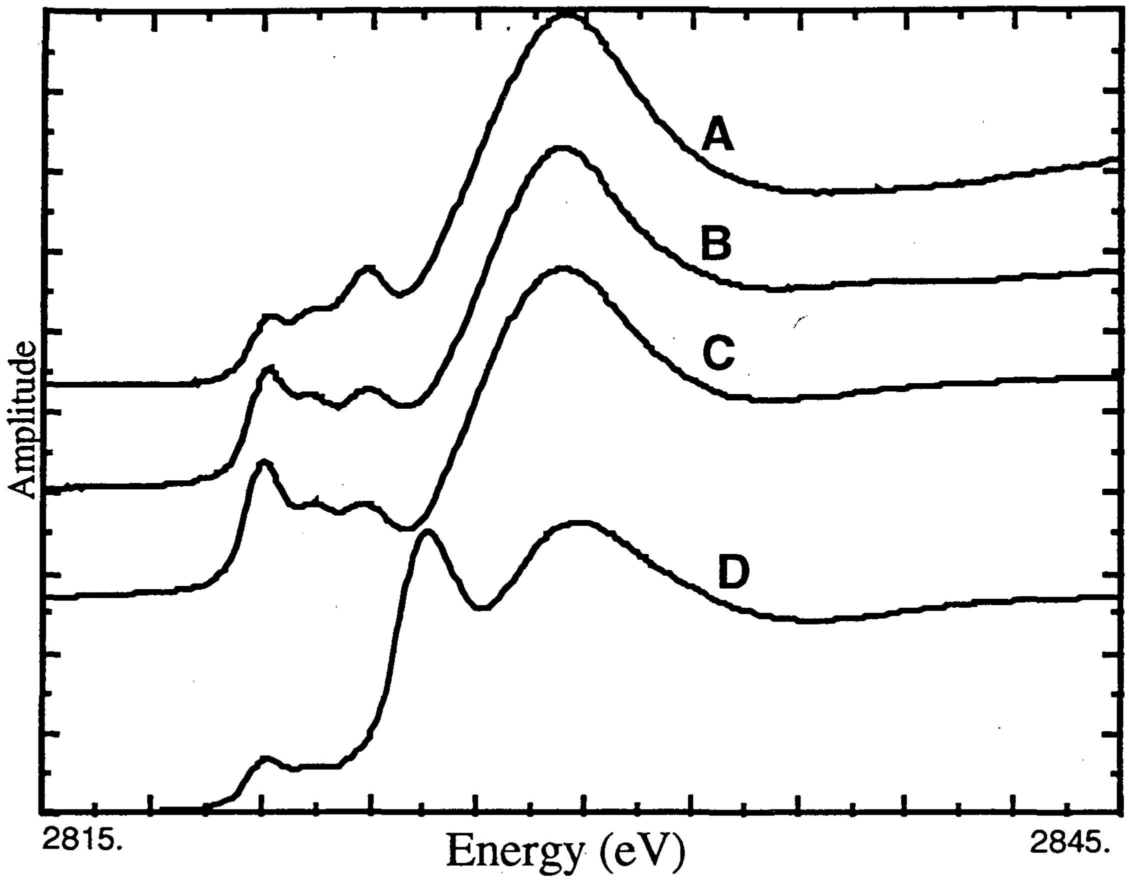

Figure 5.4: Cl K-edges of (A) $Mn_4O_3Cl(O_2CMe)_3(dbm)_3$ (1 μ_3 bridging Cl); (B) $Mn_4O_3Cl_4(O_2CMe)_6(py)_3$ (1 μ_3 bridging Cl, 3 terminal Mn-Cl); (C) $(Hpy)_3[Mn_4O_3Cl_7(O_2CMe)_3]$ (1 μ_3 bridging Cl, 6 terminal Cl); (D) $Mn_4O_3Cl_4(O_2CPh\text{-}3,5Cl_2)_3(py)_3$ (1 μ_3 bridging Cl, 3 terminal Cl, 2 Cl on phenyl ring.)

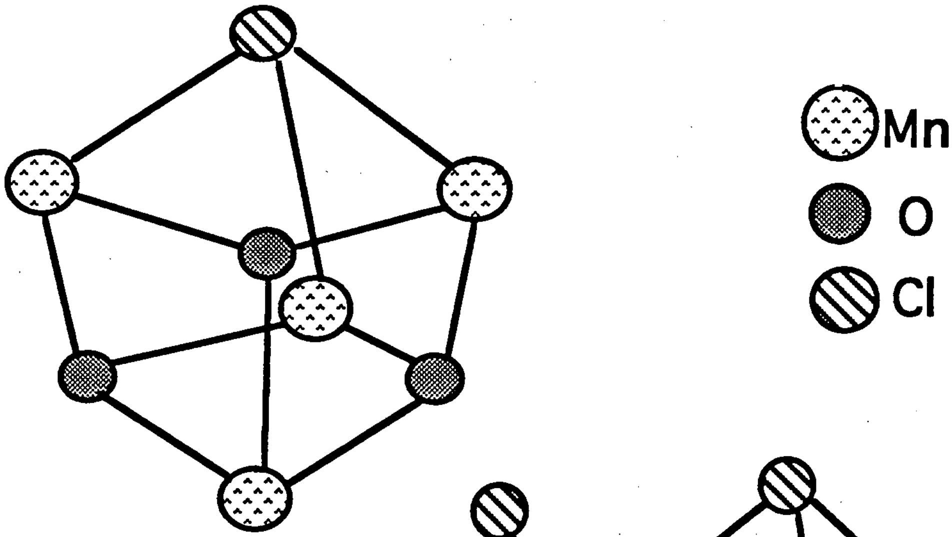

A: $Mn_4O_3Cl(O_2CMe)_3(dbm)_3$

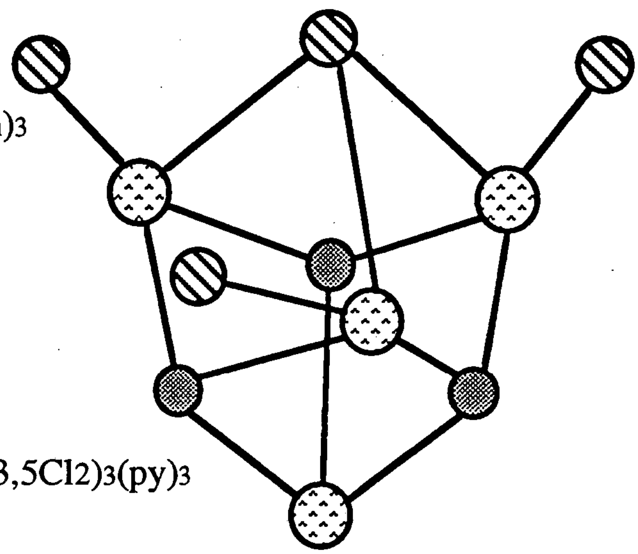

B: $Mn_4O_3Cl_4(O_2CPh\text{-}3,5Cl_2)_3(py)_3$

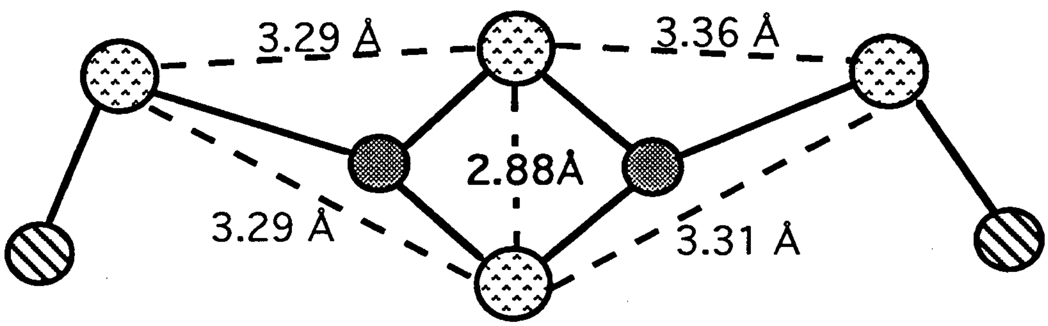

C: $Mn_4O_2Cl_2(O_2CPh\text{-}3,5\text{-}F_2)_6(py)_4$

Figure 5.5: Core structures of Mn-Cl model compounds
(A) $Mn_4O_3Cl(O_2CMe)_3(dbm)_3$; (B) $Mn_4O_3Cl_4(O_2CPh\text{-}3,5Cl_2)_3(py)_3$;
(C) $Mn_4O_2Cl_2(O_2CPh\text{-}3,5\text{-}F_2)_6(py)_4$.

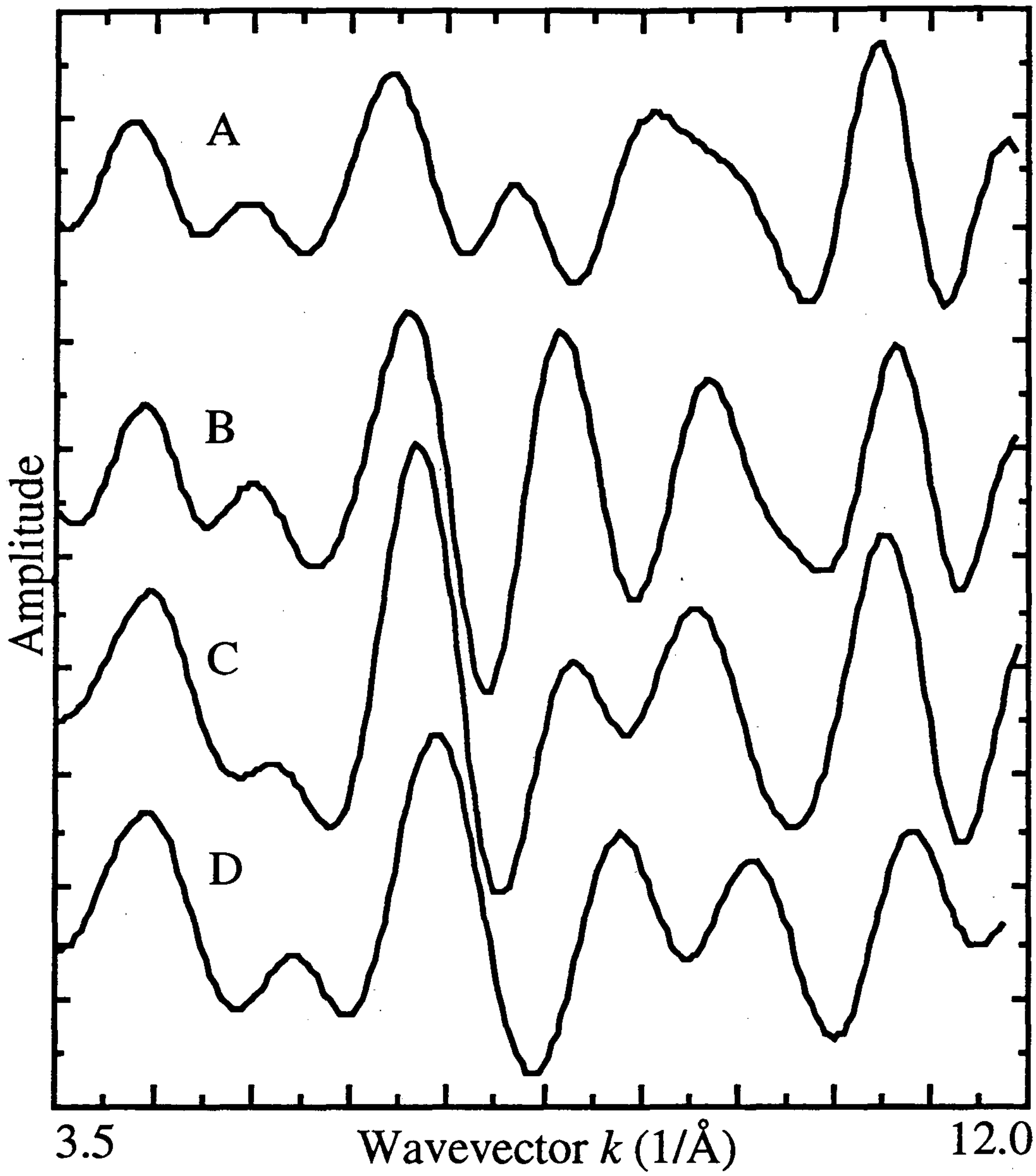

Figure 5.6: Mn K-edge EXAFS back transformed from 0 to 4 Å of (A) $Mn_4O_2Cl_2(O_2CPh\text{-}3,5F_2)_6(py)_4$; (B) $Mn_4O_3Cl_4(O_2CPh\text{-}3,5Cl_2)_3(py)_3$; (C) $Mn_4O_3Cl(O_2CMe)_3(dbm)_3$; (D) Spinach PS II in the S_2 state.

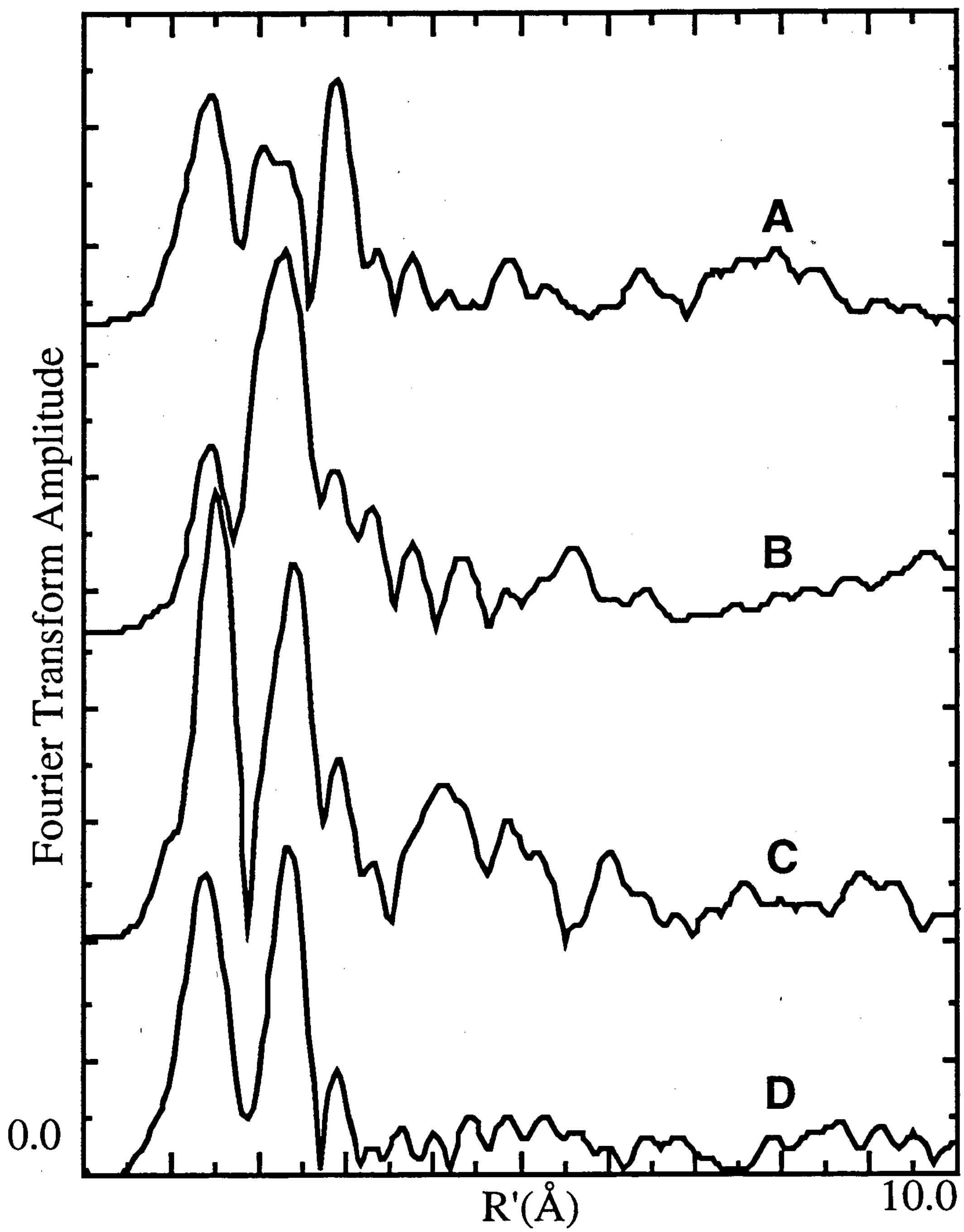

Figure 5.7: Fourier Transforms of (A) $Mn_2O_2Cl_2(O_2CPh\text{-}3,5F_2)_6(py)_4$; (B) $Mn_4O_3Cl_4(O_2CPh\text{-}3,5Cl_2)_3(py)_3$; (C) $Mn_4O_3Cl(O_2CMe)_3(dbm)_3$; (D) Spinach PS II in the S2 state.

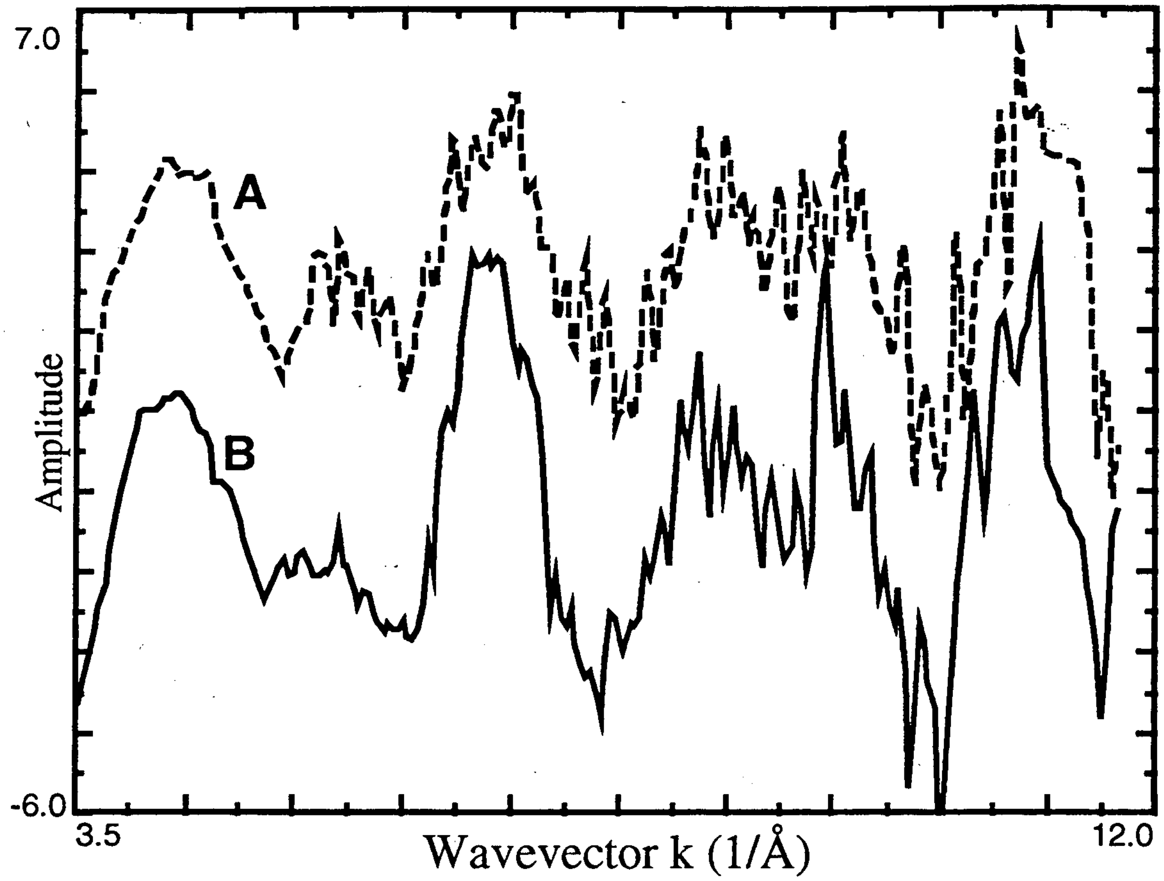

Figure 5.8: *k*-space of Mn K-edge EXAFS of oriented Br-treated PSII, at (A):10° and (B) 80°. Monochromator glitches have been removed at about 4.5 $Å^{-1}$ and 11.5 $Å^{-1}$.

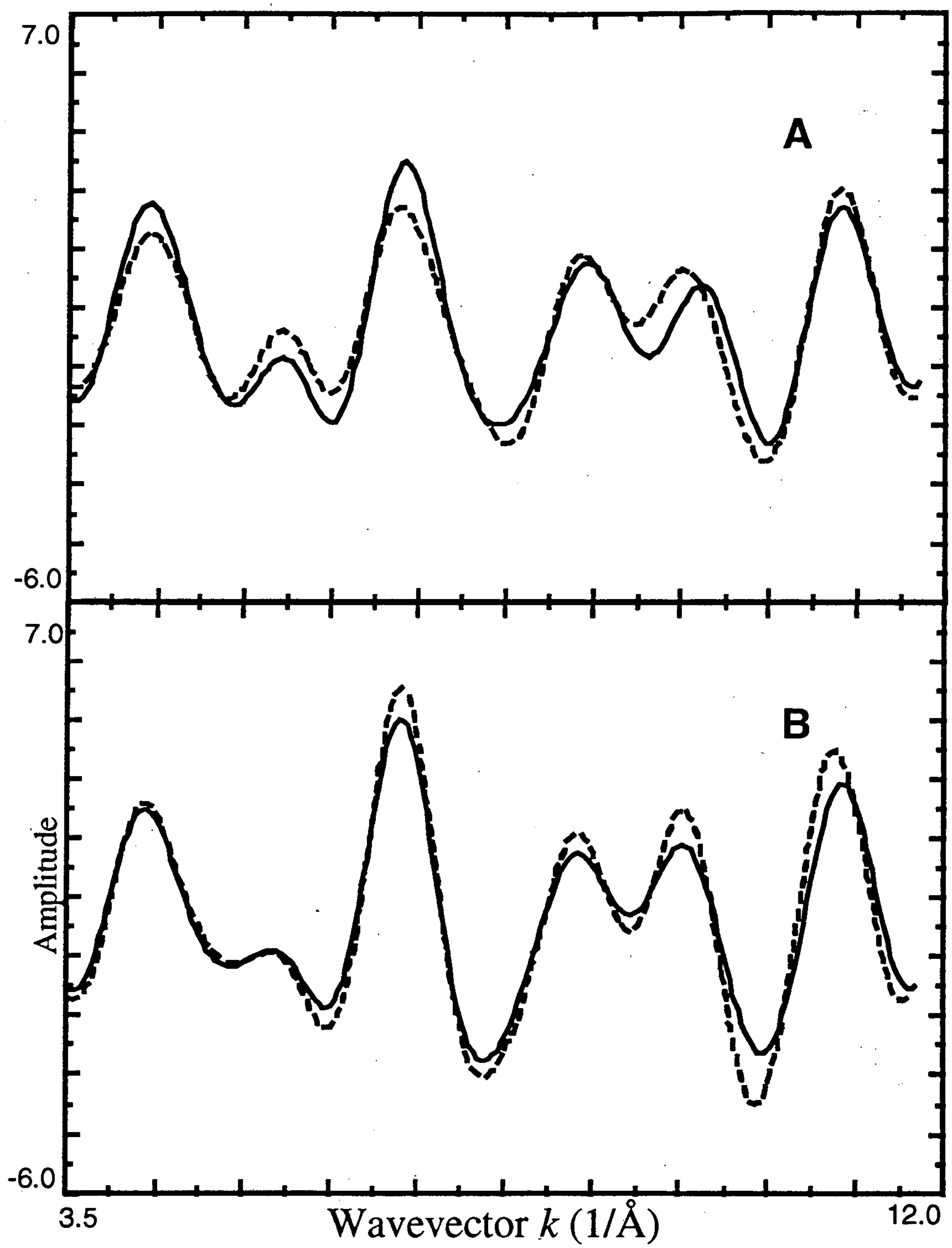

Figure 5.9: Isolates of Fourier peaks 1-4 of Br-treated (- -) and Cl control (——) PS II at (A) 10° and (B) 80°.

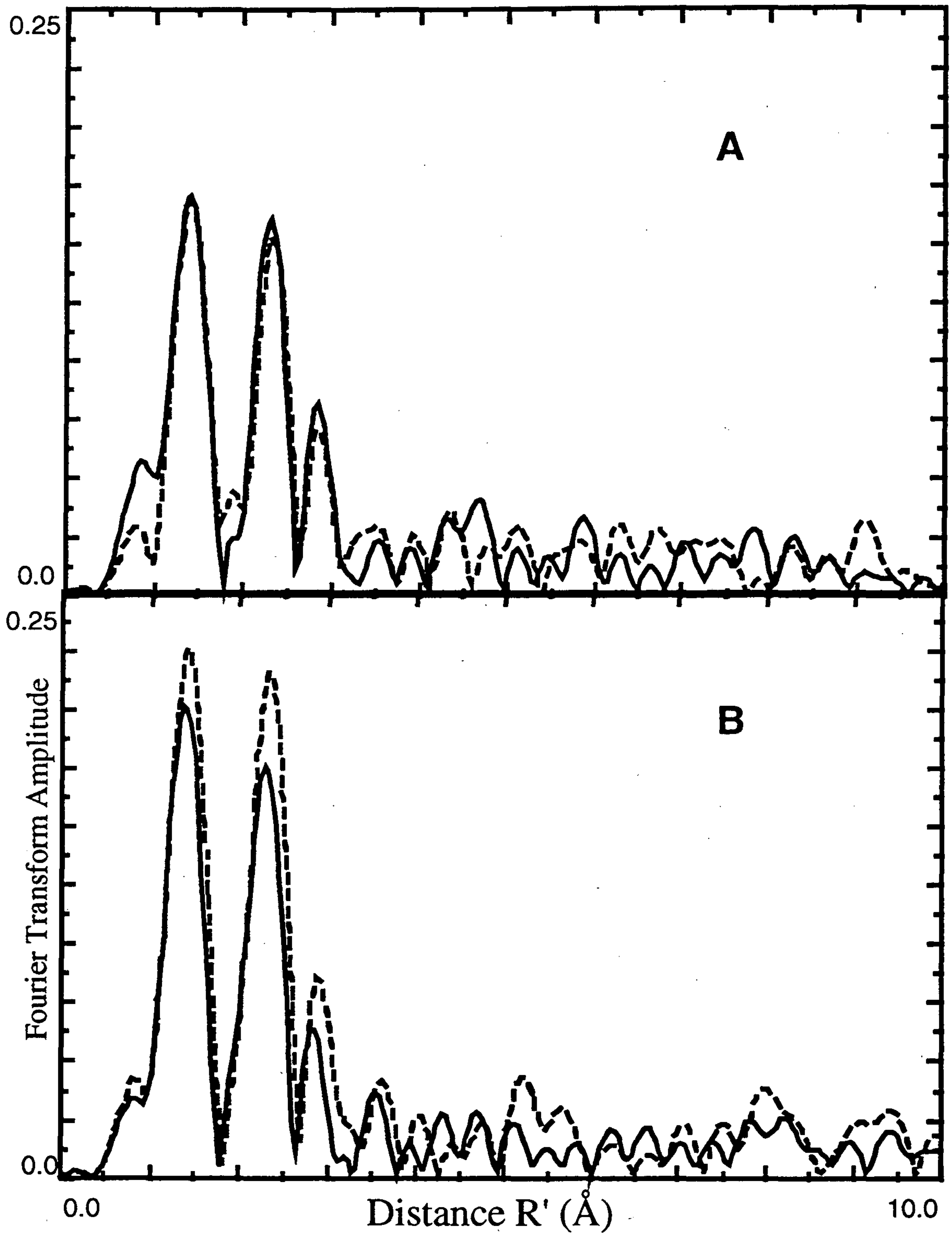

Figure 5.10: Fourier transforms of Mn EXAFS of Br-treated (- -) and Cl Control (—) PS II at (A) 10° and (B) 80°.

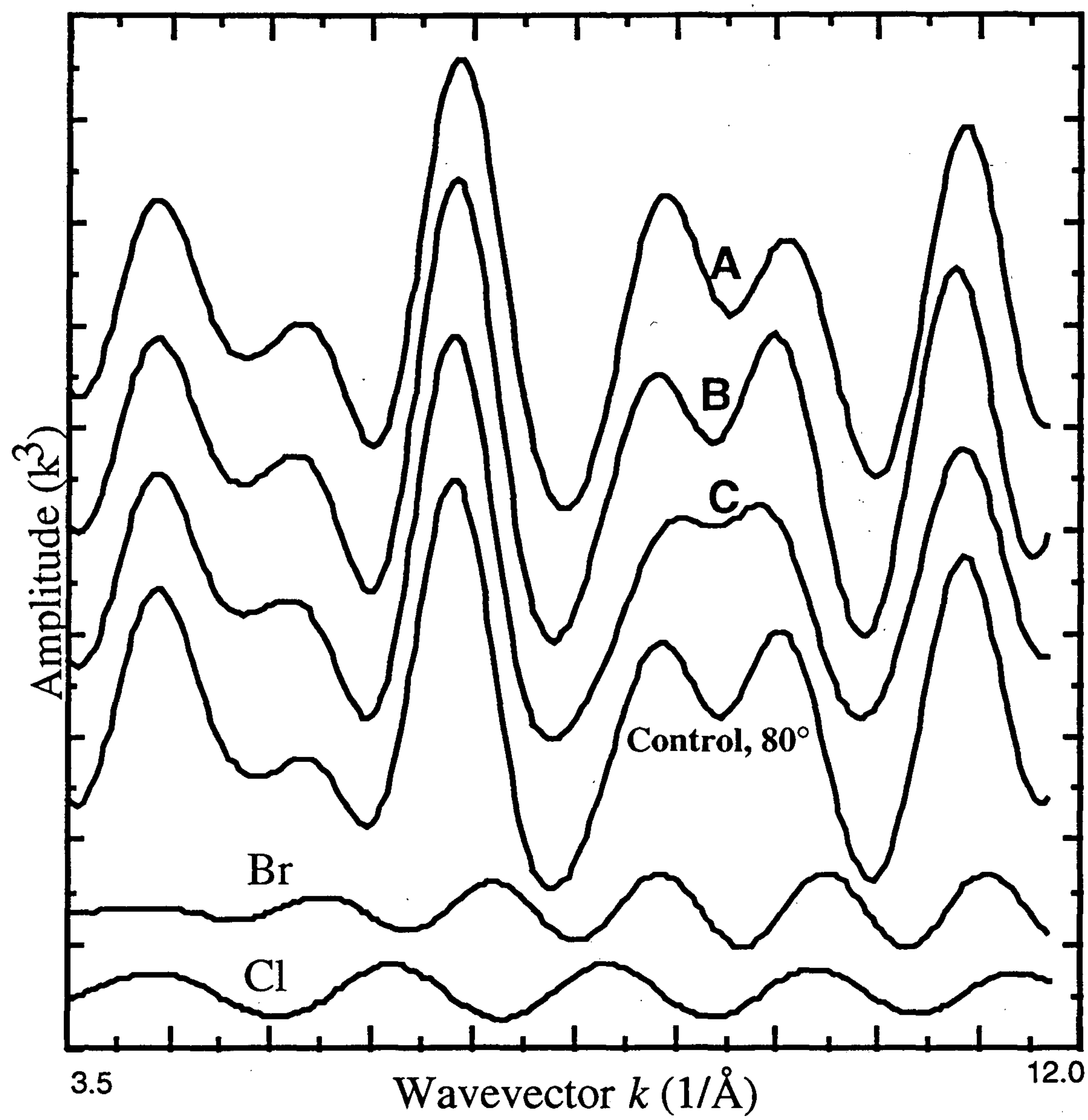

Figure 5.11: Back transform of Cl control data at 80° (Fourier peaks 1 to 4) plus simulations of Br data created by subtracting the partial wave for 0.25 Cl scatterers at 2.2 Å and adding the partial wave for Br with N=0.25, at various distances R. Simulations with Br at (A) 2.6 Å, (B) 2.7 Å and (C) 2.8 Å are seen above the Cl control data, as marked. Partial waves for Cl and Br are shown below,

LAWRENCE BERKELEY LABORATORY
TECHNICAL INFORMATION DEPARTMENT
1 CYCLOTRON ROAD
BERKELEY, CALIFORNIA 94720